Analysis of vegetation-activity trends in a global land degradation framework

Rogier de Jong

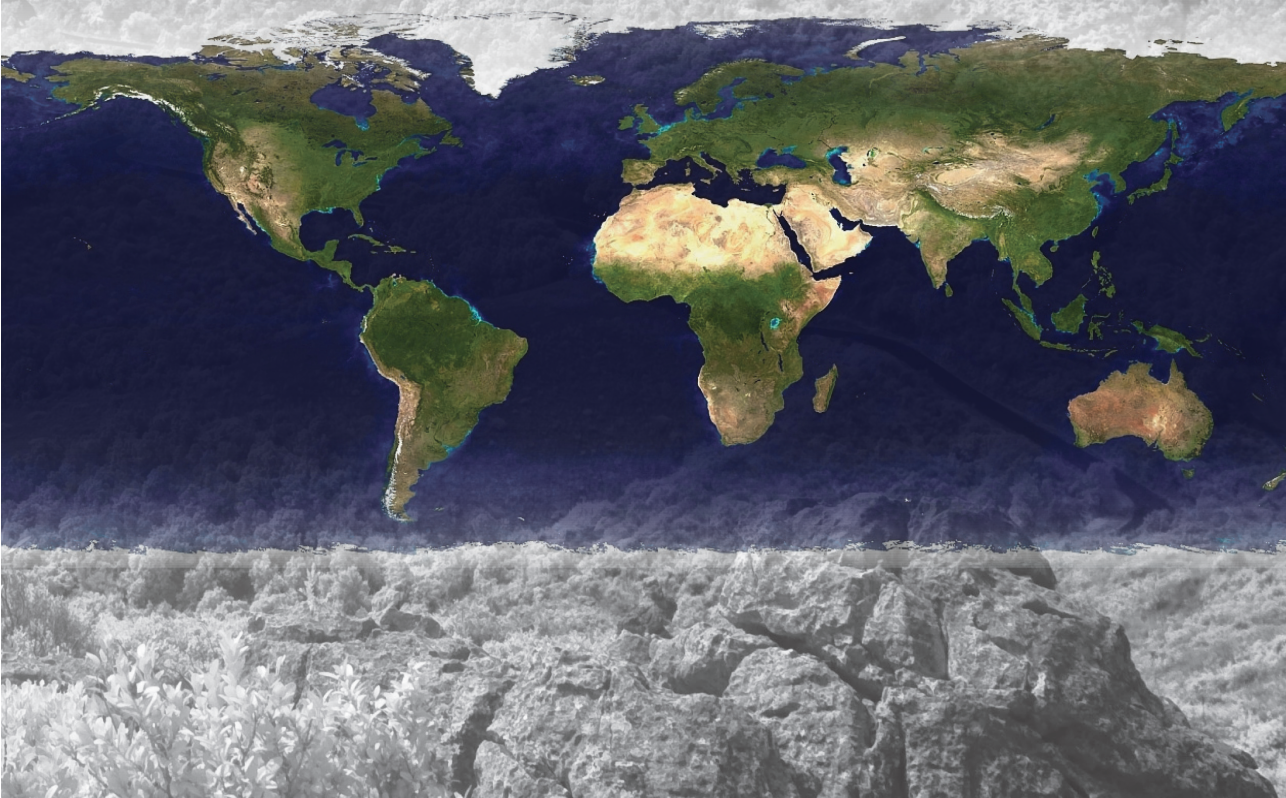

2000 2002 2004 2006 2008

Analysis of vegetation-activity trends in a global land degradation framework

Rogier de Jong

Thesis committee

Thesis supervisor
Prof.dr. M.E. Schaepman
Professor of Remote Sensing, University of Zurich, Switzerland
Professor of Geo-information Science and Remote Sensing,
Wageningen University, The Netherlands

Thesis co-supervisor
Dr.ir. S. de Bruin
Assistant Professor at the Laboratory of Geo-information Science and Remote Sensing,
Wageningen University, The Netherlands

Other members
Prof.dr.ir. G.M.J. Mohren, Wageningen University, The Netherlands
Prof.dr. S.W. Running, University of Montana, United States of America
Prof.dr.ir. P.H. Verburg, VU University Amsterdam, The Netherlands
Prof.dr. S.M. de Jong, Utrecht University, The Netherlands

This research was conducted under the auspices of the C.T. de Wit Graduate School of Production Ecology & Resource Conservation (PE&RC)

Analysis of vegetation-activity trends in a global land degradation framework

Rogier de Jong

Thesis
submitted in fulfilment of the requirements for the degree of doctor
at Wageningen University
by the authority of the Rector Magnificus
Prof.dr. M.J. Kropff,
in the presence of the
Thesis Committee appointed by the Academic Board
to be defended in public
on Monday 11 June 2012
at 4 p.m. in the Aula.

Rogier de Jong
Analysis of vegetation-activity trends in a global land degradation framework
153 pages

Thesis, Wageningen University, Wageningen, NL (2012)
With references, with summaries in Dutch and English

ISBN 978-94-6173-312-2

Table of contents

		Page
Chapter 1	General introduction	1
Chapter 2	Quantitative mapping of global land degradation using Earth observations	15
Chapter 3	Analysis of monotonic greening and browning trends from global NDVI time series	37
Chapter 4	Linear trends in seasonal vegetation time series and the modifiable temporal unit problem	57
Chapter 5	Trend changes in global greening and browning: contribution of short-term trends to longer-term change	69
Chapter 6	Spatial relationship between climatologies and changes in global vegetation activity	91
Chapter 7	Synthesis	111
References		123
Summary / Samenvatting		138
Acknowledgements		142
List of publications		144
Short biography		146
Education certificate		147

Chapter 1

General introduction

1.1 General introduction

On October 31 2011, United Nations (UN) estimated that the 7th billion living person was born in India, only 12 years after the world population reached 6 billion (United Nations Population Fund (UNPF), 2011). This refuelled discussions about the demand on agricultural production and concern about degrading land resources. Discordance between exponential population growth and linear increase in food production was foreseen as early as the 18th century (Malthus, 1798). Later, in 1968, *the population bomb* sketched dark scenarios of overpopulation (Ehrlich, 1968) and, around the same time, the *Club of Rome* argued that the human ecological footprint would soon surpass Earth's carrying capacity (Meadows *et al.*, 1972). After the golden ages of soil science during the *green revolution* in the 1950s and 1960s, when its contribution to agricultural productivity was considered a key factor in banishing global famine (Bradfield, 1960), another facet of soil science emerged by means of *land degradation* which soon appeared on the global agenda as an economic, security and environmental issue (Dent *et al.*, 2007).

Land is shorthand for the system made up of soil, water, the biota and, also, the man-made landscape and their biophysical processes (Dalal-Clayton & Dent, 2001). It can be considered as the Earth's *critical zone* – the thin veneer extending from the top of the tree canopy to the bottom of our aquifers – of which soil lies at the heart (Banwart, 2011). Land degradation and soil degradation are therefore often used interchangeably. In this work, the term land degradation is used, which is interpreted as a deterioration of the system's function in which the soil has a prominent but not an exclusive position.

Land degradation, despite the contentious nature of its exact definition (see section 3.1), is commonly measured by vegetation activity or productivity (Zika & Erb, 2009). Figure 1.1 schematizes the relationship between the two and distinguishes three different phases of land degradation separated by thresholds which are specific for the prevailing environmental conditions (Lal *et al.*, 1989). Given our interest in detecting improvement or deterioration, phase I and III are not of particular interest, since they represent stable states. According to the first global assessment of soil degradation (GLASOD), a substantial part of the terrestrial earth surface can be classified as (very) degraded, but not beyond irreversible (Oldeman *et al.*, 1990; Banwart, 2011) and thus in phase II. Figure 1.2*a* shows the spatial distribution of what are considered (very) degraded soils.

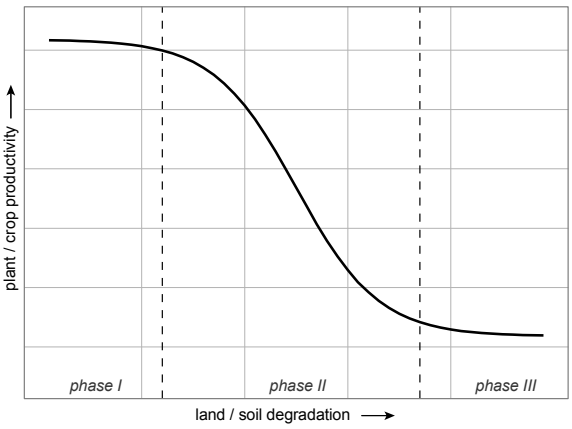

Figure 1.1 The generalized, three-phased soil degradation pattern (in relation to plant/crop productivity). Phase I represents degradation in the none-to-slight category. Soil productivity within this range is influenced by exogenous factors, e.g. climate. Phase II represents a rapid rate of soil degradation, where productivity decline accelerates and eventually decelerates. The limit B is the point-of-no-return, at which the soil is so degraded that it does not deteriorate any further and from which it cannot be restored. Within phase III the soil may be irreversibly degraded or at best, degraded beyond practical utility. The range and magnitude of the limits A and B, therefore, vary among soils and land use. Modified after Lal *et al.* (1989).

Figure 1.2 shows (*a*) a generalized version and (*b*) the full version of the GLASOD map, which is a result of cooperative research efforts of soil scientists and soil degradation experts throughout the world in the late 1980s (Oldeman et al., 1990). The delineation of map units and assessment of degradation type and severity class were qualitative and partly subjective and therefore hardly reproducible (Sonneveld & Dent, 2009). Two decennia later, this map needed a quantitative follow-up (Bai et al., 2008).

The research presented in this thesis was carried out in the broad context of the UN Food and Agricultural Association (FAO) project *global assessment of land degradation and improvement* (GLADA), which aimed at quantifying land degradation at global scale using vegetation productivity as a proxy. The main assumption here is that productivity numbers, which deviate from the long-term norm, may be taken as a measure of land degradation or improvement (Bai & Dent, 2007). The general approach developed for GLADA involves a sequence of analyses to identify land degradation hotspots using remotely sensed data: first with simple vegetation index (VI) indicators which are taken as proxy for productivity; secondly using integration with climate data and, thirdly, using stratification of the landscape and high spatial resolution imagery for local analysis. The main indicator, which plays a central role in all analyses steps, is the temporal increase or decrease in yearly VI aggregates, which is referred to as global *greening* or *browning*. In essence, these trends are to be interpreted as vegetation degradation or improvement, but in combination with other information sources they allow assessment of land degradation.

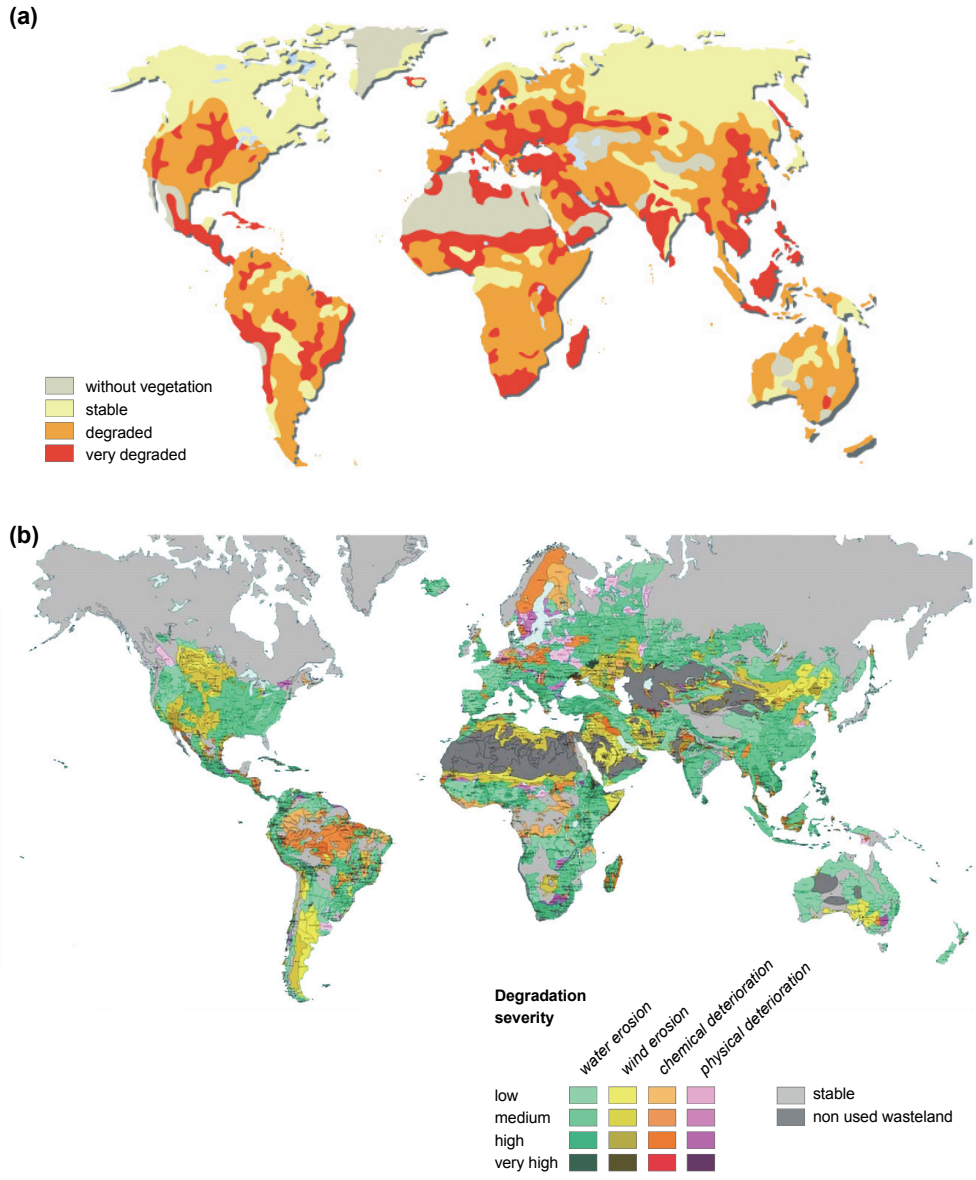

Figure 1.2 Results of the first global assessment of (human-induced) soil degradation (GLASOD). Top (a): generalization of the GLASOD map, showing the severity of soil degradation in three qualitative classes. Modified after: Philippe Rekacewicz, UNEP/GRID-Arendal. Bottom (b): the full GLASOD map, showing types and severity of soil degradation (Oldeman *et al.*, 1990).

1.2 Monitoring terrestrial vegetation activity using remote sensing

1.2.1 Definition of vegetation activity

The fixation of atmospheric carbon dioxide (CO_2) by *photosynthesis* in plants is a key process for the functioning of ecosystems and – more general – for life on Earth. It traps energy from the sun and releases oxygen to the atmosphere (Eq. 1.1). The rate at which this process occurs is termed gross primary production (GPP). Subtracting the plant's day and night respiratory losses yields net primary production (NPP), or the flux at which carbon is stored as biomass or plant dry matter (DM). It is usually measured in $gCm^{-2}year^{-1}$ or in $tCha^{-1}year^{-1}$ and referred to as *plant productivity* or *productivity* in short. NPP measures accumulation of biomass in any part of the plant, including root systems. Integration over the ecosystem and subtraction of additional respiratory losses, e.g. by soil organisms and decay processes, yields net ecosystem exchange (NEE).

$$2n\ CO_2 + 2n\ H_2O + photons \rightarrow 2(CH_2O)_n + 2n\ O_2 \qquad (1.1)$$

carbon dioxide + water + light energy → carbohydrate + oxygen

The magnitude of the yearly global GPP flux is about 15 times the value of CO_2 emissions from combustion of fossil fuels (Wang *et al.*, 2011). Therefore may a small change in vegetation photosynthesis have a large effect on the role of vegetation as a carbon sink and, as a result, on climate change (Luyssaert *et al.*, 2007). Soil resources play a large role here, as they govern annual carbon gain and they define the patterns of variation in NPP across landscapes and biomes (Chapin *et al.*, 2011, pp. 168-169).

Deriving the rate of photosynthesis from spectral data is a troublesome task, especially at large spatial scales and with dense time intervals. The only direct relationship resides in the small fraction (1-2%) of the absorbed photosynthetically active radiation (PAR), which is reradiated at a longer wavelength during the process of photosynthesis. This *chlorophyll fluorescence* can be measured with hyperspectral sensors or with other narrow-band sensors that are specifically designed for this purpose. Efforts to employ this technique at global scale using satellite sensors are still in their infancy (see Section 2.2.2). Today, the most widely used approach to quantify plant productivity is the use of spectral vegetation indices as proxies. Many different indices have been developed and it is beyond the scope of this chapter to review all of these. Some 30 different indices were listed and discussed by Jones & Vaughan (2010, Box 7.1). The one that measures chlorophyll fluorescence most closely is the photochemical reflectance index (PRI), which is based on excitation of chlorophyll pigments in the leaf (Gamon *et al.*, 1997). It needs, however, narrow-band measurements (531nm and 570nm) and application at large spatial and temporal scales is limited by availability of operational sensors.

While vegetation systems are very complex by nature, a vegetation index (VI) is a one-dimensional measure derived from few spectral bands. As mentioned above, VIs do not directly measure biomass, nor productivity or chlorophyll content. There is, however, a strong relationship between VI values, chlorophyll abundance and energy absorption (Myneni *et al.*, 1995), hence they reflect photosynthetic activity (Slayback *et al.*, 2003). Relationships with GPP and NPP have also been demonstrated (Box *et al.*, 1989), but are not straightforward. Following Zhou *et al.* (2001), *vegetation activity* was used in this work to refer to the state and dynamics of terrestrial vegetation systems as inferred by broad-band vegetation indices. Changes in vegetation activity have in literature been referred to as *greening* and *browning* for positive and negative changes respectively (Alcaraz-Segura *et al.*, 2010; Samanta *et al.*, 2010; Wang *et al.*, 2011).

1.2.2 Broad-band vegetation indices

The many existing vegetation indices can be grouped into either broad-band or narrow-band types, based on both their intended purpose and the width of the spectral bands used. Narrow-band indices are usually pigment-specific and, as such, used for spectroscopic applications. Such indices are not applicable for the purposes of this work. Therefore, this section focusses on broad-band indices and, more specifically, on the most common *normalized difference vegetation index* (NDVI).

Red radiance exhibits a nonlinear inverse relationship between integrated spectral radiance and green biomass, while the near-infrared component exhibits a nonlinear direct relationship (Tucker, 1979). The former is related to pigment (e.g. chlorophyll) absorption, while the latter is related to the cell structure of the leaf. This is a biological adaptation against overheating of the plant, which would happen if infrared radiation were absorbed. In a typical spectral signature of green vegetation, these unique properties cause a sharp increase in reflectance (ρ) between the red (~650nm) and infrared (~750nm) bands, known as the *red edge* (Figure 1.3). Bare soil, on the other hand, typically shows a positive linear relationship between red and near-infrared (NIR) reflectance, known as the *soil line* (Huete, 1988; Baret *et al.*, 1993). Practically all broad-band vegetation indices are based on this differential response of vegetation and soil in red and NIR.

Simple vegetation indices based on the red edge were developed in the 1970s and described in several publications. The paper of Tucker (1979) is often adopted as the first to describe the rationale and the wide range of applications for remote sensing of vegetation systems. The first reported use of the NDVI, however, was by Rouse *et al.* (1973), although they christened it the Vegetation Index. The majority of studies at that time used Landsat data and focussed on monitoring of crop systems. Large-scale applications, related to land-cover dynamics or climate change, were developed in

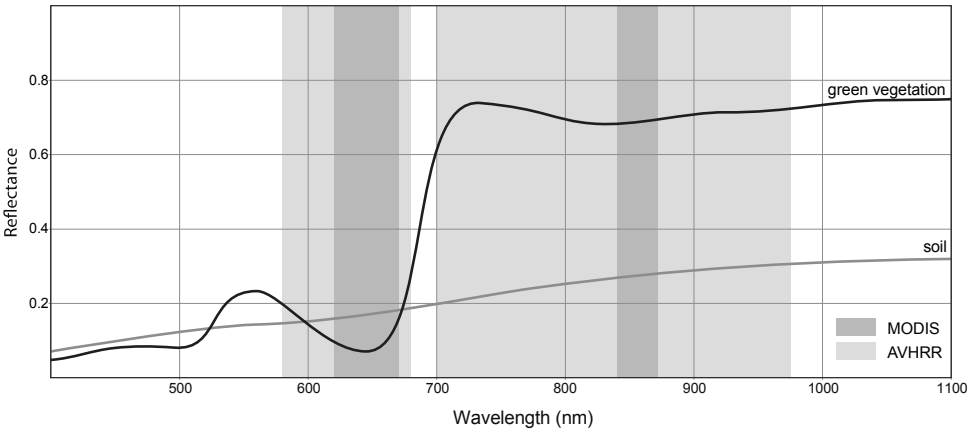

Figure 1.3 Characteristic reflectance spectra for green vegetation (black line) and soil (grey line) as well as the red and near-infrared acceptance bands of the advanced very-high resolution radiometer (AVHRR) in light grey and the moderate-resolution imaging spectrometer (MODIS) in dark grey. The sharp increase in reflectance of green vegetation between ~650nm and ~750nm is know as the *red edge*.

the 1980s when satellites started to produce high-resolution time series with global coverage (see Sections 1.2.3 and 2.2).

The NDVI is obtained by dividing the difference vegetation index (NIR reflectance minus red reflectance) by the sum of both reflectance values (Eq. 1.2). By design, NDVI is dimensionless and varies between -1 and 1 or, in case of green vegetation where NIR reflectance exceeds the red counterpart, between 0 and 1. It is beyond the scope of this chapter to review the physical basis of this type of vegetation indices, but a few relationships (given below) with properties of vegetation (canopies) may elucidate the physical meaning of greening and browning trends.

$$NDVI = \frac{\rho_{NIR} - \rho_{RED}}{\rho_{NIR} + \rho_{RED}} \tag{1.2}$$

The ultimate goal that is pursued with vegetation indices should be the quantification of state and flux of biophysical properties amenable to economic and/or environmental analysis. This includes energy fluxes, water content and fixation of dry matter. A sound understanding of these properties provides insight in processes driving plant productivity, vegetation-atmosphere and vegetation-hydrology interactions and associated feedback mechanisms. Any VI, however, yields a one-dimensional spectral measure, which can, by nature, not directly relate to all of these components. Nevertheless, assuming (linear) mixture of only soil and vegetation components within each pixel, the VI values can be used to estimate the

fractional cover of photosynthetically active vegetation (PV) for an area of interest (Eq. 1.3) (Choudhury *et al.*, 1994).

$$f_{PV} \cong \frac{VI - VI_{\min}}{VI_{\max} - VI_{\min}} \tag{1.3}$$

The PV fraction (f_{PV}) directly relates to the fraction of PAR (fPAR) absorped by the vegetation – i.e. fraction of absorbed PAR (APAR) over incident PAR. Therefore, fPAR can be estimated from the VI given a vegetation-specific conversion coefficient α_{veg} (Eq. 1.4). This was demonstrated by theoretical work of Sellers *et al.* (1992, 1997) and has been extensively documented (Gallo *et al.*, 1985; Asrar, 1989; Friedl *et al.*, 1995). It provides the theoretical connection between NDVI and NPP through the concept of light use efficiency (LUE) on which the equation of Monteith (1981) is based (Eq. 1.5). In this equation, the conversion efficiency (ε) translates fPAR (in energy units) to plant tissue growth, or NPP. The integral denotes yearly aggregation. This principle has been used in a multitude of ecological studies (Tucker *et al.*, 1981; Tucker *et al.*, 1985; Box *et al.*, 1989; Paruelo *et al.*, 1997) and implemented for large-scale monitoring systems (Myneni *et al.*, 2002).

$$fPAR = \frac{APAR}{PAR} \cong f_{PV} \cdot \alpha_{veg} \tag{1.4}$$

$$NPP = \varepsilon \times \int fPAR \times PAR \tag{1.5}$$

In conclusion, it remains unclear what the NDVI itself measures, but it is directly related to the fractional vegetation cover and, through some modeling steps, to productivity measures. Theoretical work provides strong support for the interpretation of the NDVI as a measure of carbon flux through ecosystems (Paruelo *et al.*, 1997). It has also been defined as indicator of relative growth and/or vigor of green vegetation (Wickland, 1989). In any case, the NDVI does not directly reflect a biophysical process, but it is diagnostic of various biophysical vegetation and canopy attributes and has been used (some say overused or even abused) as a proxy for biomass, leaf area index (LAI), evapotranspiration and albedo. Given these relationships, applications included the quantification of drought stress, ecosystem functioning, vegetation patterns, food security, wildfire prediction and climate change. A review of all studies would be a tedious exercise, but a concise overview of the relationships between VI measurements and a range of vegetation and canopy attributes was provided by Glenn *et al.* (2008).

1.2.3 Low-resolution satellite sensors

A paper of Cracknell (2001) was endowed with the title 'The exciting and totally unanticipated success of the AVHRR in applications for which it was never intended'. One of the key successes he had in mind was the application of the NDVI for terrestrial monitoring purposes. The sensor, or more accurately the series of sensors, is called the advanced very-high resolution radiometer (AVHRR) and is carried on-board polar-orbiting satellites of the U.S. National Oceanic and Atmospheric Administration (NOAA). The intended meteorological purpose can be deduced from its name, since the spatial resolution (~1km), also by standard of that time, is low rather than 'very high' for terrestrial purposes. By way of comparison, the Landsat multi-spectral sensor (MSS) was already well established and provided a spatial resolution of ~60m. On the other hand, the temporal resolution and spatial extent (daily global coverage) make AVHRR a perfect sensor for large-scale monitoring. Today, it provides an invaluable historical record.

In 1979, the AVHRR sensor system was modified to improve discrimination between land and oceans, as well as clouds and snow. A single broad-wavelength sensor was replaced with two sensors, which separately measure visible and NIR spectral reflectance. Fortuitously, this sensor modification made the AVHRR measurements suitable to study land vegetation dynamics (Goward *et al.*, 1993). Several vegetation datasets were prepared using this data (Table 2.1). Out of these, the global inventory for mapping and modeling studies (GIMMS) dataset is probably the most broadly used for ecological monitoring purposes (Pettorelli *et al.*, 2005). This dataset is still regularly being updated with new measurements and more enhanced calibration and correction methods and was found the most accurate in terms of temporal change (Beck *et al.*, 2011). For these reasons, we selected it for use in this work. For each study, i.e. each of the core chapters in this thesis, we used the most recent version of the dataset. For the GLADA work that implied the time span of 1981–2003 (Bai *et al.*, 2008); later this was extended until 2006 and 2008. Soon, the update until 2010 will become available (Molly Brown, pers. com.). Extensive VI studies based on AVHRR data helped improvement of instrument characterization and calibration of modern sensors (Huete *et al.*, 1994). These sensors, including the moderate-resolution imaging spectrometer (MODIS) on-board NASA Terra and Aqua satellites, provide finer spatial resolution (Table 2.1, p. 23) and narrower spectral acceptance bands (Fig. 1.3). The latter yields a cleaner NDVI measurement, since spectral water-absorption features are not any longer included (Salomonson *et al.*, 1989). Although records from these sensors are increasingly being used for analysis of temporal trends, datasets are not available for the 1980s and 1990s.

Technical details about the AVHRR sensor were provided by Cracknell (1997) and about the GIMMS processing scheme by Tucker *et al.* (2005). Baldi *et al.* (2008) and Beck *et al.* (2011) compared GIMMS with other long-term NDVI datasets. Here, we limit ourselves to a concise description.

The dataset is based on daily global area coverage (GAC) data which was collected by a suite of NOAA satellites (Table 5.3) at ~4km spatial resolution. The source data were aggregated into fortnightly scenes with 0.072deg (~8km) spatial resolution. The maximum-value compositing (MVC) technique was used for temporal aggregation, while minimizing bias caused by atmospheric conditions (Holben, 1986). This is not an atmospheric-correction method and some inaccuracy

Table 1.2 Description of the GIMMS dataset. After Baldi *et al.* (2008) and Beck *et al.* (2011).

		GIMMS[a], version g
Data origin (and its spatial resolution)		NOAA-AVHRR GAC 1B (4km)
Platforms		7, 9, 11, 9d, 14, 16, 17 (operational dates in Table 5.3)
Temporal	*extent*	1981–2008
	resolution	Fortnightly (24 scenes/year)
	compositing	Maximum value composites (MVC)
Spatial	*extent*	Global, 62.85°S – 89.22°N
	resolution	0.072deg (~8km)
	compositing	Forward, nearest neighbour mapping. Selection of the 4km pixel with the maximum NDVI value for the 8 km output pixel.
Corrections	*radiometric*	Ocean and clouds calibration NOAA[b]-7 to -14: Vermote & Kaufman (1995) coefficients; NOAA[b]-16 and -17: prelaunch coefficients. Additional calibration using invariant desert targets (Los, 1998)
	viewing and illumination / BRDF[c]	Adaptive empirical mode decomposition (EMD) method (Pinzon *et al.*, 2005)
	cloud	0 °C thermal mask (Channel 5)
	aerosol	Volcanic aerosol correction for El Chicon (04/1982–12/1984) and Mt Pinatubo (06/1991–12/1993)
	noise attanuation and gap filling	Kriging interpolation
	water-vapour / molecular absorption and scattering	None
Scaling procedures		Non-linear rescaling against SPOT-VGT[d] (Tucker *et al.*, 2005)

[a] Global Inventory for Mapping and Modeling Studies (GIMMS)

[b] National Oceanic and Atmospheric Administration (NOAA)

[c] Bidirectional Reflectance Distribution Function (BRDF)

[d] Satellite Pour l'Observation de la Terre (SPOT) Vegetation (VGT)

remains, especially in hazy and cloudy conditions (Nagol *et al.*, 2009). We applied a harmonic smoothing algorithm to further reduce these inaccuracies in areas with persistent cloud cover (see Section 3.2). Orbital decay and platform changes are known to affect AVHRR observations (de Beurs & Henebry, 2005b) but processed NDVI data have been found to be free of trends introduced from these effects (Kaufmann *et al.*, 2000). This is confirmed by a study in the Sahel to the effects of shifts in solar zenith angle on NDVI (Eklundh & Olsson, 2003). The characteristics of the GIMMS dataset are listed in Table 2.1 and further discussed in several papers (Zhou *et al.*, 2001; Brown *et al.*, 2006; Alcaraz-Segura *et al.*, 2010).

1.3 Research questions

Leaving aside deforestation and other land cover changes that accompany a growing human population, the last decades were prosperous for plants on planet Earth. In many parts of the world, the mean temperature raised and precipitation increased (IPCC, 2007), which are, in general, beneficial circumstances for plant growth. This contributed to intensification of agriculture with higher yields, but left important questions like: How will global soils cope with these climatic changes? (How long) can this trend last? Is it a global trend, or a collection of local trends? In that case, which parts of the world suffer from degradation and how hard are they hit? To get closer to answers we need more advanced analysis methods for available satellite imagery and we need to make steps towards disentangling climate effects from human-induced effects. The ultimate goal, towards which first steps were made (Symeonakis & Drake, 2010), should be the development of a universal land degradation model which is able to predict changes in land resources and their environmental and societal impacts.

The work presented in this thesis is based on the GLADA approach for quantification of vegetation changes. The main objective is: “to advance the understanding of dynamics and trends in global vegetation activity, in relation to climate variability, for use in land resource applications, including land degradation assessments, using quantitative Earth observation approaches”. We followed a step-wise approach, in which each step focuses on one of the following research questions.

1: What is the current state-of-art in large-scale quantitative land degradation assessment and what are knowledge gaps, key ecological indicators and successful methods that have not yet been exploited to their full potential?

We address this question by reviewing the currently available datasets and findings of recent research. Several disciplines are involved but our focus is on satellite remote sensing data and methods for monitoring land surface dynamics at global scale.

2: Can we use the full temporal dimension offered by satellite records for detection of vegetation-activity trends, and what is then the influence of land surface phenology?

Previous studies used yearly aggregates of satellite measurements. This is an effective way to remediate serial autocorrelation, but it also eliminates intra-annual information. The latter might provide clues towards processes driving the detected change.

3: Can we detect trend reversals within the time series and what is the implication of these reversals for detection of global vegetation-activity trends?

Changes in vegetation activity over time may consist of an alternating sequence of greening and/or browning periods. As a next step in the trend analysis, trend reversals may be considered for a closer relation to the system dynamics. We found that there is a critical need for a consistent global assessment of trend changes.

4: What are the spatial relationships between potential climatic growth constraints and trends in vegetation activity?

Previous steps aimed at enhancing change detection techniques, but trends were detected irrespective of their driving processes. Quantification of spatial relationships between trends in vegetation activity and climate variables might provide a step towards establishing links between climate change, human-induced land changes and plant growth.

1.4 Outline

The core of this thesis is a series of five peer-reviewed papers. Four papers address the before-mentioned research questions and one short technical paper (Chapter 4) addresses a statistical issue which is inherent to trend analysis. The problem and framework of quantifying land degradation using remote sensing are described in Chapter 2, while the subsequent chapters present advancements for VI trend analysis and interpretation of the detected trends.

The key principles about remote sensing of terrestrial vegetation activity and the main datasets – as they were used in this work – are described in this introductory chapter. This is not an exhaustive text on remote-sensing theories nor on ecological principles, for which purpose other textbooks can be consulted. These data and principles have been applied in a framework of land degradation. Chapter 2 provides a review of previous studies in this field and shows that degradation of land resources has many dimensions, not least of all one that involves issues of definition and perception. Leaving this aside, challenges and knowledge gaps in the quantitative aspects are described and used as starting point for the technical work.

Building further on the GLADA approach, Chapter 3 demonstrates how the full temporal resolution, i.e. without temporal aggregation, can be used to detect monotonic trends in vegetation activity with higher accuracy than on a yearly aggregated basis. The intra-annual information, which is retained in this approach, provides information about changes in land surface phenology and can be used for non-parametric analysis. In addition to the trend in yearly aggregates, the trend in intra-annual growing intensity can be used to relate vegetation changes to possible drivers.

Chapter 4 contains a short technical communication on the previously mentioned temporal aggregation. This approach for dealing with serial autocorrelation is valid for many regions where growing seasons are relatively stable, but it might affect trend detection in other cases. We demonstrate this *modifiable temporal unit problem* (MTUP) for linear trend models based on real VI time series and on synthetic data.

Both gradual and abrupt changes in vegetation activity occurred in many regions in the world, as demonstrated in Chapter 5. It provides an approach to include these changes in the afore-mentioned trend analysis. This improves our insight in the system dynamics in temporal sense.

Better change-detection methods provide tools for identifying trends in vegetation activity, but detection of trends is irrespective of the underlying driving processes. These processes find their basis in climatic or human actors and can, in part, be distinguished by the spatial scale at which they express themselves. Chapter 6 provides a step towards relating observed climate changes to trends in vegetation activity using a spatial-statistical approach. This chapter demonstrates that many trends in vegetation activity can be associated with climatic changes and provides a basis for statistical modeling of climate and human-induced land degradation in future research.

Finally, Chapter 7 concludes this thesis by integrating the main results from the core chapters and suggesting directions for future research efforts.

Chapter 2

Quantitative mapping of global land degradation using Earth observations

Rogier de Jong, Sytze de Bruin, Michael E. Schaepman, David L. Dent

"A plenty of rich land, to be had for little or nothing, is so powerful a cause of population as to overcome all other obstacles."

Thomas Malthus (1798)
An Essay on the Principle of Population, as it Affects the Future Improvement of Society

This chapter is based on:
International Journal of Remote Sensing, 32 (2011), pp. 6823-6853
DOI: 10.1080/01431161.2010.512946

Abstract

Land degradation is a global issue on a par with climate change and loss of biodiversity, but its extent and severity are only roughly known and there is little detail on the immediate processes – let alone the drivers. Earth-observation methods enable monitoring of land degradation in a consistent, physical way and on global scale by making use of vegetation productivity and/or loss as proxies. Most recent studies indicate a general greening trend but improved datasets and analysis also show a combination of greening and browning trends. Statistically based, linear trends average out these effects. Improved understanding may be expected from data-driven and process-modeling approaches: new models, model-integration, enhanced statistical analysis and modern sensor imagery at medium spatial resolution should substantially improve the assessment of global land degradation.

2.1 Introduction

Recent discussions on competition for land resources suggest that claims on fertile land and even on degraded land, have never been higher (Tilman *et al.*, 2009; Rathmann *et al.*, 2010). In the context of ever-growing human population, the global area under food crops has peaked at the end of the last century and there is a growing demand for land for production of biofuels. This puts land degradation on the global agenda as an economic, security and environmental issue (Dent *et al.*, 2007) with a strong focus on land use change science (Turner *et al.*, 2007). The IPCC argues that climate change will drive certain types of land degradation by more extreme weather events and a likely increase in total area affected by drought (Trenberth *et al.*, 2007). At the same time, land degradation interacts with atmospheric processes (Cracknell & Varotsos, 2007) and may drive climatic change through increasing greenhouse gas emissions and reducing carbon fixation in soils and biomass (Schlesinger *et al.*, 1990). Mitigation and adaptation require the ability to predict and monitor land degradation; UNEP's GEO4 report urges governments to respond with 'effective early warning, assessment and monitoring – combine remote sensing with field surveys of key indicators; measure indicators consistently at different scales over the long-term.'

This poses scientific and technical challenges (Zucca *et al.*, 2012). The distribution and intensity of land degradation are only roughly known; assessments have been local, or based on expert opinion and qualitative classifications (Oldeman *et al.*, 1990; Dregne, 2002). Satellite remote sensing provides the only viable option for quantitative estimations of degradation at global scale. Time-series imagery with dense acquisition intervals and global coverage is available since the early 1980s and can be used for change detection. Quantitative and physically-based models can be used to relate detected changes to physical processes. In reviewing the currently available datasets and findings of recent, broad-scale research on land degradation, we aimed at identification of knowledge gaps, key ecological indicators and successful methods that have not yet been exploited to their full potential. Several disciplines are involved but our focus is on satellite remote sensing data and methods for monitoring land surface dynamics at global scale.

2.1.1 Definitions

Land is shorthand for the system made up of soil, water, the biota and, also, the man-made landscape and their biophysical processes (Dalal-Clayton & Dent, 2001). Loss of 'its usefulness for human beings' (Wasson, 1987) or 'its services, notably the primary production service' (Adeel *et al.*, 2005) is considered as *degradation*. Still, different schools, according to their interests, use diverse definitions of land degradation. FAO (1979) defined land degradation as 'a process which lowers the

current and/or potential capacity of soils to produce'; the Millennium Ecosystem Assessment (MEA, 2005) defined it as 'the reduction in the capacity of the land to perform ecosystem goods, functions and services that support society and development'. The term *soil degradation* is often used interchangeably (Lal *et al.*, 1989) and *desertification* has been adopted as a synonym of land degradation in dry lands (UNCCD, 1994; Reynolds *et al.*, 2007), but common usage may also imply desert encroachment into adjacent regions (Lamprey, 1988).

Both economic loss and ecological degradation may be considered and measured against the capacity to satisfy human needs (Kassas, 1995) and this is a common viewpoint of agriculture-oriented research (FAO, 1979; Dent & Young, 1981). Standing apart from human interest, land degradation has also been defined as deterioration in the physical and chemical properties of the soil as result of environmental change (Imeson & Emmer, 1992) and, embracing both viewpoints, as 'a long-term reduction in ecosystem function and productivity from which the system cannot recover unaided' (UNEP, 2007).

Despite the lack of a common definition, there is consensus that land degradation is widespread, has severe financial and social consequences and may sometimes be irrecoverable on a human time scale at manageable cost (Okin *et al.*, 2001). Also, it can be self-accelerating so the cost of rehabilitation rises exponentially as it advances (Glantz & Orlovsky, 1983) and, in some forms, it has a reciprocal relationship with climatic systems (Schlesinger *et al.*, 1990; Prospero & Lamb, 2003), causing significant changes in global biogeochemical cycles.

2.1.2 Processes and drivers

The most common perspective on land degradation is what farmers see happening to their land – symptoms such as soil erosion and salinity. That something bad is happening might be obvious but links with the driving processes may not be. Driving processes may be categorized as biological, physical or chemical (Lal *et al.*, 1989) – though rarely political (Blaikie, 1985) – and each may have natural or man-induced causes, also called factors, that are agents or catalysts of the mentioned processes (Lal *et al.*, 1989). Figure 2.1 shows examples of these categories.

Whether land degradation is mainly human-induced, natural, or both, is often a moot point (Evans & Geerken, 2004). Early researchers focused on human-induced land (or soil) degradation (Aubreville, 1949; Dregne, 1986). Emphasising the impact of man on geology and ecology, Vitousek *et al.* (1997) state that we live on a human-dominated planet and Crutzen (2002) proposed the name *Anthropocene* for the current geological epoch. More recently, fluctuating climatic conditions have been considered a significant cause (UNCCD, 1994; Puigdefábregas, 1998; Nicholson, 2000; El Hassan, 2004; IPCC, 2007); a change of view brought about by the Sahelian droughts of the 1970s and 80s (Glantz & Orlovsky, 1983) and drying of the Aral Sea (Micklin, 1988; Small *et al.*, 2001) and Lake Chad (Haas *et al.*, 2009), among others.

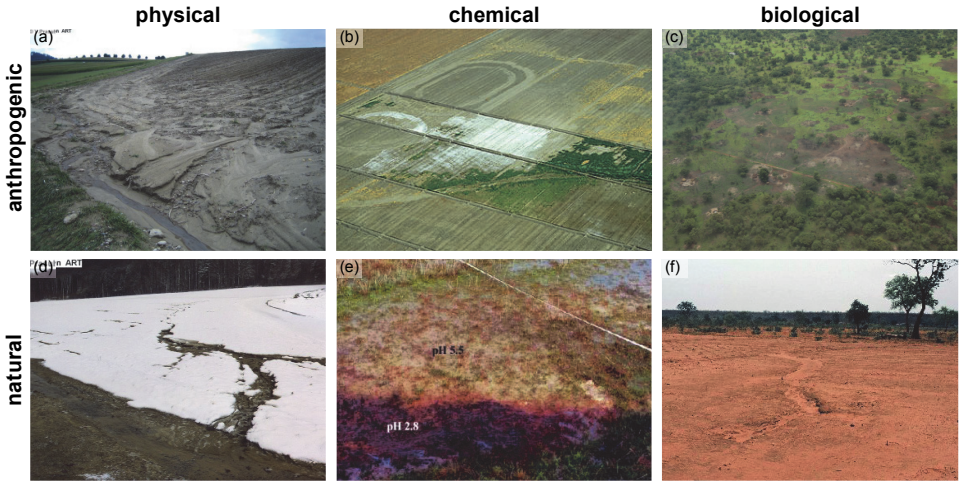

Figure 2.1 Examples of land degradation. Top: (a) Human-induced soil erosion on agricultural fields (Volker Prasuhn, website); (b) Secondary (human-induced) salinity in farmland, California (USDA Agricultural Research Service); (c) Loss of forest cover through shifting agricuture, Wau district, Sudan (UNEP website). Bottom: (d) Soil erosion induced by snowmelt (Volker Prasuhn); (e) Acid sulphate scald caused by drainage change (Gardner *et al.*, 2004) which may be natural or man-made; (f) Drought -induced vegetation decline and soil erosion (WMO).

Climatic variations are believed to be a greater factor in, for instance, biodiversity in arctic and boreal areas, whereas land-use change is considered a greater factor in other biomes (Chapin *et al.*, 2000). Most authors agree that various human and environmental processes interact along complex pathways and that both biophysical and socio-economic indicators should be considered jointly (Lambin *et al.*, 2001; Baartman *et al.*, 2007). Despite this, biophysical variables other than climatic change have received relatively little attention as causal factors of land degradation (Turner *et al.*, 2007).

The interaction of the human and the biophysical sub-systems on the land system and the schematic positioning of land degradation within the latter is depicted in Figure 2.2. The biophysical sub-system interacts with the human sub-system by delivering environmental goods and services (Turner *et al.*, 2007) that might be diminished by land degradation as defined by UNEP (2007). Land degradation, in this sense, is an issue beyond the field scale and has become part of the emerging land change sciences (LCS). Research is undertaken by various disciplines including remote sensing, resource economics, landscape ecology and biogeography. It is a challenge to capture the whole system with its interrelationships between acting processes and to scale-up understandings gleaned from field studies to regional, biome and global perspectives.

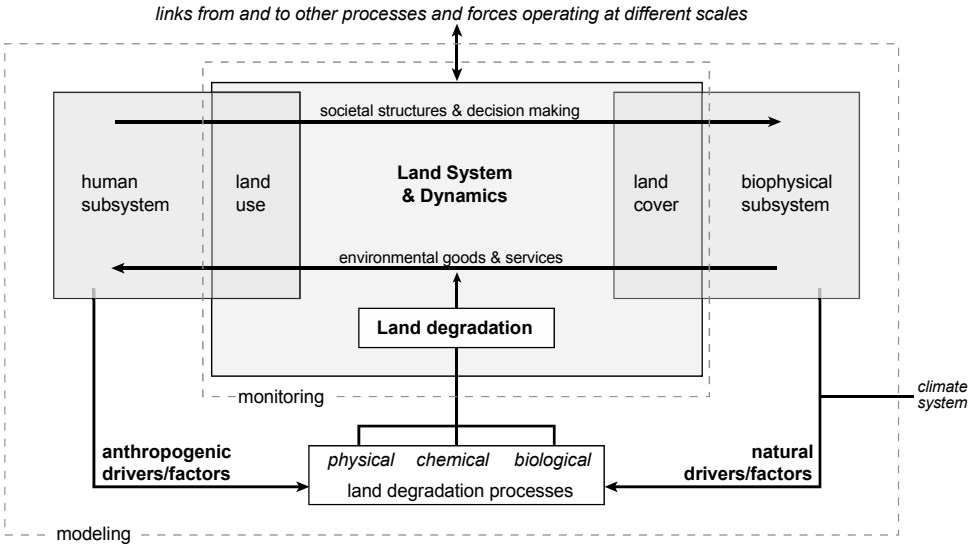

Figure 2.2 The positioning of land degradation within the land change science framework. Modified after Turner *et al.* (2007).

2.1.3 Classification methods

Land degradation may be assessed qualitatively or quantitatively. The first approach, using expert opinion, may be able to embrace several processes in a single assessment that usually considers the consequences or symptoms of degradation – such as decline of land quality, biomass or vegetation health. The quantitative approach uses proxy measures like spectral reflectance. Remote-sensing methods are most frequently employed and depend on establishing relationships between the proxy and the 'real thing'. Most land-degradation processes affect the vegetation cover, for which reason vegetation dynamics, which is relatively easy to quantify using remote sensing, has been widely adopted as an indicator of land degradation at regional to global scales; this approach has the strength of being repeatable and transferable between scales and regions.

In early years, qualitative research included systematic and detailed soil survey. Two approaches emerged (Bergkamp, 1996; Boer, 1999): one focusing on the sensitivity of *land mapping units* to external changes which imposes limitations to the farmers' freedom of action; the other focusing on the actual change induced by external factors. The first is represented by the well-known Land Capability Classification (Hockensmith & Steele, 1949; Klingebiel & Montgomery, 1961) which defines land capability classes, each having a defined degree of limitation or conservation problems. This is a rules-based approach, depending on expert

judgment. Similarly, the FAO Land Quality Classification relates risk of degradation to crop yields and management factors like germination conditions (FAO, 1976). The second approach is represented by the global assessment of human-induced soil degradation (GLASOD; Oldeman & van Lynden, 1997), an expert assessment of land degradation by classes applied to a common base of landform units depending on the degree (light − severe) and the frequency (percentage occurrence within the mapping unit) of degradation by soil erosion, nutrient depletion, salinity and/or chemical contamination. Experts are comfortable with both of these approaches; they deliver a familiar perspective of land degradation but they are time-bound and not reproducible.

Air-photo interpretation was employed extensively from the 1960s and, later, satellite imagery. In the beginning these were used in a qualitative way. Later, more quantitative methods emerged which often employ several indicators in combination with modeling (Kirkby *et al.*, 2004) or statistical methods to define the contribution of various processes (Feoli *et al.*, 2002; Riedler & Jandl, 2002; Stroppiana *et al.*, 2009). For instance, Vargas *et al.* (2007) used a fuzzy clustering algorithm to calculate classes combining loss of vegetation, soil chemical degradation and soil physical degradation and employed a decision tree to derive a land degradation map.

Various criteria for monitoring ecological status have been proposed respecting scalability, reproducibility, consistency, cost-effectiveness, transferability and statistical rigor (Boer, 1999); remote sensing meets many of these criteria.

2.2 Earth-observation datasets and methods

2.2.1 Time series of global vegetation status

Land degradation is often linked to a decline in biomass or vegetation cover, which may be measured in terms of biomass productivity, or undesirable changes in composition (Bertiller *et al.*, 2002; Hanafi & Jauffret, 2007; Wessels *et al.*, 2007; Salvati & Zitti, 2009; Zika & Erb, 2009). Green vegetation has a characteristically high reflectance in the near-infrared (NIR) and a low reflectance in the red part of the electromagnetic spectrum. Many broadband vegetation indices (VI) using this characteristic have been developed (see Section 1.2.2).

The most common VI is the normalized difference vegetation index (NDVI), which is a normalized ratio between NIR and red reflectance (Tucker, 1979). It is sensitive to the amount of photosynthetically active vegetation and, therefore, is useful for monitoring biomass (Tucker *et al.*, 1985; Prince & Tucker, 1986). Correlation with biomass is highest in the mid-range of NDVI values (Asner *et al.*, 2004; Phillips *et al.*, 2008). In areas of dense vegetation, the NDVI signal saturates and other indices, like EVI (Enhanced Vegetation Index) and SAVI (Soil-adjusted Vegetation Index) or narrow-band measures perform better (Huete *et al.*, 2002a;

Asner *et al.*, 2004). NDVI has been used for many other applications, including as a proxy for vegetation water content and drought stress. Its spectral resolution, however, does not allow to separate water absorption features and its reliability decreases with mixed vegetation types (Ceccato, 2001).

Frequently-acquired imagery from the advanced very high resolution radiometer (AVHRR) has yielded unprecedented insights into our changing planet, by analyses of land cover dynamics, biomass and primary production (Tatem *et al.*, 2008). The availability of a long time-series of global NDVI data, in combination with detailed studies of its relationship with many biophysical parameters, prompted the use of NDVI trends as a proxy for land degradation. It has already been used extensively to study vegetation change and its interactions with climate (Townshend, 1994; Loveland *et al.*, 2000), global primary production (Prince & Goward, 1995), land cover (DeFries *et al.*, 1995) and yield prediction and crop modeling (Chen *et al.*, 2008; Stöckli *et al.*, 2008; Boschetti *et al.*, 2009). The 8km spatial resolution – a characteristic of many AVHRR datasets – is considered to be suitable for global vegetation monitoring (Justice *et al.*, 1985; Moulin *et al.*, 1997; Pinzon *et al.*, 2004; Tucker *et al.*, 2005) and constrains the spatial variability between different NDVI products (Tarnavsky *et al.*, 2008). The problem for land degradation studies is to discount false alarms raised by factors that are not commonly understood as land degradation, notably fluctuations in rainfall, rising temperatures, atmospheric CO_2 and nitrate precipitation and land-use change – which may not be accompanied by land degradation as commonly understood (Bai *et al.*, 2008).

Global VI time series are available from several sensors; Table 2.1 lists the most commonly used examples. The longest run consists of AVHRR NDVI maximum-value composites (Holben, 1986). The global inventory modeling and mapping studies (GIMMS) dataset has been compiled from daily AHVRR 4km global area coverage (GAC) data, geometrically and radiometrically corrected to produce fortnightly 8-km resolution NDVI data from 1981 through 2006 (Tucker *et al.*, 2005). These NDVI values are comparable to NDVI products from other sensors such as MODIS, SPOT Vegetation, SeaWiFs and Landsat ETM+ (Brown *et al.*, 2006). Other AVHRR NDVI datasets include Fourier-adjusted, sensor and solar zenith angle corrected interpolated and reconstructed monthly time-series (FASIR; Los *et al.*, 2000), Pathfinder AVHRR land (PAL; James & Kalluri, 1994) and global vegetation index (GVI; Goward *et al.*, 1993). Although the various datasets started with nearly identical composited AVHRR measurements, different processing has produced absolute NDVI values that can differ substantially, especially in the tropics and northern high latitudes (Hall *et al.*, 2006). Also, compared with new-generation time-series data like the moderate resolution imaging spectrometer (MODIS), there are limitations including orbital drift, atmospheric interference, wide spectral bands and discontinuities due to platform changes (de Beurs & Henebry, 2004; Fensholt *et al.*, 2009; Nagol *et al.*, 2009).

Shorter time series of about 10 years are available from MODIS, SPOT and SeaWiFs. MODIS imagery is acquired every three days, providing aggregated products every 3-16 days. MOD13 is an NDVI dataset with a spatial resolution of 250-1000m and appears to be more accurate than NOAA AVHRR, especially in areas with high atmospheric water vapour content (Huete *et al.*, 2002a). MODIS also provides a continuous NPP dataset (Running *et al.*, 2004) derived from the fraction of absorbed photosynthetically active radiation (fPAR), which is a more direct physical measurement than NDVI (Phillips *et al.*, 2008). The spectral bands used are narrower than for the AVHRR NDVI product (Figure 1.3) so there is less interference with (water) absorption features; importantly, the derived NPP is less sensitive to saturation over dense vegetation. On the other hand, fPAR is generally overestimated in semi-arid areas (Fensholt *et al.*, 2004; Turner *et al.*, 2006). The French *satellite pour l'observation de la terre* provides global vegetation datasets (SPOT VGT) of 1km spatial resolution. Replacement of SPOT VGT1 by VGT2 in 2003 involved a change in the spectral response functions of channels 1 and 2 (Figure 2.3*b*) but, after correction, the NDVI products of AVHRR and SPOT are comparable, except for regions with high biomass (Swinnen & Veroustraete, 2008). In semi-arid areas, Fensholt *et al.* (2009) show that GIMMS and MODIS NDVI agree better than SPOT VGT, as a result of the SPOT discontinuity (Figure 2.3*a*). The OrbView-2/SeaWiFs (Sea-viewing Wide Field-of-view Sensor) was originally designed to monitor the colour of the oceans, but thanks to convenient spectral bands

Table 2.1 Most commonly used time series of vegetation imagery for broad-scale land degradation studies, limited to datasets with a high temporal resolution and global coverage.

Dataset / Product	Indicator	Sensor	Platform	Time range	Spatial resolution	Temporal resolution
Pathfinder Land (PAL)	NDVI	AVHRR	NOAA satellites	1981-2006	8km (GVI 16km)	10-day MVC
Global Vegetation Index (GVI)						Weekly MVC
GIMMS						15-day MVC
FASIR						15-day MVC
MOD13 / MYD13	NDVI / EVI	MODIS	Terra / Aqua	2000-present	250m – 1km	8 or 16-day MVC
MOD17A2 / MYD17A2	GPP				1km	8-day composite
VGT-S10	NDVI	VGT	SPOT-4	1998-present	1km	10-day synthesis
L3-SMI NDVI	NDVI	SeaWiFS	OrbView-2	1997-present	4.63km	Weekly MVC

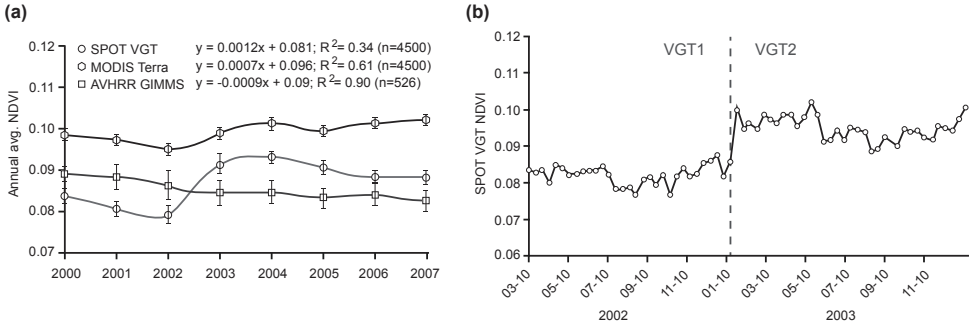

Figure 2.3 Comparison of GIMMS, MODIS NDVI and SPOT VGT for a test site in Senegal. Reproduced from Fensholt *et al.* (2009).

and a detector and amplifier that does not saturate over land, it also allows monitoring of the land surface (Gobron *et al.*, 2003). Differences between SeaWiFs and AVHRR NDVI data can be neglected for land degradation studies, especially in drylands (Laneve & Castronuovo, 2005).

Many other remotely sensed datasets have been used for regional land degradation studies. It is beyond the scope of this review to list them all and, therefore, we restrict ourselves to radar remote sensing and satellite based imaging spectroscopy, which we expect to be useful to global land-degradation research in the near future. For other sensors, the reader is referred to recent reviews of remote sensing for land degradation assessments, including local to regional scales, by Metternicht *et al.* (2010) and Zucca *et al.* (2012).

2.2.2 Space-borne radar and imaging spectroscopy

Radar was brought into space in the 1980s and has the advantage over optical remote sensing that it can sense through cloud cover and without daylight. Synthetic Aperture Radar (SAR) interferometry has been investigated for identification of potential degradation sites (Liu *et al.*, 2004), for monitoring of wind erosion (Del Valle *et al.*, 2010), for measurements of soil water (Walker *et al.*, 2004) and carbon stock (Goetz *et al.*, 2009), for crop monitoring (Baghdadi *et al.*, 2009) and to study ecological processes (Kasischke *et al.*, 1997). The latter include vegetation mapping and above-ground biomass estimation which, in combination with change-detection methods, can provide information on land degradation. For instance, SAR using multiple frequencies and polarizations is better for estimating woody biomass in tropical forest than optical remote sensing (Wang & Qi, 2008). There are more and more radar instruments in orbit, especially in C and X bands, with recent launches of TerraSAR-X and COSMO-SkyMed and forthcoming launches of TanDEM-X and SAOCOM. However, consistent time series needed for land degradation assessment are not yet available.

Methods have been proposed for broad-scale degradation assessment by space-borne imaging spectroscopy. At the moment, Hyperion (on board NASA EO-1 launched in 2000) has been successfully tested for land degradation research (Huete *et al.*, 2002b; Asner & Heidebrecht, 2003). The spectral analyses for dryland degradation (SAND) mission was proposed to specifically target dryland degradation (Mueller *et al.*, 2001; Kaufmann *et al.*, 2002) but not realized; it was followed up by the German environmental mapping and analysis program (EnMAP) to be launched in 2013 (Kaufmann *et al.*, 2006). The lauch of the Italian counterpart *precursore iperspettrale della missione applicativa* (PRISMA) is also planned for 2013. All these sensors have a spatial resolution of about 30m, which currently limits global applications by the welter of data that attend high resolution. Preliminary results from plant physiological studies, however, indicate the potential power of using imaging spectroscopy for monitoring chlorophyll fluorescence emission as a measure for heat or drought stress (Krumov *et al.*, 2008; Soukupova *et al.*, 2008). Recently, ESA published plans for the FLEX (fluorescence explorer) mission, which will comprise weekly global mapping of fluorescence at 300m spatial resolution (Rascher *et al.*, 2008). Potential pigment shifts as indicators for plant stress and plant community composition change are also available at leaf and canopy level (Kokaly *et al.*, 2009) from imaging spectrometer data. Data assimilation techniques (Dorigo *et al.*, 2007) and angular sampling (Schaepman, 2007; Verrelst, 2010) will further improve the use of imaging spectrometer data in process modeling for land degradation.

2.2.3 Climatic and land-use / land-cover data

Various complementary global datasets may be used in concert with satellite imagery to constrain index-based assessment of land degradation. Global or near-global climatological datasets are available from satellites, including tropical rainfall measuring mission (TRMM) and the AVHRR-based PATMOS-x project and also from long-term, station-based observations (Beck *et al.*, 2004; Mitchell & Jones, 2005). From these, rain-use efficiency (RUE), light-use efficiency and energy-use efficiency can be calculated (Le Houérou, 1984; Goetz *et al.*, 1999; Bai *et al.*, 2008). If productivity is limited by rainfall, RUE accounts for variability of rainfall and, to some extent, local site characteristics. The combination of NDVI and rainfall or RUE has been widely applied (e.g. Hein & de Ridder, 2006) but direct use of RUE has its critics (Holm *et al.*, 2003; Prince *et al.*, 2007).

Soil characteristics and variability are important variables in land degradation studies (Nicholson & Farrar, 1994), but the available datasets such as the soil map of the world (FAO-UNESCO, 1988), the harmonized world soil database (Nachtergaele *et al.*, 2008) and SOTER (Van Engelen & Wen, 1995) are hardly compatible with Earth-observation data, although a rigorous application at a regional scale has been in China under the global assessment of land degradation and improvement (Bai &

Dent, 2009). Improved global soil and terrain datasets are being developed in the e-SOTER project (e-SOTER website, 2010) and the GlobalSoilMap.net project (Sanchez *et al.*, 2009).

Land use and management are largely influential for land degradation and certain land-use changes make land degradation more or less likely (Vacca *et al.*, 2000); information about land-use and land-cover change is therefore essential for studying land degradation. Global land-cover maps have been derived from several remotely-sensed datasets including AVHRR (IGBP-DIS), SPOT-VGT (GLC2000), ENVISAT MERIS (Glob-Cover) and MODIS (Herold *et al.*, 2008). At finer resolution, Landsat-based land cover datasets include NLCD2001 (USA), CORINE (Europe) and AfriCover (Africa). However, each is specific to its own date and data; they are not mutually comparable. In China, a SPOT VGT-based land cover classification has been used to detect areas at risk of desertification (Huang & Siegert, 2006) and is claimed to be superior to GLC2000 and MODIS Land Cover products but, for establishing the causes, the use of higher resolution, Landsat or ASTER, imagery was recommended. The same SPOT data were used to monitor land cover changes in West-Africa by NDVI and SAVI (Lupo *et al.*, 2001). Several climate-driven processes of land-cover change were detected but it was also concluded that the data suffered from an incomplete cloud mask and sensor noise. There have been efforts to derive dynamic land cover maps from AVHRR or MODIS time-series (Julien & Sobrino, 2009) but there is still need for reliable, readily-available products.

2.3 Broad-scale land degradation studies

Global assessments of land quality and dynamics became feasible with the first AVHRR images (Justice *et al.*, 1985). Since then, studies using time series of satellite imagery have mainly focussed on the areas generally considered to be prone to degradation. The Sahel attracted attention because of a succession of severe droughts since the 1960s, with driest years in the early 1980s (Nicholson, 2000; Anyamba & Tucker, 2005; Govaerts & Lattanzio, 2008). It is an important validation site for general circulation models because of the uncertainty about the system's reaction (Cook, 2008) and of human-environment models because of the disputes about human influences on land degradation in the Sahel (Helldén, 2008). It has often been asserted that the Sahara is encroaching as a result of human activities (Cloudsley-Thompson, 1974; Lamprey, 1988) but assessment of time-series imagery in the Sudan showed no systematic advance of the desert or reduction in vegetation cover (Hellden, 1984). This was confirmed by Tucker *et al.* (1991) and Schlesinger & Gramenopoulos (1996) who found that vegetation density on the margins of the Sahara varies with rainfall, by Seaquist *et al.* (2008) who found no relation between demographics and model-based vegetation dynamics and by Prince *et al.* (1998) on the basis of rain-use efficiency (RUE). Still, Hein & de Ridder (2006) argue for

human-induced vegetation degradation over the last two decades based on temporal RUE variability – an interpretation disputed by Prince *et al.* (2007). A systematic increase in vegetation productivity around the Sahara has been measured using satellite imagery (Anyamba & Tucker, 2005; Herrmann *et al.*, 2005; Olsson *et al.*, 2005; Heumann *et al.*, 2007; Karlsen *et al.*, 2007). Probably, much of what has been identified as human-induced land degradation is a response to climatic fluctuations (Nicholson, 2000).

There is also controversy about land degradation in South Africa, both about the existence of severe degradation and about the causes. Several studies identified land degradation, mainly in rangelands (Ross, 1963; Adler, 1985; Hoffman & Simon, 2000), but Dean *et al.* (1995) found no evidence for increasing degradation and other studies in South Africa and surrounding countries concluded that vegetation change could be attributed to natural conditions such as drought and restrictive soil conditions (Dahlberg, 2000). In Zimbabwe, Prince *et al.* (2009) recently found that detected degradation could not be related to natural conditions and thus concluded that it was caused by human land-use practices. Wessels *et al.* (2007), in South-Africa, used the trends of the residuals of NDVI vs. time regressions (RESTREND) to distinguish human-induced land degradation. They concluded that observed changes could have resulted from several processes, including natural ecological processes and land-use changes. Not explicitly assigning causes, Bai & Dent (2007), in the GLADA project, found that almost half of the cultivated land experienced a decline in productivity over the last quarter century and one third of the whole country, mostly rangeland, showed increasing productivity.

Broad-scale assessments using NDVI in several other parts of the world show a general greening trend (Table 2.2), but also regions of decline. Like the Sahel, the Northern Hemisphere has become greener during recent decades (Myneni *et al.*, 1997; Slayback *et al.*, 2003; Hüttich *et al.*, 2007), although a browning trend was found between 1994 and 2002 (Angert *et al.*, 2005). Pouliot *et al.* (2009), in Canada, found that AVHRR NDVI data compared well with Landsat data and show an overall positive trend since 1985. Alcaraz-Segura *et al.* (2010), also in Canada, confirm this but remark that AVHRR NDVI exhibit other greening and browning trends than the CCRS (Canadian Centre for Remote Sensing) NDVI dataset. In Australia, an increase in vegetation cover, especially in winter, recorded by fPAR derived from AVHRR PAL has been attributed to an increase in available moisture (Donohue *et al.*, 2009).

Table 2.2 Selected studies of broad-scale vegetation trends.

Extent	Indicator	Spatial resolution	Time range	Remote sensing data	Conclusion	Reference
Global	NPP (PEM)	0.5deg	1982-1999	PAL / GIMMS	6% increase in global NPP	Nemani *et al.* (2003)
Global	NPP (CASA)	1deg	1983-1988	FASIR	Increase in global NPP, 6-month to 1-year offset in timing of anomalies	Potter *et al.* (1999)
Global	NDVI	8km	1981-2003	GIMMS	Greening and browning trends globally	Bai *et al.* (2008)
Northern hemisphere	NDVI	8km	1982-1999	GIMMS/FASIR	Significant greening trends (61% of vegetated area)	Slayback *et al.* (2003) Tucker *et al.* (2001) Zhou *et al.* (2001)
Northern hemisphere	NDVI	1deg	1982-2002	GIMMS	Shifting greening and browning trends, net greening	Angert *et al.* (2005)
Northern Eurasia	NDVI		1998-2005	SPOT VGT	Greening trend	Hüttich *et al.*, (2007)
Northern high latitudes	NDVI	8km	1981-1991	PAL / GIMMS	Photosynthetic activity increased, suggesting increase in plant growth	Myneni *et al.* (1997)
Sahel	NDVI / RUE	8km	1982-1990	GIMMS	No evidence of desertification	Prince *et al.* (1998)
Sahel	NDVI / rainfall	8km	1982-2003	GIMMS	Greening trend	Herrmann *et al.* (2005)
Sahel	NDVI	8km	1982-1999	PAL	Greening trend	Olsson *et al.* (2005)
Sahel	Albedo		1984 - 2003	MeteoSAT	Greening associated with decreasing albedo	Govaerts & Lattanzio (2008)
Australia	fPAR	0.08deg	1981-2006	PAL	Increase in vegetation cover	Donohue *et al.* (2009)
South America	fPAR / NDVI		1981-2000	AVHRR	Overall increase of 1.3%	Paruelo *et al.* (2004)
China	NPP (PEM)	0.5deg	1981-2000	AVHRR	Increase in NPP (0.32% / year), decrease in net ecosystem productivity between 80s and 90s due to global warming	Cao *et al.* (2003)

NDVI has proved capable of assessing vegetation dynamics and relations to land degradation. However, assessment of land degradation at global scale remains a challenge. One of the first attempts was Dregne's 1977 map of the status of desertification for the UN Conference on Desertification which was based on expert opinion and restricted to drylands. The later GLASOD map (Oldeman *et al.*, 1990) provided full global coverage, also based on expert opinion. The situation has been revolutionised by the availability of more than 25 years of consistent Earth-observation data. These are the basis of the first quantitative assessment of global land degradation and land improvement (GLADA) which applied trend analysis to the GIMMS dataset and corrected for trends in rainfall using rain-use efficiency and temperature using energy-use efficiency (Bai *et al.*, 2008). The GLADA map detected potential degradation hotspots (Figure 2.4) and yielded quantitative estimates of lost productivity in terms of NPP. However, much potential information in the dataset is not revealed by the linear regression of yearly aggregated values.

Assessments of land degradation using NDVI focused mainly on areas where the NDVI signal does not saturate, such as semi-arid and temperate regions with relatively low LAI. But land degradation is not confined to these areas and also occurs in humid tropical and sub-tropical areas with dense vegetation. Deforestation is one of the most common kinds of human-induced land degradation but there are many other facets that may be referred to as forest degradation (Köhl *et al.*, 2009) – monitoring of which is technically more challenging than monitoring deforestation (DeFries *et al.*, 2007). The estimated extent of deforestation in humid tropic forests is 1.4% of the total area (2000-2005) and another 20% is affected by some kind of logging (Asner *et al.*, 2009). Accurate broad-scale estimations are difficult, because clearing mostly occurs at a fine scale, but MODIS data have been used to create indicator maps (Hansen *et al.*, 2008). The impact of natural factors like droughts has also been assessed using MODIS. For instance, in the Amazon there has been debate about whether the 2005 drought caused greening or not (Saleska *et al.*, 2007; Samanta *et al.*, 2010). Both studies used EVI but the latter concluded that the data were corrupted by atmospheric factors that explained the apparent greening effect. At global scale, FAO undertakes a decennial forest resource assessment but there is no global forest degradation inventory available.

Biogeochemical models can assess changes in vegetation productivity with and without human activity: a decline in productivity that cannot be explained by climatic variations might be attributed to human influences (Seaquist *et al.*, 2008). At global scale, Nemani *et al.* (2003) applied a biome-specific production efficiency model with two AVHRR datasets (GIMMS and PAL) and found that global climatic and atmospheric changes have eased several constraints on NPP, which had increased by 6 percent over the period 1982-1999 (Figure 2.5).

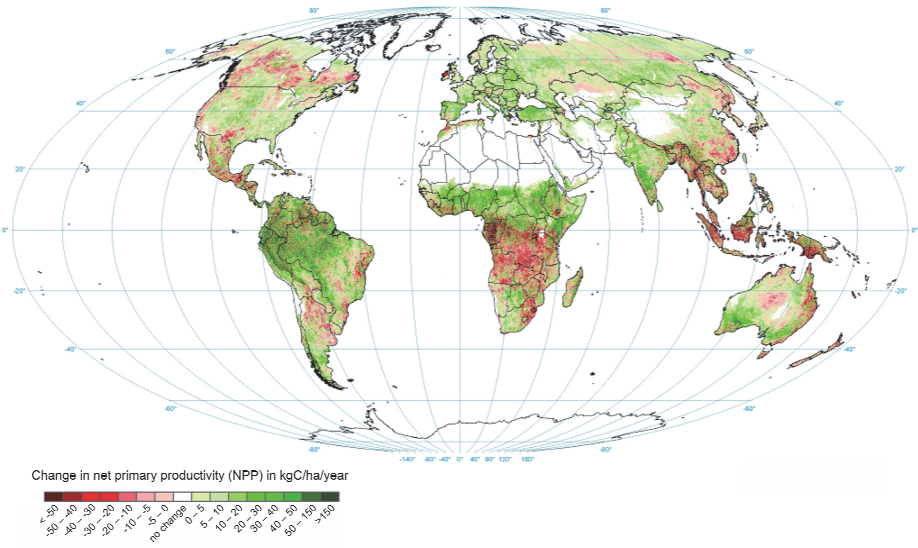

Figure 2.4 Linear trends in net primary production (NPP) from the 1981-2003 global assessment of land degradation and improvement (GLADA). Reproduced from Bai et al. (2008).

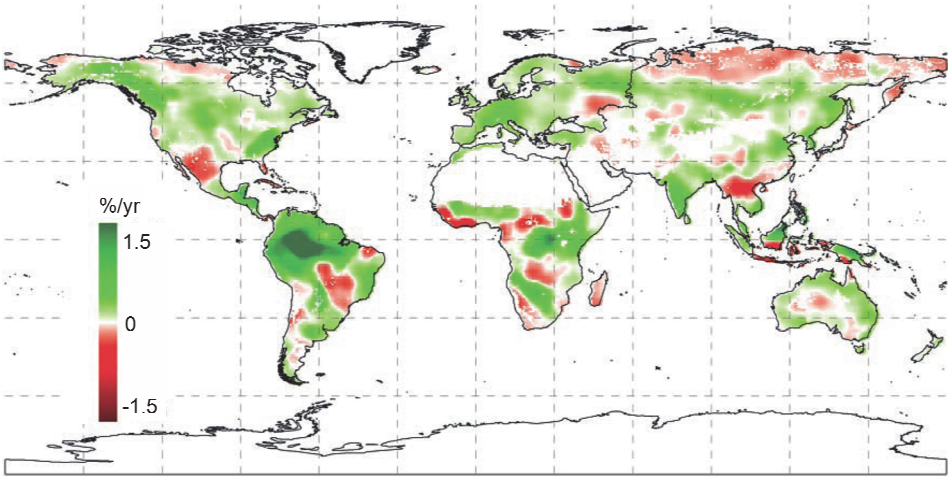

Figure 2.5 Linear trends in yearly accumulated net primary production (NPP) from 1982-1999 using a global production efficiency model (PEM). Reproduced from Nemani *et al.* (2003).

Similarly, Cao *et al.* (2003), in China, used AVHRR data and two biogeochemical models to estimate inter-annual variations of NPP. One of the models, the global production efficiency model (GLO-PEM) uses only remotely-sensed input data and, thus, delivers independent estimates of NPP (Goetz *et al.*, 2000). They concluded that, in contrast with the global trend, the net ecosystem production in China decreased in the past decades because of stronger warming than the global average. Seaquist *et al.* (2003) built a LUE model for estimation of GPP in the Sahel, which was parameterized with satellite data (PAL). In a follow-up they used the model to disentangle the effects of climate and human influence and concluded that the identified changes could not be associated to human activity (Seaquist *et al.*, 2008). To address human appropriation of NPP (HANPP) at global scale, Haberl *et al.* (2007) used the Lund-Potzdam-Jena (LPJ) dynamic global vegetation model for calculating potential NPP. They concluded that almost 24% of yearly potential NPP was lost due to human activities (based on the year 2000) including harvesting (53%) and land-use change (40%). These data have also been used to focus on human-induced dryland degradation at global scale (Zika & Erb, 2009). The extent of degrading areas was taken from a compilation of mainly qualitative land degradation assessments, including GLASOD. They found a loss in NPP of 1.6% with respect to the global terrestrial NPP but emphasized, that results are hard to interpret because of uncertainties in the underlying assumptions. Another model that has been regularly used in combination with Earth observations for modeling NPP is the Carnegie-Ames-Stanford (CASA) biogeochemical (BGC) model (Potter & Klooster, 1997; Yu *et al.*, 2009).

So far, biomass decline has been considered as a gradual process on the human time scale, but it may equally well be considered an abrupt, or catastrophic, shift induced by gradual environmental change (Scheffer *et al.*, 2001; Rietkerk *et al.*, 2004). The latter is caused by positive feedback mechanisms like the effect of vegetation on soil erosion and the other way around (Janssen *et al.*, 2008). Mid-Holocene desertification in North Africa has been identified as such a catastrophic shift (Dakos *et al.*, 2008). The concept has been used in a study to resilience of tropical forest and savanna ecosystems (Hirota *et al.*, 2011) but assessment of catastrophic land degradation using remote sensing is yet an unexplored field of research.

2.4 Broad-scale monitoring of physical and chemical land degradation processes

Soil erosion by runoff water is considered to be the most widespread process of land degradation (Eswaran *et al.*, 2001; Vrieling, 2007). Most commonly, it is assessed by measuring or modeling the detachment of particles by rain splash and overland flow and up-scaling to the catchment. Vrieling (2006) and Metternicht *et al.* (2010) review

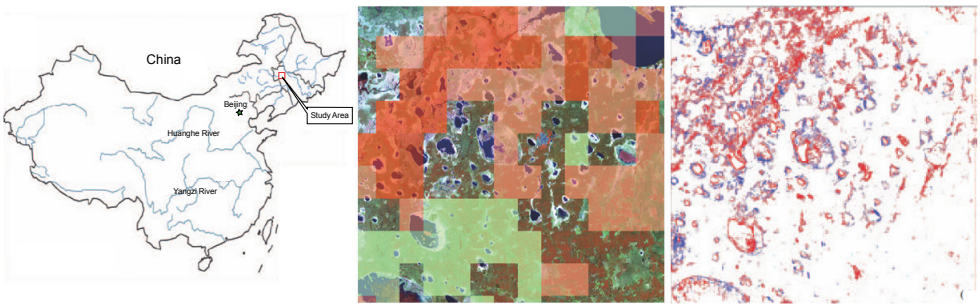

Figure 2.6 Salinization study in China: middle- Landsat image of study area, overlaid by GLADA NDVI trend (Figure 2.4); right - red indicates degradation and blue improvement (1988-1996). Modified after Chen & Rao (2008).

the application of satellite remote sensing, which can show the larger erosional features such as rills, gullies and land slips. Smaller features like crusting or soil compaction may be spectrally distinguishable on bare ground (Goldshleger *et al.*, 2001) but attempts to quantify them in remotely sensed imagery have been limited to small plots. The same holds for monitoring of gully erosion (Marzolff & Poesen, 2009) and quantification of soil properties (Summers *et al.*, 2011), which are mostly done using high-resolution, often airborne, remote sensing. Nevertheless, a recent modeling approach for soil erosion at continental scale for sub-Saharan Africa by Symeonakis & Drake (2010) found that the estimates are within the same order of magnitude as field measurements. In drylands, wind is an important agent of erosion and deposition (Ravi *et al.*, 2010) but it is hard to quantify at broad scales Symeonakis & Drake (2004). Radar remote sensing has been tested for mapping of wind-driven land degradation by mapping its primary factors: surface roughness, soil moisture, local incidence angle and vegetation cover (Del Valle *et al.*, 2010). The acute processes of chemical land degradation are salinization and chemical contamination. Salt accumulation may arise from groundwater, coastal flooding or irrigation; chemical contamination may be natural, for instance in volcanic areas, or, most often, man-made (Gardner *et al.*, 2004). Salinity may be detected with relatively high-resolution imagery like Landsat (Chen & Rao, 2008) but comparison with the GLADA assessment at 8km resolution shows some sensitivity at the broader scale as well (Figure 2.6). However, the coarse resolution of most satellite imagery compared with the variability of salt concentrations in the soil and the interference of other soil properties with the detected signal limit its value for detailed mapping (Mougenot *et al.*, 1993; Ben-Dor, 2009). At the same time, high-resolution data impose a practical constraint on broad-scale mapping. Metternicht & Zinck (2003, 2009) provided an overview.

2.5 Future steps for Earth observations

There is broad agreement that efficient action to arrest land degradation requires 'effective early warning, assessment and monitoring – combining remote sensing with field surveys of key indicators' (UNEP, 2007); but it remains a contentious field (Bai *et al.*, 2008). Field observations and experiments combined with expert synthesis measure physically different things at a different scale from those measured by remote sensing. Expert judgement of 'the real thing' is local and time-bound and it is hardly possible to validate 25 years of NDVI measurements in the field, after the event, at 8km spatial resolution. Remote sensing can take us several steps towards accurate and consistent monitoring of land degradation at the global scale, but interpretation of imagery and derived products comes with challenges. Some important steps towards better understanding of time series of satellite imagery are listed below.

2.5.1 Advanced time-series analysis

The value of a 30-year record of AVHRR can hardly be over-stated. Land degradation nearly always affects vegetation and NDVI is one of the few, consistent indicators available at global scale over the long term. In spite of the limitations of AVHRR data already discussed, data-driven approaches can derive several biophysical variables (Goetz *et al.*, 2000). Since 2000, MODIS, SPOT VEG and SeaWiFS provide improved datasets in terms of accuracy or spatial resolution. Each dataset contains information on inter- and intra-annual variability, phenological cycles, frequency and shift of growing seasons and distinction between gradual and abrupt changes (Azzali & Menenti, 1999; Jönsson & Eklundh, 2002; Zhang *et al.*, 2003; Verbesselt *et al.*, 2010a) which might be linked to climatic changes, changes in land use and management and/or land degradation. Current assessments eliminate intra-annual information by reducing the temporal resolution, while existing methods can account for phenological variation without averaging to yearly values, for instance by harmonic analysis of NDVI time-series (Jakubauskas *et al.*, 2001; Hird & McDermid, 2009). For this purpose, the HANTS algorithm (Verhoef *et al.*, 1996; Roerink *et al.*, 2000; Jun *et al.*, 2004) performs well in comparison with several others (White *et al.*, 2009). If more measurements are maintained in the analysis, it is also possible to capture trend breaks or shifts. For instance, certain regions exhibit combined greening and browning trends (Angert *et al.*, 2005), which are averaged out by simple linear trends analysis.

When using vegetation dynamics as indicator for land degradation, it is essential to account for phenological variation and, when using regression to quantify trend slopes, it is essential to deal with trend shifts and breaks. The analysis of the full temporal domain of AVHRR and other datasets is needed to achieve these goals.

2.5.2 Spatial-contextual analysis

The spatial-contextual approach, which includes the pixel location and interaction with adjacent pixels as source of information, is relatively unexplored. For coarse resolution data, this might include stratification by phenological zones, while at finer resolution changes in land use may be incorporated (Friedl *et al.*, 2002; Lupo *et al.*, 2007). In any case, the spatial resolution of the imagery should correspond with the scale at which the processes act. In case of climate-driven land cover changes (e.g. warming, change in precipitation) a 1km spatial resolution will suffice, whereas most human-driven land cover changes (e.g. land transformation, logging, over exploitation) occur at 250m–500m scale (Townshend & Justice, 1988). Patchiness, or spatial configuration, of vegetation is often used to study ecosystem health or degradation (Bastin *et al.*, 2001; Ludwig *et al.*, 2007). In water-limited ecosystems, patchiness might be self-organizing due to a positive feedback relation between vegetation and water availability (Rietkerk *et al.*, 2004): dense vegetation allows for high water infiltration into the soil and lower soil evaporation. As a result, vegetation may persist where it is already established but bare soil does not allow for vegetation to establish. The catastrophic shift between vegetated patchy state and bare homogeneous state, e.g. due to overgrazing, might have severe consequences for land degradation in drylands (von Hardenberg *et al.*, 2001). It is a challenge and urgent issue to anticipate these changes using earth observation and include these in dryland degradation models (Kéfi *et al.*, 2007).

2.5.3 Modeling

Satellite-based Earth observation methods are confined to physical measurement – in most cases radiances or reflectance factors (Schaepman-Strub *et al.*, 2006). Mapping of indicators of land degradation relies on empirical models, mostly using statistical methods, to establish relationships between the physical measurement and the degradation process. Models that aim at predicting catastrophic shifts need a long time-series of sufficient quality and resolution to capture the dynamics of the system (Dakos *et al.*, 2008). Currently available remotely-sensed time series enable trend analysis of some fast-reacting sub-systems but large climatic systems are known to react over centuries (deMenocal, 2008). At shorter time-scales, remotely sensed data can be coupled to outputs from vegetation dynamics or light-use efficiency models like Biome-BGC (White *et al.*, 1999), LPJ (Bonan *et al.*, 2003), CASA (Potter *et al.*, 1999) or crop growth simulation models (Jongschaap, 2006); differences between observed productivity and simulated productivity without human interference might indicate land degradation. Although many studies have shown the potential of this approach, it remains a challenge to combine these models with others, e.g. soil-erosion models (Symeonakis & Drake, 2010) and land-change models / human-

environment models (Turner *et al.*, 2007; Helldén, 2008) into a generic land-degradation model.

2.5.4 Validation

Validation is crucial for remote sensing studies. We have consistent satellite data of the past 30 years, but no compatible field data. Field validation is hardly feasible for pixels ranging from 1–8km (Running & Nemani, 1988) and, because of heterogeneity on the ground, extrapolation is often problematic. Every study of scalability issues deals with the trade-off between local precision, which is improved by on-the-spot assessment (Baartman *et al.*, 2007) and global accuracy which needs a consistent, world-wide overview but which is hard to recognize in the field. The AVHRR dataset captures the typical temporal scale on which degradation processes occur, whereas the new generation sensors capture the typical spatial scale (Townshend & Justice, 1988). If the 1981–2006 AVHRR data were to be processed in a manner quantitatively comparable to that of the new generation of sensors, many advantages of MODIS and SPOT Vegetation data could be realized while retaining historical information (Tucker *et al.*, 2005). Many regional and national studies will remain essential to validate broad-scale degradation estimates – either qualitative or quantitative.

2.6 Conclusions

Land degradation is a global environmental and development issue but there is no consensus on its causes, severity and extent. Many scientific and political fields are involved in research and policy making and there is agreement about the need for up-to-date, quantitative information at national and global scales to support mitigation. This requires consistent monitoring of key indicators at a range of scales. Loss of vegetation productivity or cover has been widely used to quantify land degradation, not least because of the availability of long-term NDVI time series. Broad-scale studies show a general greening trend over recent decennia but, also, regions of productivity decrease, e.g. in south China. The first quantitative global assessment of land degradation and improvement (GLADA) used yearly averaged linear trends in NDVI, translated in terms of NPP as a proxy measure. However, the results of global studies are disputed because they are different from traditional expert assessments and they are hard to validate in the field. At the same time, local assessments are only snapshots of small areas, generally too detailed for global application. Steps towards improvement of broad-scale assessments include more advanced time-series analysis, integration of state assessments using statistical methods with model based links to processes or drivers, the use of spatial-contextual information and validation using regional assessments. The first might include recognition of intra-annual variation, non-linear trends and breaks or shifts in greening and browning trends. The

others might include the use of regional studies at medium spatial resolution, for instance land degradation assessments, but also dynamic land use mapping and other land dynamics or land change studies for validation and identification of driving processes. A truly global assessment, empirical or deterministic, requires more than NDVI measurements, which have limited application in densely vegetated (high LAI) regions. Integration with a future global forest-degradation assessment is needed.

The long-term AVHRR-NDVI record provides an invaluable historical record but there is still a gap in the methodology to couple this dataset to the datasets from the new generation of improved sensors. Using the full potential of all available datasets – in all temporal, spectral and spatial dimensions – will be a significant step towards global-scale assessment of land degradation. Advances in satellite-based remote sensing will improve its measurement, but further development of physically-based process models is needed to establish cause-and-effect relationships. Until then, Earth observation-based mapping of indicators will continue to reveal ambiguities.

Acknowledgements

This work is partly financed through the FAO contract PR35852. The authors thank Dr Zhanguo Bai for his data and constructive criticism.

Chapter 3

Analysis of monotonic greening and browning trends from global NDVI time series

Rogier de Jong, Sytze de Bruin, Allard de Wit, Michael E. Schaepman, David L. Dent

"When you're making decisions, you can't just take anecdotal information. You need quantified, explicit information, which really will let you determine: is this bad, is this really bad, so we don't over respond, and we don't ignore a real problem."

Molly Brown (2011)
Geospatial Revolution, Episode Four

This chapter is based on:
Remote Sensing of Environment, 115 (2011), pp. 692-702
DOI: 10.1016/j.rse.2010.10.011

Abstract

Remotely sensed vegetation indices are widely used to detect greening and browning trends; especially the global coverage of time series normalized difference vegetation index (NDVI) data, which are available from 1981. Seasonality and serial auto-correlation in the data have previously been dealt with by integrating the data to annual values; as an alternative to reducing the temporal resolution, we apply harmonic analyses and non-parametric trend tests to the GIMMS NDVI dataset (1981–2006). Using the complete dataset, greening and browning trends were analyzed using a linear model corrected for seasonality by subtracting the seasonal component, and a seasonal non-parametric model. In a third approach, phenological shift and variation in length of growing season were accounted for by analyzing the time series using vegetation development stages rather than calendar days. Results differed substantially between the models, even though the input data were the same. Prominent regional greening trends identified by several other studies were confirmed but the models were inconsistent in areas with weak trends. The linear model using data corrected for seasonality showed similar trend slopes to those described in previous work using linear models on yearly mean values. The non-parametric models demonstrated the significant influence of variations in phenology; accounting for these variations should yield more robust trend analyses and better understanding of vegetation trends.

3.1 Introduction

Vegetation, as the main component of the terrestrial biosphere, is a crucial element in the climate system (Foley *et al.*, 2000) and there is high confidence that global warming is now strongly affecting the terrestrial biosphere (IPCC, 2007). Vegetation status is commonly used in assessments of productivity of natural and agricultural lands (Sims *et al.*, 2008; Yu *et al.*, 2009; Cai & Sharma, 2010) and a declining, or browning, trend is considered to indicate land degradation (Wessels *et al.*, 2007; Zika & Erb, 2009; Metternicht *et al.*, 2010). The normalized difference vegetation index (NDVI), based on red and near-infrared reflectance (Tucker, 1979), is correlated with vegetation activity measures (see Section 1.2.2) and trends in NDVI can thus be used as a proxy for greening or browning (Bai *et al.*, 2008; Alcaraz-Segura *et al.*, 2010). However, it is difficult to attribute cause-and-effect relationships to the detected trends, since variations in vegetation activity are driven by various factors, including climatic cycles and management practices (Lupo *et al.*, 2001; Evans & Geerken, 2004; Wessels *et al.*, 2007). NDVI trends have been used for many purposes, including assessment of ecological response to global warming (Pettorelli *et al.*, 2005), phenological change (White *et al.*, 2009), crop status (Tottrup & Rasmussen, 2004), land-cover change (Hüttich *et al.*, 2007) and desertification (Symeonakis & Drake, 2004). For example, systematic greening has been found in the Sahel (Anyamba & Tucker, 2005; Olsson *et al.*, 2005; Heumann *et al.*, 2007), most likely due to climatic variations and recovery from severe droughts (Nicholson, 2000; Herrmann *et al.*, 2005). The effects of human-induced land degradation are highlighted by some studies (Hein & de Ridder, 2006) and disputed by others (Prince *et al.*, 2007; Seaquist *et al.*, 2008). Most analyses established trends by linear regression of NDVI, integrated annually (Bai *et al.*, 2008) or seasonally (Eklundh & Olsson, 2003) but it is not always clear whether the derived slope coefficient differs significantly from zero (de Beurs & Henebry, 2004) or what may be the effect of integration by calendar year in the Southern Hemisphere where growing seasons straddle the year end (Wessels, 2009).

Trends and inter-annual variability in vegetation phenology – the timing of seasonal activities of plants – affect the exchange of carbon, water and energy between the vegetation and the atmosphere (Baldocchi *et al.*, 2001). A range of studies using station observations of phenology and temperature has shown a widespread trend of earlier onset of greening and longer growing seasons, especially in the Northern Hemisphere (Menzel *et al.*, 2006; Rosenzweig *et al.*, 2007; Sparks *et al.*, 2009); these findings are substantiated by satellite observations since the early 1980s (Myneni *et al.*, 1997; Tucker *et al.*, 2001; Zhou *et al.*, 2001; Karlsen *et al.*, 2007) and are in line with the increase in net primary production (NPP) suggested by modeling studies (Nemani *et al.*, 2003). Longer and warmer growing seasons

increase evapotranspiration and drought stress (Barber *et al.*, 2000; Zhang *et al.*, 2009), wildfire incidence (Westerling *et al.*, 2006) and intensity of carbon sequestration (Goulden *et al.*, 1996; White *et al.*, 1999). Therefore, a decrease in the growth rate within the growing season might be a more sensitive measure than total production as an indicator of stress and soil degradation. Unfortunately, information on growth rate, or intensity, is concealed by integration of NDVI data to annual values.

When analyzing complete NDVI time series for trends, without yearly aggregation, linear regression needs to be used with care. Any auto-correlation within the dataset will violate some model assumptions (McBride & Loftis, 1994; de Beurs & Henebry, 2004; Beck *et al.*, 2006) and trends may be less significant than they appear. Either seasonality must be removed (Hussian *et al.*, 2005) or a non-parametric trend test that accounts for seasonality may be applied (de Beurs & Henebry, 2004). In the Sahel, growth intensity has been measured by combination of the seasonal amplitude and the seasonal total but the amplitude appeared to be affected by saturation of the NDVI signal (Eklundh & Olsson, 2003). The non-parametric analysis will not be so affected because NDVI values near the beginning and end of the season are well below saturation level.

This paper considers monotonic trends; accordingly it is assumed that trends preserve their increasing or decreasing order throughout the time series. We examine differences between previously-published methods using the 1981-2006 global inventory modeling and mapping studies (GIMMS) dataset (Bai *et al.*, 2008; Bai & Dent, 2009) and suggested improvements that do not require temporal aggregation: 1) a linear model applied to NDVI residuals after the seasonal component has been removed; 2) a non-parametric model applied to the original NDVI data; 3) a non-parametric model applied to vegetation development stages (NDVI data adjusted for the growing season). Long-term and annual harmonic analyses were used to filter cloudiness and seasonality, and to derive phenological measures.

3.2 Materials and Methods

Harmonic analysis was applied to the NDVI data to remove residual cloud and haze effects and seasonality. Greening and browning trends were then investigated using linear and non-parametric models, summarizing the outputs by land-cover class.

3.2.1 The GIMMS dataset

NDVI is the most-used product derived from NOAA-AVHRR data (Cracknell, 2001). We used GIMMS version G (Tucker *et al.*, 2004), consisting of 26 years of NDVI data from 1981 through 2006, summarized fortnightly at 8km resolution. The fortnightly time series was derived from daily 4km global area coverage data from a suite of NOAA satellites (Tucker *et al.*, 2005), applying the maximum-value

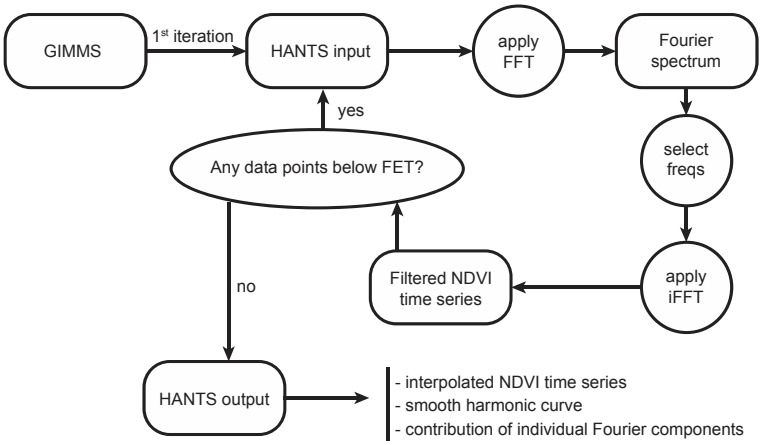

Figure 3.1 Harmonic analysis of NDVI time series flowchart.

composite (MVC) technique to remove bias caused by atmospheric conditions (Holben, 1986). See Section 1.2.3 and Table 1.2 for more details about the GIMMS dataset.

3.2.2 Harmonic analysis of NDVI time series

Phenological patterns were extracted from the GIMMS data using a modified implementation of the harmonic analysis of NDVI time series (HANTS) algorithm (Roerink *et al.*, 2000; de Wit & Su, 2005) which describes seasonal effects in vegetation using a limited number of low-frequency cosine functions with different phases, frequencies and amplitudes. The algorithm uses Fourier analysis, complemented with detection of outliers, which are flagged and replaced iteratively (Figure 3.1).

First, the raw GIMMS data were used as input for a fast Fourier transform (FFT). The frequencies representing the yearly, 6-monthly and 4-monthly signals were selected from the Fourier spectrum. Based on these frequencies, the spectrum was transformed back into a filtered NDVI time series using inverse FFT. Outliers were filtered using a fit-error tolerance (FET): each original NDVI value that deviated

Table 3.1 Parameters used for the harmonic analysis of NDVI time series (HANTS) algorithm.

Parameter	Single year	Full temporal extent (26yrs)
Number of data points	26	624
Fourier frequencies	0,1,2,3	0,26,52,78
Fit error tolerance (FET)	0.1	0.1
Max. number of iterations (i_{MAX})	6	12
Min. number of retained data points	16 (66.7%)	416 (66.7%)

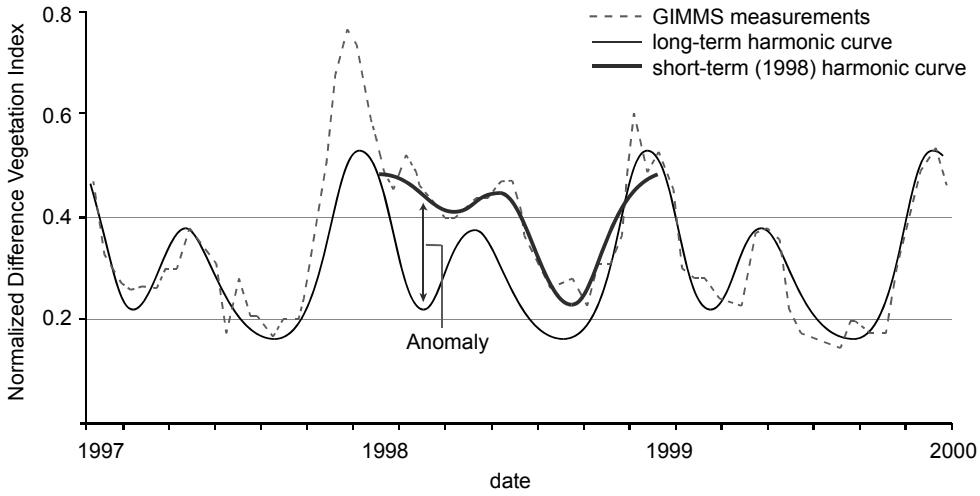

Figure 3.2 Example of NDVI anomalies as derived from the long- and short-term fits of the harmonic analysis.

from the harmonic curve by more than the FET-value was considered noise and was replaced by the filtered value. This procedure was repeated until either no points exceeded the FET or a pre-defined constraint was reached; the constraints concern the maximum number of iterations (i_{MAX}) and a threshold on retained data points, which is closely related to the degree of over-determinedness as defined by Roerink *et al.* (2000). The number of retained data points may be taken as a measure of the performance of the algorithm. A disadvantage of HANTS is the lack of objective rules to determine its control parameters; parameterization requires experience and running several parameter combinations.

We used HANTS in two ways. First, the per-pixel long-term harmonic patterns were determined using the full-length GIMMS dataset (HA_{full}). Secondly, the harmonic pattern was extracted for each year separately (HA_{year}). Differences between the two were considered NDVI anomalies (A) and used for temporal trend analysis. Figure 3.2 and Equation 3.1 illustrate how the anomalies were calculated.

$$A(t) = HA_{year}(t) - HA_{full}(t) \tag{3.1}$$

Using anomalies, seasonality could be almost fully eliminated from the data, as illustrated by the autocorrelation functions in Figure 3.3. The algorithm was tuned to disregard values lower than zero, as these correspond to water or null-values in the GIMMS data. Fills, having value zero, replaced the eliminated values. The FET was fixed to 10% of the NDVI range (0.1), so observations with a lower anomaly were retained. The number of iterations required depended on the biome and the length of

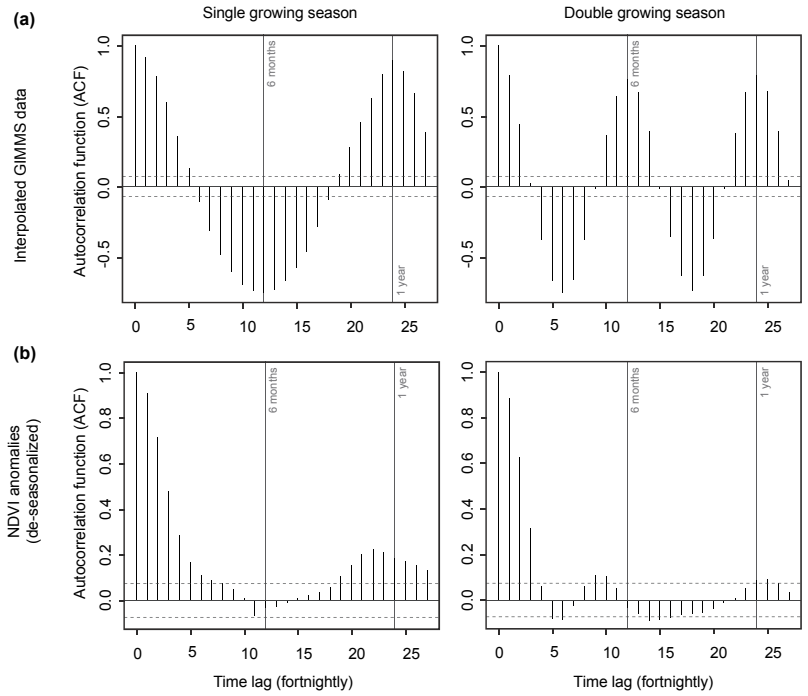

Figure 3.3 Average autocorrelation functions (ACF) of GIMMS data (A: interpolated, B: anomalies) with fortnightly lags (lag 24 = 1 year). The dotted lines indicate the 95% confidence interval of zero autocorrelation. For both, single and double growing seasons, 30 pixels were used.

the time series. For a single-year analysis, 1 or 2 iterations proved sufficient for all except some tropical areas in which the amplitude was limited and cloudiness affected even the fortnightly MVC images (Julien & Sobrino, 2010); in these cases a stable fit was obtained after 3 or 4 iterations. The i_{MAX} was fixed to 6 iterations in the yearly analysis. The full time series is 26 times longer and needed more iterations for a stable fit. In this case, the i_{MAX} was doubled to 12. The minimal number of retained data points was set to 16 and 416 for the yearly and the full datasets, respectively. This implies that the output curve is always fitted to at least two-thirds of the original data points, even if the FET is not achieved. Table 3.1 lists the parameters used for analysis of both the full dataset and each year separately.

3.2.3 Extraction of phenological measures

Although satellite-observed phenology – also referred to as land-surface phenology (LSP) – is not identical to plant phenology, it is considered to be related (Doktor *et al.*, 2009; Liang & Schwartz, 2009; White *et al.*, 2009) and LSP has been

used to define developmental stages of vegetation. Analyzing trends in NDVI by vegetation development stage rather than by day of the year eliminates variations in the start and length of growing season – since the growing season is fully contained within the first developmental stage (start of season, SoS), and the last stage (end of season, EoS). Various approaches have been described to derive SoS from NDVI time series: half-maximum (White *et al.*, 1997), 10% amplitude (Jönsson & Eklundh, 2002), inflection point (Moulin *et al.*, 1997), maximum curvature (Zhang *et al.*, 2003), delayed moving average and forward-looking moving average (Reed *et al.*, 2003). Following White *et al.* (2009), we used the first derivative of the HANTS-smoothed NDVI profile, where SoS is defined as the maximum of the first derivative (maximum NDVI increase), and EoS is defined as the first occasion after SoS where the NDVI value drops below the value at the start of the growing season. Between SoS and EoS, ten equally spaced vegetation development stages were defined. This approach is reliable in comparison with several other methods (White *et al.*, 2009), but it can be anticipated that the approach only works for single growing seasons and that it will not be able to detect multiple growing seasons. This limits the applicability of the method in multi-cropping regions. For illustration, Figure 3.4 shows an example of a growing season in which several measures are indicated.

The NDVI values at each development stage ($NDVI_{ds}$) were calculated using the yearly harmonic fit (Eq. 3.2*a*), where *FC* represents the Fourier Component, $NDVI_{mean}$ is the mean NDVI (FC0), *A* is the amplitude, Φ is the phase shift and *x* is the day number represented in radians (Eq. 3.2*b*).

$$NDVI_{ds} = NDVI_{mean} + \sum_{i=FC_1}^{FC_{\max}} A_i \cdot \cos(i \cdot x + \Phi_i) \qquad (3.2a)$$

$$x = day / 365 \cdot 2\pi \qquad (3.2b)$$

For each growing season, this provided 12 $NDVI_{ds}$ values, which were used as input for the seasonal Mann-Kendall (SMK) model described below.

3.2.4 Trend analysis

NDVI time series are characterized by outliers, seasonality and serial auto-correlation. The GIMMS data were analyzed for trends using three different strategies that take account of these effects – all involving harmonic smoothing to remove outliers and seasonality.

The first approach – here referred to as the linear model (LM) – uses the smoothed time series (624 fortnightly values from 1981 through 2006) to analyze trends in anomalies (*A*) between the long-term harmonic fit and yearly fits (Eq. 3.1). In the case of a perfectly stable seasonal pattern without additional trend, there would be no anomalies; conversely, differences between the long-term and yearly fits may

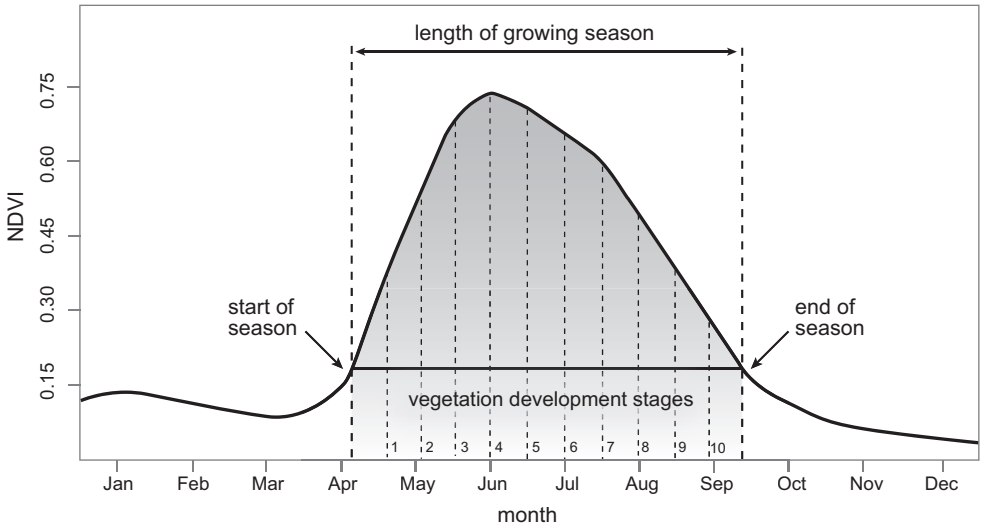

Figure 3.4 Example of single growing season and related phenological measures. Start of season (SoS) is defined as the date of the inflexion point of the NDVI curve and end of season (EoS) as the date at which NDVI drops below the SoS value. In between these dates, 10 equally distanced vegetation development stages (VDS) are defined, covering the entire growing season (shaded area).

indicate land degradation or improvement, particularly if there is a significant negative or positive trend over time. Trends were quantified by the slope of the regression line derived from a simple linear model of the NDVI anomalies against time. The fitted slopes were tested for significance using analysis of variance (ANOVA) with a significance level (α) of 0.1. Only slopes that significantly differed from zero have been considered to indicate greening or browning trends.

The second approach used the HANTS-interpolated data without removing seasonality. This dataset would violate the assumption of independent residuals, which is a basis for ordinary least-squares regression. For this reason, the seasonal Mann-Kendall test was used as a non-parametric test for monotonic trends. The test may be used with missing or tied data and its validity does not depend on the data being normally distributed. Mann (1945) first suggested using the Mann-Kendall test for significance of Kendall's τ for temporal trends and this approach has since been applied to seasonal data, mainly for hydrological analyses (Hirsch *et al.*, 1982) and, more recently, with NDVI data (Chamaille-Jammes *et al.*, 2006; Pouliot *et al.*, 2009; Alcaraz-Segura *et al.*, 2010). The test consists of computing the Kendall Score (S) and its variance separately for each season (p). In this case, p equals the number of observations in a year (24). For each season, n equals the number of observations in the record (26). S denotes the sign (sgn) of the change between subsequent samples and attains the value -1, 0 or +1 (Hirsch & Slack, 1984). These individual values are summed over all samples to obtain the seasonal statistic S_g (Eq. 3.3). The sum over

all seasons provides the final test statistic *S'* (Eq. 3.4). Subsequently, the Kendall's rank correlation coefficient (τ) ranging between -1 and 1 (Kendall, 1938), is calculated (Eq. 3.5). The null hypothesis H_0 is that for each of *p* seasons the *n* samples are randomly ordered (mean $S = 0$), versus the alternative hypothesis H_A of a monotonic trend in one or more seasons (Hirsch & Slack, 1984). H_0 was tested 2-sided against H_A and rejected when Kendall's τ of NDVI versus time is significantly different from zero ($\alpha = 0.1$). We then conclude that there *is* a monotonic trend in NDVI over time: a *greening trend* if $\tau > 0$ and a *browning trend* if $\tau < 0$.

$$S_g = \sum_{i<j} \mathrm{sgn}(X_{jg} - X_{ig}) \qquad g = 1,2,...,p \tag{3.3}$$

$$S' = \sum_{i=1}^{p} S_g \tag{3.4}$$

$$\tau = \frac{S'}{n(n-1)/2} \tag{3.5}$$

In a further step, the slope of this trend may be quantified using a Kendall slope estimator, but we preferred using the Kendall's rank correlation coefficient τ (Eq. 3.5) directly.

The seasonal approach compares events linked to the same seasonal phase (e.g. the first half of January); each scene is compared with the corresponding scene in other years but no cross-phase comparisons are made. In reality, phenological cycles vary in start and length according to the weather (Moulin *et al.*, 1997; Zhou *et al.*, 2001; Cleland *et al.*, 2007); such variability may produce trends that can be falsely interpreted as land degradation. Therefore, we propose a third method in which we use the SMK method to analyze trends by vegetation development stages (VDS) rather than by month or calendar day. This approach eliminates phenological shifts and variations in length of season (LoS). A linear model of yearly LoS values was used to find regions where greening or browning may be caused by a longer or shorter thermal growing season, and the coefficient of variation (CoV) was used as a measure of reliability: a large variation in the identified LoS might indicate limitations to the model's capability to extract phenological parameters, for instance as a result of multiple growing seasons or low seasonal amplitude.

The International Geosphere-Biosphere Program (IGBP) global land cover characteristics database (Loveland *et al.*, 2000) was used to calculate statistics of our results according to land-cover class. The 1km dataset was resampled to 8km resolution. In this process, the IGBP biome with the highest occurrence was assigned to each pixel (majority resampling). To minimize edge effects and mixed pixels, only

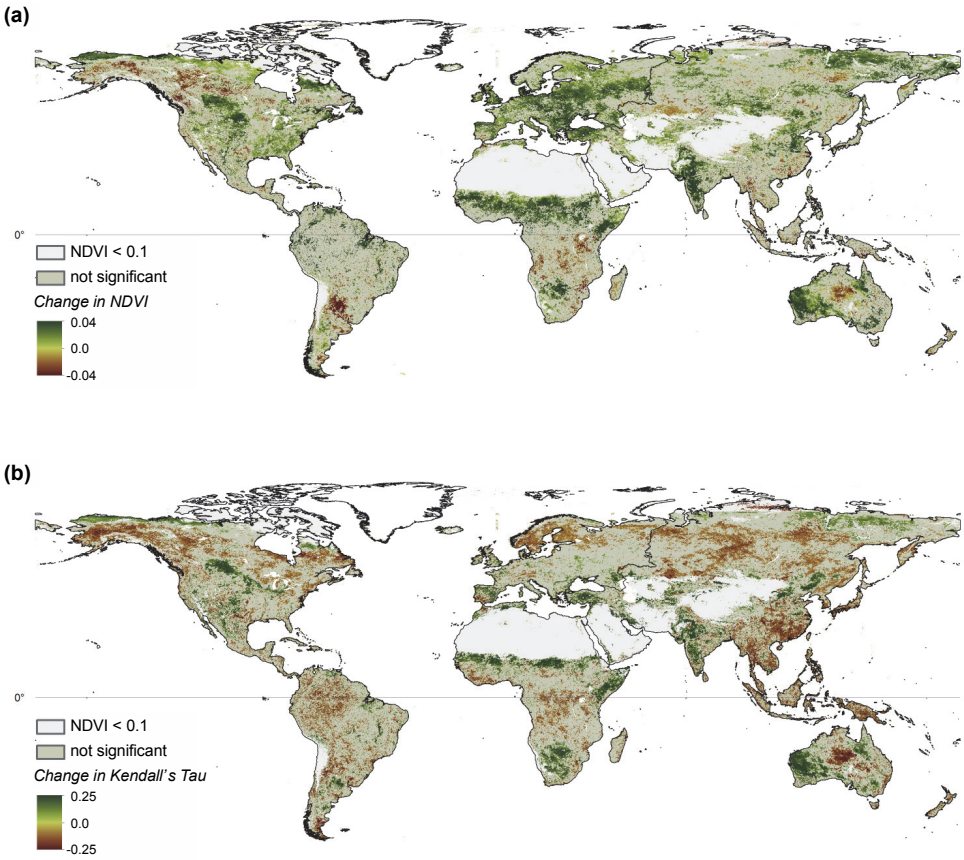

Figure 3.5 (a) Change in NDVI (dNDVI/dt, t in years), based on linear model of NDVI anomalies (1981–2006). (b) Kendall's tau from seasonal Mann-Kendall model on data adjusted by vegetation development stage (VDS). In both cases trends were assessed for significance ($\alpha = 0.1$) using analysis of variance (ANOVA). Weak trends were masked.

clusters of more than 50 adjacent pixels belonging to the same IGBP class were used in the calculation of statistics. A land-cover map, based on the same classification scheme but resampled to 0.5deg spatial resolution, is shown in Figure 6.1*a* (p. 98).

3.3 Results

3.3.1 Linear trends in NDVI anomalies

Figure 3.5*a* shows the results of the linear model based on the NDVI anomalies: green and red colors indicate greening and browning, respectively; areas with little or

no vegetation (NDVI < 0.1) were masked. Overall, greening predominates, especially in the Northern Hemisphere and most notably in the boreal forests, eastern Europe, Asia Minor, the Sahel, and western India. In the Southern Hemisphere, greening is apparent in Western Australia and Botswana; and browning in the tropical Africa and Indonesia / Oceania and in northern Argentina.

3.3.2 Seasonal trends in interpolated NDVI

The SMK model seconded some of the conspicuous regions of greening as identified by the linear model, including western India and the Sahel, but it showed a different picture for some other regions. In some cases the detected trend is even inverted (e.g. parts of Botswana, Nigeria, Argentina and Australia). With few exceptions, the absolute Kendall τ scores were not larger than 0.25, which indicates rather weak trends and therefore, the map is not illustrated here.

The extent to which the SMK model is influenced by phenological variations is determined by the variation in SoS (phenological shift) and LoS (variation in length of the growing season). If the growing season is stable, then the inter-annual VDS dates are close to each other, which is essential for the SMK model. Figure 3.6 shows the variation in LoS using the slope of the linear trend (days/year) analysis and the CoV. It is clear that the growing season is not stable everywhere: most regions showed a positive or negative trend in LoS (Figure 3.6*a*). This trend was significant (α=0.1) in parts of the Sahel, Asia, North-America and northern Europe, with lowest p-values in Sweden and Russia. The CoV values indicate that the extraction of LoS is stable (low CoV) across most of the Northern Hemisphere but less stable in the tropics and some parts of the Southern Hemisphere (Figure 3.6*b*).

3.3.3 Seasonal trends in phenology-adjusted NDVI

The map of Kendall's τ scores from the VDS model (Figure 3.5*b*) identifies the same areas of distinct greening but the absolute Kendall τ values are higher than those from the SMK model (commonly higher than 0.3 in areas with a greening or browning trend). Results from the VDS model should be interpreted in combination with the trend in LoS (Figure 3.6) because greening might be caused either by a longer growing season or by a higher rate of production. The former effect is not captured by this method because the data were adjusted for changes in length of growing season.

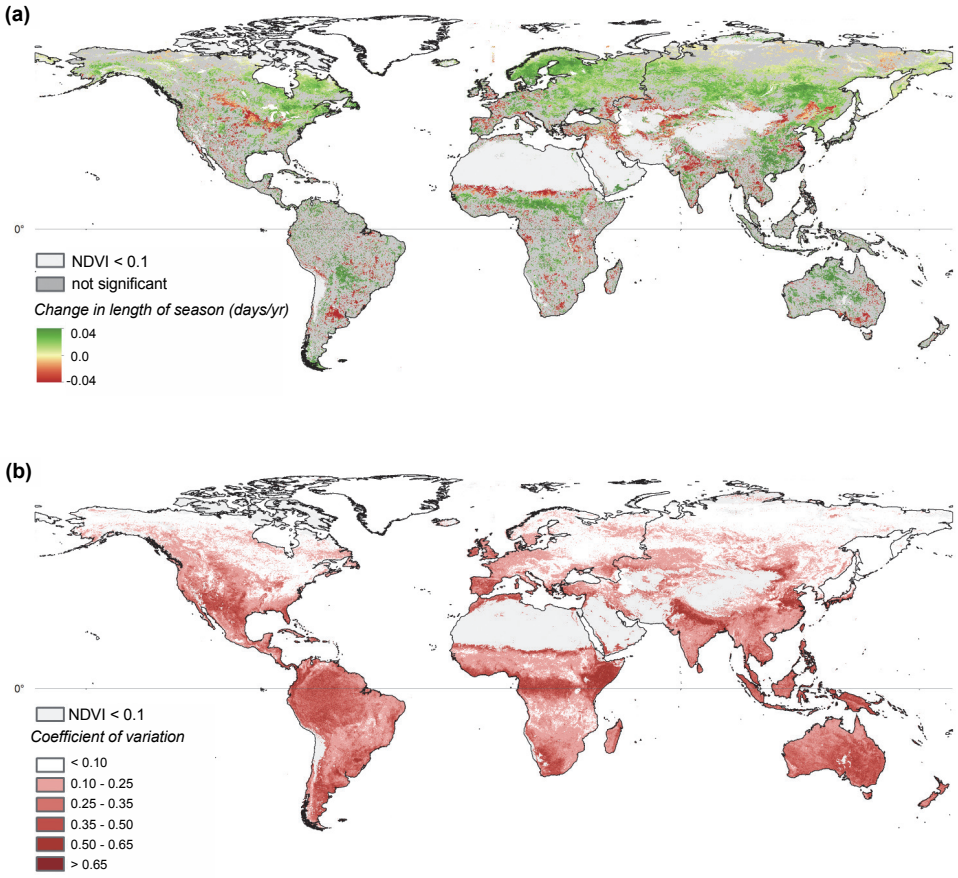

Figure 3.6 Change in length of growing season. (a) Magnitude of change in days per year; insignificant ($\alpha = 0.1$) changes were masked. (b) Coefficient of variation (standard deviation / mean) of the observed growing season length.

3.3.4 Significance of trends

In Figure 3.5, the non-masked pixels show significant trends, green indicates a positive trend and red a negative trend. The analysis of variance (ANOVA) of the LM results shows that the identified trends are significant in large parts of Europe, western India, Western Australia, the Sahel, Botswana and in some parts of Argentina, North America and Canada. Trends are weak in most tropical and tundra regions. The SMK model had non-significant values in most places and these results are not shown in Figure 3.5; only few pixels with significant trends were found in western India, Western Australia and parts of the Sahel and Asia Minor. The VDS

model was more powerful in rejecting the no-trend hypothesis: significant trends are revealed in the northern Sahel, Asia Minor, Scandinavia, Western Australia and Botswana and smaller parts of western India, China, Canada and the Horn of Africa (Figure 3.5*b*).

3.4 Discussion

3.4.1 Model results

The slopes found using the linear model and fortnightly NDVI values were very close to the linear trend analysis of yearly cumulative values published by Bai *et al.* (2008). On average, the difference in change is < 0.001 units and never as much as 0.01 units – which supports the contention that reducing the temporal resolution to yearly values and the choice of annual break-point does not affect the trend slopes (Dent *et al.*, 2009), given that the time series start and end in the same phase.

The SMK model is valid only when it is conceptually correct to compare measurements based on calendar date. In case of NDVI time series, this assumes that there is no phenological shift or variation in length of growing season throughout the measured period – which is not the case. Therefore, the SMK model identified only the most conspicuous greening regions; the likeliness (according to Kendall's τ) and significance (according to p-values) were generally low.

In the VDS model, Kendall's τ values were higher and p-values lower than in the SMK approach but VDS measures a different attribute of vegetation activity. The LM and SMK models use values with equal intervals (continuous fortnightly measurements) whereas VDS is based on an equal number of values for each growing season (the interval between these values might differ between years). Therefore, the VDS model does not show greening or browning associated with variation in growing season; it measures activity within a growing season (changes in *photosynthetic intensity*) rather than of the total yearly activity (changes in integrated NDVI).

3.4.2 Land-cover stratification

The LM indicated greening in all biomes except deciduous needle-leaf forest, where no trend was observed (Figure 3.7*a* no. 3). Figure 3.7*b,e* show that the LoS trend opposed the photosynthetic intensity trend in all biomes except shrubland and savanna. For cropland, the detected LoS trend was negligible. In all forest types but especially in Scandinavian boreal forest, the VDS model indicated a decrease in photosynthetic intensity which was counterbalanced by an overall increase in LoS (Figure 3.5*b* and Figure 3.6*a*). This might indicate that vegetation growth was no longer limited by temperature but by other constraining factors such as exhaustion of soil water or nutrients, which is in line with results from evapo-transpiration models

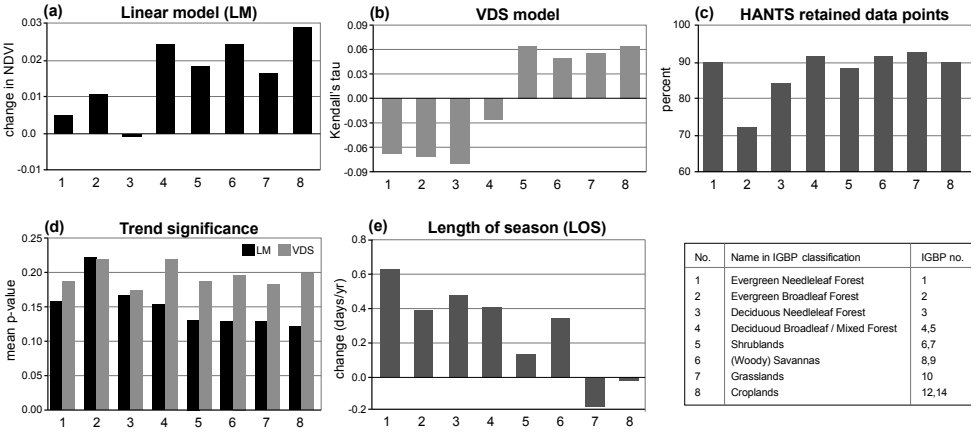

No.	Name in IGBP classification	IGBP no.
1	Evergreen Needleleaf Forest	1
2	Evergreen Broadleaf Forest	2
3	Deciduous Needleleaf Forest	3
4	Deciduoud Broadleaf / Mixed Forest	4,5
5	Shrublands	6,7
6	(Woody) Savannas	8,9
7	Grasslands	10
8	Croplands	12,14

Figure 3.7 Statistics based on selected IGBP land clover classes. (a) change in NDVI from linear model, (b) Kendall's tau of vegetation development stage (VDS) model, (c) Fraction of retained data points (RDP) from HANTS algorithm, (d) p-values of linear and VDS models, (e) change in length of growing season (LoS). Some land cover classes (Table 2) have been merged based on similar response. Classes which are not shown are: urban, snow and ice, barren / sparsely vegetated, permanent wetlands and water bodies.

(Zhang *et al.*, 2009). On the other hand, the significance of the trends appeared to be highest outside of the forest biomes (Figure 3.7*d*) but, as already remarked, the power of the LM might be over-estimated (the predictive power of the models used and the performance of HANTS are discussed in Section 3.4.4).

3.4.3 Assessment of greening and browning trends

All three methods agreed on a significant greening across western India, Western Australia, Asia Minor, parts of the Sahel, Canada and the USA. Validation, however, is a moot point. Even if field observations were available, they are usually limited to a few points in time that may not be representative for 8km pixels (Running & Nemani, 1988). We therefore compared our results with regional studies.

An inherent problem with time series is that the initial status is often not known. The Sahel, for instance, experienced severe droughts in the late 1960s, 1970s and the early 1980s (Nicholson, 2000; Zeng, 2003; Govaerts & Lattanzio, 2008); recovery from these droughts shows as greening that is confirmed by several studies (Anyamba & Tucker, 2005; Herrmann *et al.*, 2005; Olsson *et al.*, 2005; Heumann *et al.*, 2007) and there is controversy about this greening trend concealing the role of human-induced land degradation (Hein & de Ridder, 2006; Prince *et al.*, 2007). The VDS model showed strong positive trends in the northern parts of the Sahel, e.g. central Chad and northern Burkina Faso, indicating that greening is caused by a more intense growing season rather than a longer season, in line with recovery from drought. Greening in the Deccan thorn forests of west India can be explained, in part,

by recovery from degradation that occurred prior to the start of the GIMMS record (Champion & Seth, 1968); nowadays, parts of these shrublands are protected (Chape *et al.*, 2003) and recovering from human-induced degradation.

In Western Australia, Donohue *et al.* (2009) identified greening by an increase in fPAR (from AVHRR PAL) for the period 1981–2006; greening in north-eastern Australia is also in line with the increase in fPAR. In contrast, central Australia browned during this period; this might be explained by an 0.1 ºC/yr increase in temperature (Nemani *et al.*, 2003). Also in the Southern Hemisphere, there has been greening in Botswana, which is in line with the 1% yearly increase in NPP found by Nemani *et al.* (2003) using AVHRR data and a production-efficiency model.

In Canada and the USA, all models showed three notable greening regions: (1) the Low-Arctic tundra in Alaska, North West Territories and Yukon; (2) tundra and taiga east of Hudson's Bay; and (3) the prairie of southern Saskatchewan. These trends are most conspicuous in the VDS model and confirmed by other studies. Pouliot *et al.* (2009) used a similar Mann-Kendall approach with GIMMS data and found NDVI changes of about 0.01 units in all three regions. Goetz *et al.* (2005), using the same input data, confirm two out of three greening regions and also browning in Alaska, close to the British Columbia / Alberta border, and some parts of Quebec; they conclude that growth in tundra had increased due to rising CO_2 concentration and temperature but, in the boreal forest, various other factors including fire complicated the issue. Alcaraz-Segura *et al.* (2010) showed that the GIMMS dataset largely misses greening due to post-fire recovery. This is also mentioned by Neigh *et al.* (2008) who attribute greening of the tundra to an increase in temperature and associated growing season lengthening and greening of the prairies mainly to an increase in rainfall, which was the limiting factor for growth and lead to much higher crop yields and conversion of land to arable.

There is some discrepancy between the models for Eurasia. According to the linear model, greening prevailed over browning, most conspicuously towards the east, in line with the relation between PAL NDVI and land surface temperature (Julien *et al.*, 2006) – drier areas in the south have become hotter and even drier while northern Europe has become cooler. Stöckli & Vidale (2004) found a related positive trend in LoS of 1.4 days per year in central Europe (Germany) and a negative trend of -0.54 days per year in Scandinavia but our harmonic analysis showed an increase in LoS in Scandinavia (Figure 6), which might indicate warming (Hüttich *et al.*, 2007; Karlsen *et al.*, 2007). A longer growing season would explain the differences between the LM and the VDS model: greening due to a longer growing season does not necessarily produce a greater intensity of vegetation activity in the growing season. The VDS model showed a decline in vegetation activity in Scandinavia, whereas the LM showed a slight increase.

In their global assessment and in detail in China, Bai *et al.* (2008) and Bai & Dent (2009) used GIMMS data in another way to assess land degradation and

improvement. They applied a linear model but introduced additional criteria of rain-use efficiency and energy-use efficiency to screen NDVI trends caused by drought and climatic warming. By translating NDVI to NPP using the relationship with MODIS NPP data, they derived a tangible measure of severity that can be subjected to economic appraisal. For China, they concluded that land degradation is most conspicuous in the rapidly-developing humid south, rather than in the drylands of the north and west, where land reclamation initiatives have been concentrated. This conclusion is supported by our results from the LM and the VDS models.

3.4.4 Limitations and lessons learned

Harmonic analysis dealt effectively with some of the limitations of previous work that used yearly-aggregated NDVI data. HANTS removed cloud interference and eliminated the influence of phenological shift between the Northern and Southern Hemispheres – but it did not remediate inter-annual phenological shifts from which the LM and, especially, the SMK model suffer. This problem was targeted by the single-growing-season normalization used in the VDS method.

Serial autocorrelation remained an issue for short temporal lags with the use of the linear model (Figure 3.3). The reason for this resides in the fact that a possible deviation from the long-term norm is likely to show for much of the growing season under consideration, rather than for a single biweekly observation. Providing that seasonality is accounted for, the power of the statistical methods is mainly determined by the sample size. Serial auto-correlation is an issue if the value of a sample is partly determined by its neighbors – so a dataset with serial auto-correlation contains less information than one of the same length with truly independent samples. As such, serial auto-correlation spuriously inflates the power of the test (McBride & Loftis, 1994). It is a challenge to distinguish between *statistically significant changes* and *practically significant changes* and, in this sense, non-parametric models should be more robust than parametric models or, from a different perspective, the linear trend is more powerful in rejecting H_0 (Hirsch & Slack, 1984) – which might explain that the LM trends appear more significant (Figure 3.5).

The performance of HANTS is biome-dependent. Most IGBP biomes showed harmonic fits with more than 90% retained data points (Figure 3.7*c*) so the fitted NDVI curve lost less than 10% of the original observations. Exceptions are tropical evergreen broadleaf forest, deciduous needle-leaf forest, and shrubland. In the IGBP classification, latter includes most tundra – where NDVI is zero, or a *fill* value, under snow cover and increases quickly to high values upon snowmelt (a situation that would be better described by double logistic functions (Beck *et al.*, 2006). In the tropics, by contrast, NDVI is high throughout the year so noise in the phase-shift estimates makes it hard to extract phenological measures.

Better analysis requires a globally applicable method for deriving the start and length of growing season, which is neither simple nor straightforward (Hird & McDermid, 2009). With the HANTS technique used in this study, phenological measures can be derived automatically only for areas with a single annual growing season but it is essential to extract multi-season measures, for instance in eastern China, the Horn of Africa and the Indian Ganges plain. For these regions, Figure 6*b* shows a large coefficient of variation in the extracted LoS, probably caused by slight variations in the minimal NDVI between the growing seasons, which implies that, in one year, EoS occurs at the end of the first growing season and, in another year, at the end of the second season. This requires a procedure to extract multiple growth periods (e.g. Zhang *et al.*, 2003) and, ideally one globally applicable method. Although several methods are available, each is suitable for only one or few biomes. The method proposed by Geerken (2009), defining a set of reference curves, is a step towards global application.

Applying NDVI trends for land degradation assessment, definition of land degradation remains contentious. Since the initial status is often not known, greening might represent recovery from drought or other disturbance; and greening resulting from the replacement of old-growth forest by crops or grassland might be considered as either degradation or land improvement, depending on the researchers point of view. In the humid tropics, the NDVI proxy is less reliable due to saturation of the signal (Myneni *et al.*, 2002) and cloud cover; although most trends are in line with decreasing NPP (Nemani *et al.*, 2003), there are also contradicting trends.

At present, choice of NDVI time series presents a trade-off between temporal coverage and spatial resolution: between 10 years at 250–500m resolution (e.g. MODIS) or almost 30 years at 1–8km spatial resolution (AVHRR). The longer period captures more climatic cycles and significant changes in land use and management, but a single pixel might contain several land-use types or ecosystems. These datasets, nevertheless, are more suitable for capturing temporal dynamics.

We have assessed monotonic trends in NDVI but vegetation trends are often complex and breaks or interruptions of trends are common (Tucker *et al.*, 2001; Slayback *et al.*, 2003; Angert *et al.*, 2005; Xin *et al.*, 2008; Verbesselt *et al.*, 2010a). Major volcanic eruptions can cause sudden breaks in a trend; fast-acting climatic cycles like El Niño or broad-scale land management practices may bring about large fluctuations. Gradual changes may be associated with slow-acting climatic cycles or the accumulation of changes in management but these gradual changes might, ultimately, trigger a catastrophic shift in the ecosystem (Scheffer *et al.*, 2001). Trend breaks will be easier to identify within long time series of global observations.

3.5 Conclusions

We used harmonic analysis to enhance linear and monotonic trend analysis of GIMMS NDVI time series. Greening and browning trends were revealed but these could not be quantified unambiguously. Variations in phenology confused simple greening or browning trends but this aspect may be illuminated by using the seasonal Mann-Kendall (SMK) model with normalization of the growing season using vegetation development stages (VDS), rather than analysis by calendar day. The VDS model showed that greening or browning depends on growing intensity as much as yearly-aggregated NDVI.

At global scale, phenological shifts and variation in length of growing season render comparisons of NDVI values by calendar date unsatisfactory. However, it is difficult to extract phenological measures using a generalized method; the explaining power of the VDS model may be increased by, for instance deriving these measures by several methods, according to the phenology or climate zone, but this has yet to be undertaken.

Linear-model slopes derived from anomalies between long-term and yearly harmonic fits hardly differ from the slopes of yearly-aggregated NDVI data – so it unlikely that aggregating to yearly values severely influences NDVI trend analysis. However, the explaining power will decrease with a decreasing number of observations.

All models were consistent in detecting a greening trend in western India, the Sahel and parts of Asia Minor, Canada, northern China and Western Australia; the land-cover classes showing most conspicuous greening were shrubland, savanna and cropland.

Acknowledgements

This work is partly financed through FAO contract PR35852. The authors thank Zhanguo Bai for providing data and results from previous studies. We appreciate the NASA GIMMS group providing the latest version of their NDVI data set. We also thank the reviewers for their helpful comments.

Chapter 4

Linear trends in seasonal vegetation time series and the modifiable temporal unit problem

Rogier de Jong, Sytze de Bruin

"Numbers do not lie, but they have the propensity to tell the truth with intent to deceive."

Eric Temple Bell (1986)
Men of Mathematics.

This chapter is based on:
Biogeosciences, 9 (2012), pp. 71-77
DOI: 10.5194/bg-9-71-2012

Abstract

Time series of vegetation indices (VI) derived from satellite imagery provide a consistent monitoring system for terrestrial plant productivity. They enable detection and quantification of gradual changes within the time frame covered, which are of crucial importance in global change studies, for example. However, VI time series typically contain a strong seasonal signal which complicates change detection. Commonly, trends are quantified using linear regression methods, while the effect of serial autocorrelation is remediated by temporal aggregation over bins having a fixed width. Aggregating the data in this way produces temporal units which are modifiable. Analogous to the well-known modifiable areal unit problem (MAUP), the way in which these temporal units are defined may influence the fitted model parameters and therefore the magnitude of change detected. This chapter illustrates the effect of this modifiable temporal unit problem (MTUP) on a synthetic data set and an actual VI data set. Large variation in detected changes was found for aggregation over bins that mismatched full lengths of vegetative cycles, which demonstrates that aperiodicity in the data may influence model results. Using 26 years of VI data and aggregation over full-length periods, deviations in VI gains of less than 1% were found for annual periods (with respect to seasonally adjusted data), while deviations increased up to 24% for aggregation windows of 5 years. This demonstrates that temporal aggregation, even for bins corresponding to full calendar years, needs to be carried out with care in order to avoid spurious model results.

4.1 Introduction

Vegetation systems provide a quick and measurable response to many environmental changes at a wide range of spatial and temporal scales. The availability of historical time series from satellite observations with daily global coverage makes operational monitoring of vegetation condition a matter of detecting and interpreting changes within these datasets. Change detection, however, is often complicated by a number of statistical preconditions that are intrinsic to time series of spectral vegetation indices with dense sampling intervals. Literature is replete with the most frequently used approach for detecting temporal trends, i.e. fitting linear regressions of a (temporally aggregated) vegetation index (VI) against time (Paruelo *et al.*, 2004; Herrmann *et al.*, 2005; Olsson *et al.*, 2005; Heumann *et al.*, 2007; Bai *et al.*, 2008), but this needs to be done with care in order to avoid spurious trends. The detected slope (or gain) coefficient can be used to calculate the amount of change, but it is not always tested for significant deviation from zero, nor are standard statistical assumptions always respected (de Beurs & Henebry, 2005a). Seasonal variation is an important cause for the data to violate assumptions like homogeneous variation and absence of serial correlation in the residuals. In few cases linear models were fitted directly to seasonal data (e.g. Pelkey *et al.*, 2000), but seasonality is typically remediated using temporal aggregation, where the aggregation window (or bin size) corresponds to the length of a calendar year. The resulting bins can be regarded as temporal units, which, like spatial units, are modifiable (Taylor, 2010). In case of spatial units, it has been demonstrated that the size may influence the model results, which is known as the modifiable areal unit problem (MAUP) (Openshaw & Taylor, 1979). This problem may affect a myriad of spatial studies in geography (Dark & Bram, 2007) and remote sensing (Marceau *et al.*, 1994). Similarly, there is a modifiable temporal unit problem (MTUP) that is as troublesome as the MAUP, as it essentially entails the question of scale in the temporal dimension (Çöltekin *et al.*, 2011). In analysis of time series of satellite vegetation indices this problem is easily disregarded, although it may result in misjudgements of temporal trends in the data. Aspects of the problem include the starting phase of a time series or segment, its extent and the level of temporal aggregation. Some studies, which analyse temporal trends in vegetation activity, have been debated in literature, in part because of such issues (Wessels, 2009; Samanta *et al.*, 2011). The aim of this paper is to demonstrate possible MTUP effects in analysis of time series of satellite imagery using both real and simulated VI data and to provide, in this sense, a framework for linear time-series regression.

4.2 Data and methods

4.2.1 Trend analysis and the modifiable temporal unit problem

Many trend analysis methods exist, including parametric and non-parametric approaches. The most common method to detect changes in cyclic time series is the use of a linear model (Equation 4.1) obtained using ordinary least-squares (OLS) regression. The slope coefficient β, or gain, was used to calculate the change in Y as β times the number of bins. This number is determined by the aggregation level (or: number of observations per bin), which is equivalent to the sample interval. Given that the datasets consist of 24 observations per year, aggregation level 24 corresponds to yearly bins and so on.

$$y = a + \beta t + \omega_t \tag{4.1}$$

Where ω_t, the residual, is ideally independent and identically distributed (iid), i.e. white noise. The dependent variable Y can be any kind of VI or cyclical environmental parameter in general. The most common spectral vegetation indices are based on the rapid change in reflectance of chlorophyll between the red and near infrared (NIR) ranges. Here, we used the normalized difference vegetation index (NDVI), which is a commonly used proxy for terrestrial photosynthetic activity. A decrease over time is referred to as browning, whereas an increase indicates greening (de Jong *et al.*, 2011a). Given this, we used a three-step approach to demonstrate the MTUP effect:

(step 1) The influence of starting phase and data extent is illustrated using a perfectly harmonic model, without trend or noise components. Using a sample size of 24 observations per cycle this implies that the model residuals are far from independent, which invalidates linear regression by OLS. However, it provides a theoretical scenario to demonstrate our point that spurious slopes can be detected from cyclical data.

(step 2) Next, the sample was aggregated into bins of fixed width. These bins represent different temporal units (or aggregation levels). The MTUP effect is demonstrated by calculating the change in NDVI from linear models (Equation 1) fitted for different bin sizes. The minimum number of bins over the full length of the synthetic time series was set to 5.

(step 3) Finally, step 2 was repeated using actual data from Advanced Very High Resolution Radiometer (AVHRR) sensors. The detected

changes were compared to the corresponding change obtained using seasonally adjusted data without temporal aggregation. The seasonal adjustment was carried out using a Fourier method (Roerink et al., 2000) with four components, following de Jong *et al.* (2011a). The significance of the slopes in the seasonally adjusted data was assessed using generalized least-squares (GLS) in order to account for remaining short-lag serial correlation. A sample of 1,000 pixels was used for calculation of deviations introduced by the MTUP and the state of Queensland in north-eastern Australia was used to illustrate possible spatial patterns introduced by different temporal aggregation schemes.

Provided that the level of serial autocorrelation can be disregarded after aggregation, the significance of the detected trends can be tested using OLS-based t-tests conform the hypotheses H0: $\beta = 0$ and HA: $\beta \neq 0$. Analogous to step 3 (described above), we used GLS-based tests to account for remaining serial autocorrelation. Slopes coefficients beyond the 0.05 confidence level were considered significant. All analyses were performed using standard R functionality (R Development Core Team, 2011).

4.2.2 Time-series data

Synthetic data

Synthetic time series were used to illustrate the effect of cyclic data on regression analysis. For this purpose, model parameters were chosen in such a way that they approximate the AVHRR time series described below for a temperate (non-forest) environment with a single growing season. As such, the peak-to-peak amplitude was set to 0.6 – fluctuating around a mean of 0.4 – and the number of observations per year to 24. NDVI (Y) was simulated using a cosine model with no underlying positive or negative trend (Equation 4.2*a*). In this equation, *a* denotes the amplitude, *t* the radians equivalent of the observation number (*x*) (Equation 4.2*b*) and Φ the phase shift.

$$y_t = \bar{y} + a \cdot \cos(t + \Phi) \qquad (4.2a)$$

$$t = x / 24 \cdot 2\pi \qquad (4.2b)$$

AVHRR data

The longest run of NDVI measurements is available from AVHRR sensors on board a series of National Oceanic and Atmospheric Administration (NOAA) satellites. Acquisition started in 1981 and is still on-going, but pre-processed datasets are for

now available until the year 2006. Pre-processing includes correction for orbital decay, satellite changes and several atmospheric effects. The resulting NDVI values were aggregated into biweekly composites with ~8km spatial resolution. The full description of the dataset and the processing steps is provided by Tucker *et al.* (2005). A sample of 1'000 pixels was used for the MTUP analysis. Other vegetation indices, including the enhanced vegetation index (EVI) or the soil-adjusted vegetation index (SAVI), have similar statistical characteristics and therefore the problem described here is not restricted to NDVI.

4.3 Results and discussion

4.3.1 Synthetic data

In case of seasonal data with a dense sampling interval, both starting phase and extent influence the linear model. Figure 1*a* illustrates the *ad absurdum* case that a fit on a perfectly harmonic model without linear trend results in a range of slope coefficients – positive or negative, varying with the starting phase – but never zero. Zero slopes are obtained only if both sides of a minimum or a maximum are equally sampled. This might, however, result in over- or underestimation of the mean NDVI from the model intercept (α). The slope coefficient is linearly related to the amplitude used for the seasonal model and is inversely related to the extent of the time series (or segments). The latter is illustrated in Figure 4.1*b*, which shows 4 different extents (respectively 2, 4, 6 and 8 years) and the associated linear models for a given starting phase.

The slope coefficient changed with the level of temporal aggregation, which influenced the detected change in NDVI. This is illustrated in Figure 4.2 using a similar synthetic data set as above but now having a length of 26 full cycles, which is comparable to that of AVHRR datasets. The variation in detected NDVI change increased with the level of aggregation, which resulted in larger uncertainty in model predictions. The true change in NDVI (i.e. zero) is only obtained by aggregation over complete cyclic periods, i.e. 1 or more years. Given the perfect periodicity of this synthetic example, this is true by definition, but in reality calendar years may not fit the periodicity of VI time series because of shifts in vegetation phenology and variations in growing season length. For this reason, the same analysis was also performed on actual AVHRR time series (see Section 4.3.2).

As mentioned, the starting phase and extent influence each segment of the linear analysis. The effect reduces with longer extents, but it appeared that the change for the longest available run of NDVI data (AVHRR) is of the same magnitude as changes found by trend studies which account for seasonality (e.g. Zhou *et al.*, 2001; de Jong *et al.*, 2011a; Wang *et al.*, 2011). Table 4.1 lists the calculated changes in NDVI for a perfectly periodic model without trend component (Figure 4.1) for time

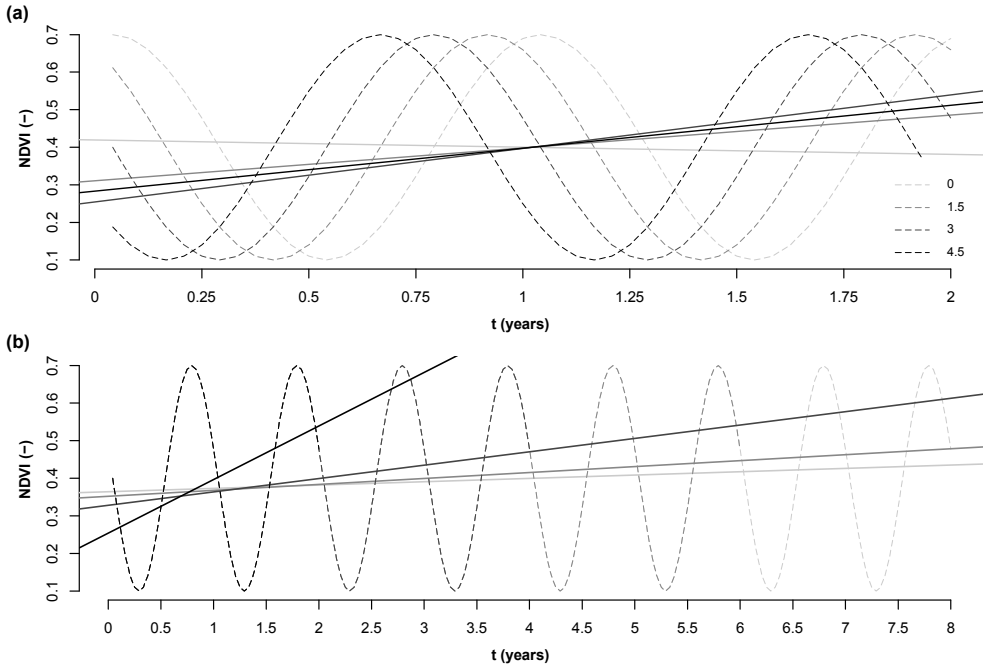

Figure 4.1 The effect of phase shift (a) and extent (b) on linear regression of NDVI against time for seasonal data. The legend in (a) shows the phase shift in months. In (b), each shade of grey represents an additional extent of 2 years. Accordingly, black to light grey refer to extents of 2, 4, 6 and 8 years respectively.

spans of AVHRR (26 years), MODIS (11 years) and 1 year. The seasonal peak-to-peak amplitude was set to 1 for ease of comparison to other amplitudes. Given that the order of maximum change reported in literature is $\sim 4.0 \times 10^{-2}$ for AVHRR data, trends induced by phase shift might introduce errors varying from 10% to 90% if seasonality is not accounted for.

	change in NDVI * 100		
phase shift (months)	*26yr*	*11yr*	*1yr*
0	-0.48	-1.14	-12.52
1.5	2.24	5.30	58.40
3	3.65	8.63	95.11
4.5	2.92	6.91	76.11
6	0.48	1.14	12.52
7.5	-2.24	-5.30	-58.40
9	-3.65	-8.63	-95.11
10.5	-2.92	-6.91	-76.11

Table 4.1. Detected changes in NDVI using linear regression on synthetic seasonal data for different starting phases and extents. Change values were calculated as the slope coefficient β (Eq. 4.2) times the length of the time series and were multiplied by 100 for numerical convenience. The lengths of 26 and 11 years (yr) correspond to the approximate length of AVHRR and MODIS time series respectively. The applied harmonic model had peak-to-peak amplitude 1 for which values can be multiplied by the actual amplitude. Due to serial autocorrelation, *t*-values could not be calculated.

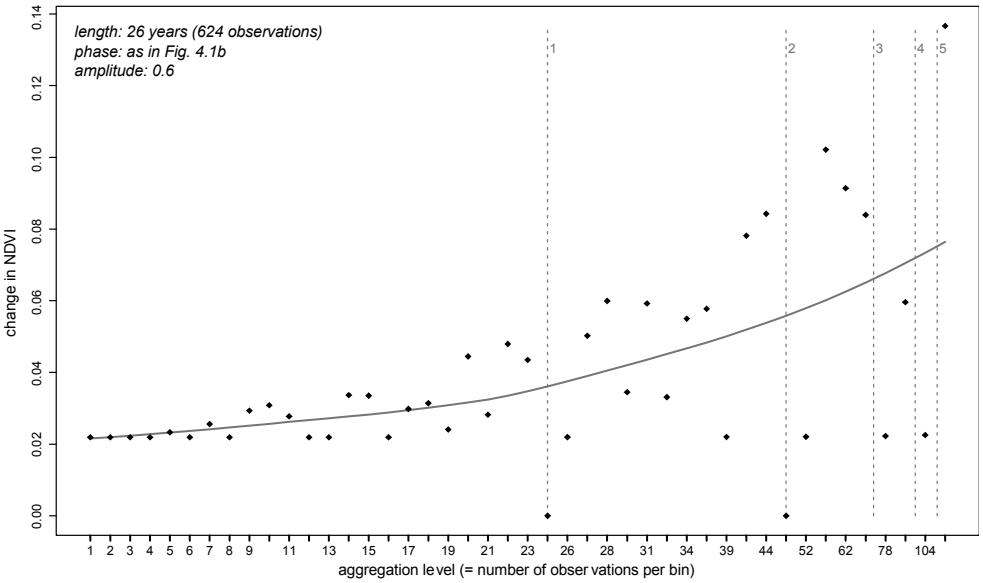

Figure 4.2 Change in NDVI detected using linear models depending on the temporal aggregation level. The plot illustrates the MTUP effect for a harmonic model of 26 years (length of common AVHRR datasets) and an amplitude of 0.6 NDVI units. The points shown are the ones that resulted in a change in the number of bins, while increasing the aggregation level. The vertical dotted lines indicate aggregation levels corresponding to 1, 2, 3, 4 and 5 years respectively and the grey line shows a LOESS curve indicating an average trend.

4.3.2 AVHRR data

An example of the MTUP effect for an AVHRR pixel with a significant ($p < 0.05$) trend component is shown in Figure 4.3. The change in NDVI was found to vary among aggregation levels: slight differences with respect to seasonally adjusted data occurred for 1 or 2-year windows and substantial differences for all other cases. This illustrates that aperiodicity in the data or in the aggregation window might result in considerable deviations from the change in NDVI found using seasonal correction instead of temporal aggregation.

If temporal aggregation is used to account for seasonality, the characteristics of the commonly used harmonic functions dictate the use of whole periods as aggregation windows, in order to force the deviation in slope coefficient to zero (Figure 4.2). Aiming for bins holding complete seasons, the MTUP analysis was carried out on AVHRR data for aggregation levels of exactly 1 to 5 calendar years. It appeared that the significant changes in NDVI (i.e. significant for all aggregation levels) varied considerably with respect to trend analysis with seasonal adjustment instead of temporal aggregation. Table 4.2 lists the mean deviation and mean absolute deviation for the AVHRR sample and for the example in Figure 4.3. This table shows that the mean deviation and the variation for the sample are low (around

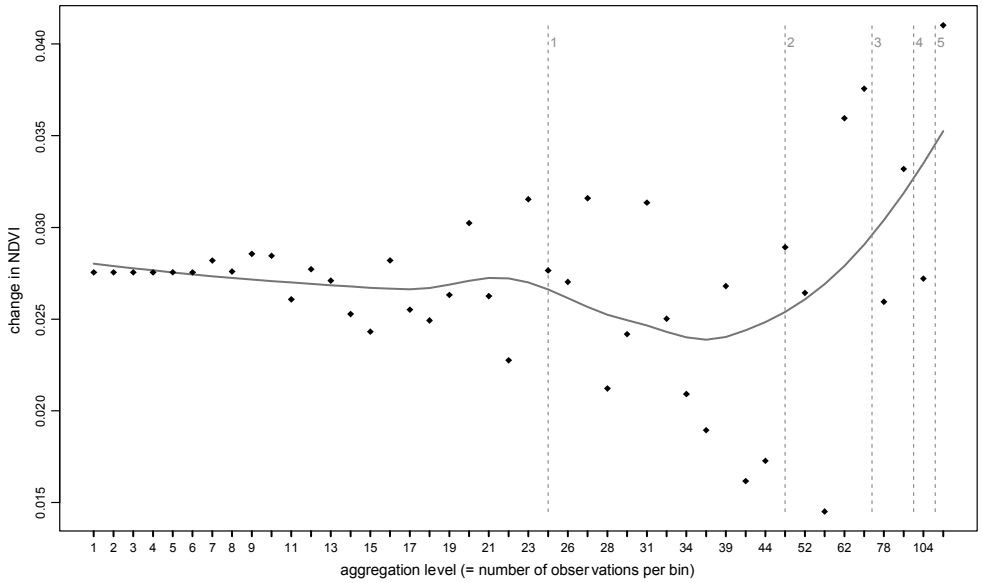

Figure 4.3 Change in NDVI detected using linear models depending on the temporal aggregation level. The plot illustrates the MTUP effect for an AVHRR pixel with significant ($p < 0.05$) trend component (location: 46.21N/110.65E, Montana, USA). See the caption of Figure 4.2 for additional information and Table 4.2 for the NDVI values corresponding to full-year aggregation levels.

1%) for fine aggregation levels but considerably higher in case of coarser aggregation: a mean absolute deviation of 24 per cent was found for 5-year aggregation. In few cases the detected change in NDVI switched between positive (greening) and negative (browning), although these trends could not be confirmed using significance tests. It was almost exclusively found that the amount of detected change increased with the level of aggregation, so greening and browning trends appeared stronger after aggregation. Figure 4.4 illustrates this by showing spatial patterns of deviations for the state of Queensland in Australia. The different panels show the change in NDVI with respect to the change detected without temporal aggregation. Spatial patterns are hardly perceivable at fine temporal aggregation levels, but they become apparent at coarser levels.

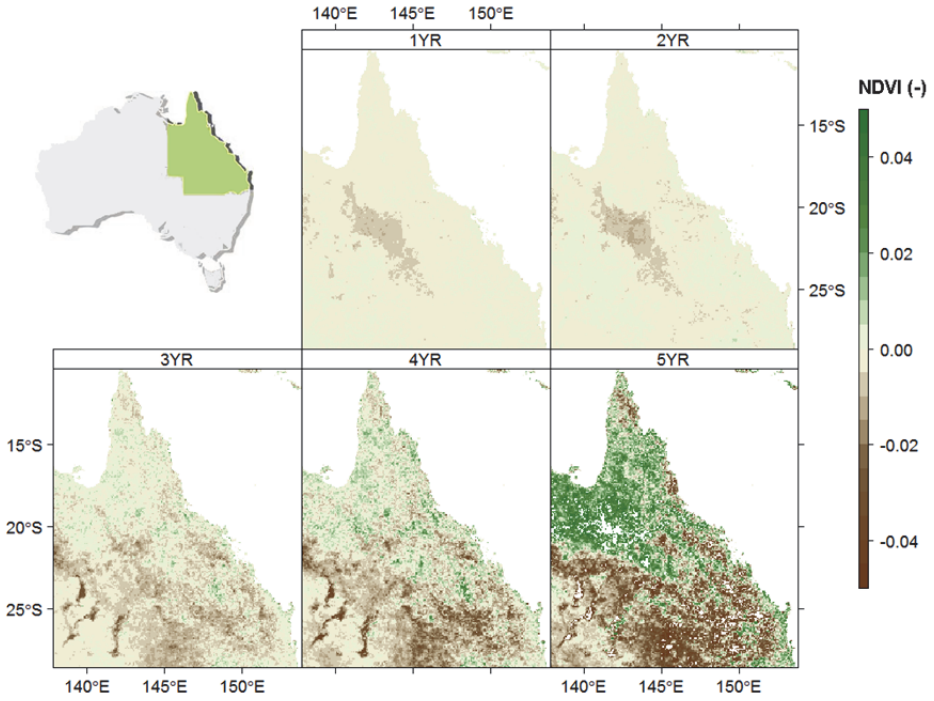

Figure 4.4 Detected changes in NDVI for different levels of temporal aggregation – example for Queensland (Australia). The top-left map shows the location of Queensland and the 5 panels show the change in NDVI with respect to changes found using seasonal adjustedment without temporal aggregation. The aggregation levels correspond to 1, 2, 3, 4 and 5 years (YR) respectively.

Temporal aggregation will only lead to unbiased estimates of VI trends if the following requirements are met:

1. The regarded time series is perfectly periodic. Any type of aperiodicity, including phase shift or incomplete periods at the start or end, may result in incorrect model parameters.

2. The aggregation level corresponds exactly to the period of the seasonal signal (often one calendar year). Aggregating over multiple periods increases the risk of MTUP effects.

Other analysis methods may implicitly require similar conditions. For example, non-parametric trend tests such as the seasonal Mann-Kendall method (Hirsch & Slack, 1984) and related slope estimators like Theil-Sen selection (Birkes & Dodge, 1993) rely strongly on the absence of seasonal changes. In case of vegetation indices, this assumption often renders the method unsuitable for large spatial and temporal scales (de Jong *et al.*, 2011a). The results from this study indicate that similar effects may disturb linear regression. The effects, however, may not be as conspicuous because parametric models are less robust against this type of error than non-parametric models (McBride & Loftis, 1994). Seasonally adjusting the data using a decomposition method (e.g. Cleveland *et al.*, 1990) provides another approach for eliminating serial autocorrelation and the MTUP. In that case, the seasonal model used should be appropriate for the growing regime and ideally should take possible seasonal changes into account. An example of such an approach is provided by Verbesselt et al. (2010b). Yet other methods to describe seasonal time series include data generating processes without the use of deterministic functions. Changes in NDVI are likely to persist from one period to the next. As such, it may be reasonable to represent the process using an autoregressive (AR) model (Equation 4.3).

$$y_t = \sum_{i=1}^{p} \alpha_i \cdot y_{t-i} + \omega_t \tag{4.3}$$

Where p represents the autoregressive order (or maximal lag), α_i are stochastic model parameters and ω_t is white noise (Cowpertwait & Metcalfe, 2009). Under these conditions, fitting a temporal trend to y_t (e.g. using Eq. 4.1) will generate misleading results termed *spurious regressions* (Granger & Newbold, 1974). The spuriousness resides in the effect of autocorrelated residuals which bias the test towards rejection of the null hypothesis, even when the series are generated as

Table 4.2 The MTUP effect for a sample of 1'000 AVHHR pixels and aggeregation levels (AL) of 1 to 5 years. Detected changes in NDVI (dNDVIagg) were compared to those found using seasonally adjusted data (dNDVIref) and listed as dNDVIagg–dNDVIref (*dNDVI*), dNDVIagg/dNDVIref (*pct*) and square root of the sample variation of pct (*sd*). The last columns list the detected changes in NDVI for the pixel in Figure 4.3. In all cases, slopes were significant ($p < 0.05$). NDVI values were multiplied by 100 for numerical convenience.

	mean deviation			**mean absolute deviation**			**Figure 3**	
AL (yr)	dNDVI	pct	sd	dNDVI	pct	sd	NDVI	pct
0							2.75	
1	0.015	100.5%	1.6%	0.044	101.0%	1.3%	2.77	2.0%
2	0.019	100.6%	3.0%	0.084	102.2%	2.2%	2.89	14.0%
3	-0.016	102.4%	9.0%	0.264	107.2%	5.8%	2.96	21.0%
4	0.022	105.4%	15.7%	0.469	112.9%	10.5%	3.47	72.0%
5	0.066	106.6%	31.4%	0.950	124.1%	21.1%	2.28	-47.0%

statistically independent random walks (Phillips, 1986). This problem is analogous to the MTUP effects described in Section 4.3.1 and will be subjected to the effects described in Section 4.3.2, were y_t temporally aggregated before fitting the temporal trend.

Using temporal aggregation, slopes may be found significant at a given aggregation level while not at another level. False positives (trend is found to be significant while it is not in reality) are likely to occur more frequently at low aggregation levels, but examples of the opposite case were found as well (not shown). If the significance of trends is not considered in the analysis, the MTUP may not only affect the amount but also the sign of detected changes in NDVI. These effects can be expected to be largest in regions with high seasonal amplitudes. MTUP as described here cannot affect analysis of time series without seasonal amplitude, e.g. in dense tropical forests or very sparsely vegetated areas. On the other hand, the use of vegetation indices is such regions is disputed; either because of signal saturation issues (Huete *et al.*, 1997) or because of over-estimation of NDVI or related parameters (Fensholt *et al.*, 2004).

4.4 Conclusions

Ordinary least squares (OLS) time series regression can be used to quantify trends in cyclic data but temporal aggregation needs to be carried out carefully in order to avoid spurious results. The risk of artefacts is minimal at an aggregation level corresponding to a full period, for instance a calendar year. Coarser aggregation levels tend to overestimate the magnitude of change and result in higher variation in model predictions, especially from 3 periods onwards. However, the use of a full-period window may be impractical because VI time series are hardly ever free of changes in seasonality. Aperiodicity within long-term time series of vegetation indices is intrinsic to certain land cover types and may arise from variations in start and length of growing seasons as a result of variations in temperature and/or precipitation. The starting phase and the choice of aggregation level – or temporal unit – affect the estimation of model parameters, including the slope coefficient or gain. In this study, the amount of absolute change that was attributed to the modifiable temporal unit problem (MTUP) varied between 1% and 24% for full-period aggregation levels.

Acknowledgements

We would like to thank the editor of Biogeosciences and the anonymous reviewers for their constructive comments to earlier versions of the manuscript.

Chapter 5

Trend changes in global greening and browning: contribution of short-term trends to longer-term change

Rogier de Jong, Jan Verbesselt, Michael E. Schaepman, Sytze de Bruin

"Each time wave has its own driver and its own cyclicity. A composite curve, originating from integration of all individual cycles, like the climate curve, can only be accurately extrapolated if all individual components are known. As long as this is not the case, it cannot be determined when the next trend break will occur. ... 'Punctuated cyclicity' one could call it, with a blink at Eldredge and Gould"

[my English, original text in Dutch]

Salomon Kroonenberg (2006)
De Menselijke Maat (The Human Measure)

This chapter is based on:
Global Change Biology, 18 (2012), pp.642-655
DOI: 10.1111/j.1365-2486.2011.02578.x

Abstract

Field observations and time series of vegetation greenness data from satellites provide evidence of changes in terrestrial vegetation activity over the past decades for several regions in the world. Changes in vegetation greenness over time may consist of an alternating sequence of greening and/or browning periods. This study examined this effect using detection of trend changes in Normalized Difference Vegetation Index (NDVI) satellite data between 1982 and 2008. Time series of 648 fortnightly images were analyzed using a trend breaks analysis (BFAST) procedure. Both abrupt and gradual changes were detected in large parts of the world, especially in (semi-arid) shrubland and grassland biomes where abrupt greening was often followed by gradual browning. Many abrupt changes were found around large-scale natural influences like the Mt Pinatubo eruption in 1991 and the strong 1997/98 El Niño event. The net global figure – considered over the full length of the time series – showed greening since the 1980s. This is in line with previous studies, but the change rates for individual short-term segments were found to be up to 5 times higher. Temporal analysis indicated that the area with browning trends increased over time while the area with greening trends decreased. The Southern Hemisphere showed the strongest evidence of browning. Here, periods of gradual browning were generally longer than periods of gradual greening. Net greening was detected in all biomes, most conspicuously in croplands and least conspicuously in needleleaf forests. For 15% of the global land area, trends were found to change between greening and browning within the analysis period. This demonstrates the importance of accounting for trend changes when analyzing long-term NDVI time series.

5.1 Introduction

Over the last decades of the 20th century, terrestrial ecosystems acted as net carbon sink, as evidenced by ecosystem process models and satellite vegetation data (Myneni *et al.*, 1997; Schimel *et al.*, 2001; Zhou *et al.*, 2001). The easing of climatic constraints on plant growth as a result of increased CO_2 concentrations and higher temperatures is a likely explanation for this effect (Nemani *et al.*, 2003). Indications for increased biological activity were found in the Northern Hemisphere between 35° and 75° latitude (Zhou *et al.*, 2001; Slayback *et al.*, 2003) and in several hot-spot regions, including the Sahel (Olsson *et al.*, 2005; Fensholt *et al.*, 2009) and parts of Australia (Donohue *et al.*, 2009). On the other hand, many forested biomes experienced a decline in biological activity (de Jong *et al.*, 2011a) and especially large parts of the boreal forests showed evidence of this, likely driven by late summer drought (Goetz *et al.*, 2005). Since instrument measurements began, record high global mean temperatures were reached in the past decade (Hansen *et al.*, 2010). This was found to induce a drying trend and a productivity decline in large parts of the Southern Hemisphere (SH), which counterbalanced the Northern Hemisphere (NH) green-up and resulted in a net global reduction in productivity (Zhao & Running, 2010). These findings may indicate a major change in the global greening regime. However, such trends may not be significant at large temporal extents and productivity estimates are often highly uncertain (Samanta *et al.*, 2011). For this reason, there is a need to better understand the temporal and spatial dynamics of ecosystem productivity (Sjöström *et al.*, 2011). The focus regarding such environmental changes is shifting towards increasingly large spatial and temporal extents (Niemi & McDonald, 2004; Pettorelli *et al.*, 2005; Verbesselt *et al.*, 2010a). As a result, long-term trends (i.e. time scales of decades) are becoming more likely to be composed of more extreme shorter-term changes (i.e. several years), which might balance themselves out. An analysis of this effect at global scale is presented in this study.

A common way to derive indicators on environmental change is the use of spectral vegetation indices (Pettorelli *et al.*, 2005). Such indices, based on the red / near infrared spectral region, are indicative of chlorophyll abundance and as such correlate to vegetation amount and photosynthetic capacity (Myneni *et al.*, 1995). Positive and negative changes in time can be referred to as *greening* and *browning* respectively. Here, time series of satellite data are particularly valuable because they provide a monitoring system with repeatable vegetation index (VI) measurements at scales at which climate- and human-induced changes take place (e.g. Wessels *et al.*, 2007). Detecting changes within the time series is the first step towards assessing their environmental impact or attributing drivers or acting processes. Changes within VI time series can be divided into three major classes (Verbesselt *et al.*, 2010a):

seasonal changes, gradual changes and abrupt changes. The first type occurs when the land surface phenology changes, e.g. driven by temperature or rainfall, without necessarily affecting the underlying trend component. For example, earlier onset of greening in spring might be counterbalanced by lower productivity late summer (Angert *et al.*, 2005). The gradual and abrupt changes refer to the trend component beyond the seasonal variation. Slowly acting environmental processes, including climate change, certain land management practices or land degradation, may cause *gradual changes* in the time series. Over time, these gradual changes may stall or reverse (Scheffer *et al.*, 2001; Zhao & Running, 2010), which involves a trend break. Following Verbesselt *et al.* (2010a), we define such an event, together with the associated magnitude and/or change in direction, as an *abrupt change*. Abrupt changes can also be induced by land-use changes (Turner *et al.*, 2007), wildfires (Kasischke *et al.*, 1993; Boles & Verbyla, 2000), floods (Domenikiotis *et al.*, 2003) or other fast-acting processes (Potter *et al*., 2003). The nature of abrupt and gradual changes can be further illustrated by the equilibrium concept. Vegetation systems are dominated by negative feedbacks, for which they are in equilibrium. This implies some sort of balance as well as the maintenance of that balance (Inkpen, 2005). The seasonal variation around an invariant mean provides the basis for a steady-state equilibrium, while changes in the mean render equilibriums either dynamic (gradual changes) or meta-stable (abrupt changes). This study focused on these abrupt and gradual VI changes.

Previous regional and global studies showed trends in vegetation activity using VI time series from spaceborne sensors like the American AVHRR (Advanced Very Hight Resolution Radiometer) and MODIS (Moderate Resolution Imaging Spectrometer) or the French VEGETATION sensor onboard SPOT (Satellite Pour l'Observation de la Terre). The direction and rate of change – together referred to as trend – have commonly been determined by the slope of a linear regression model in which the VI values or derived metrics depend on time (e.g. Paruelo *et al.*, 2004; Herrmann *et al.*, 2005; Olsson *et al.*, 2005; Heumann *et al.*, 2007; Bai *et al.*, 2008). As a next step, trend changes may be considered within the analysis for closer relation to the system dynamics. In the case of trends in vegetation productivity since the early 1980s, many areas in the world are known or expected to show trend changes (Schimel *et al.*, 2001; Slayback *et al.*, 2003; Angert *et al.*, 2005; Wang *et al.*, 2011). For instance, trend changes were found early 1990s in the Northern Hemisphere (Slayback *et al.*, 2003), possibly related to the June 1991 Mount Pinatubo eruption, which depressed incoming short-wave radiation and caused an anomalous cooling (Stenchikov *et al.*, 1998; Lucht *et al.*, 2002). Furthermore, the Northern Hemisphere greening seems to have stalled or even reversed towards browning in the last decade (Zhao & Running, 2010; Wang *et al.*, 2011). All this illustrates the critical need for a consistent global assessment of trend changes within long-term vegetation time series. Here, we applied a data-driven change detection

approach that is capable of quantifying trend changes without prior knowledge on location or timing. Regions in the world where trend changes have occurred were identified and net greening and browning for the 1982–2008 period was derived from a sequence of abrupt and gradual trend changes.

5.2 Methods

5.2.1 NDVI data

In an effort to monitor fluctuations in vegetation and understand interactions with the environment, the National Oceanic and Atmospheric Administration (NOAA) has been collecting images of vegetation condition using AVHRR sensors. The non-linear combination of red and near infrared (NIR) spectral radiance (Eq. 1.2), known as normalized difference vegetation index (NDVI), exhibits a strong relationship with green biomass and is commonly used for vegetation assessments from space.

NOAA AVHRR sensors provide the longest available run of NDVI data, including the Global Inventory for Mapping and Modeling Studies (GIMMS) which was used in this study (see Section 1.2.3). The data spans from 1981 through 2008 and has a temporal resolution of two weeks and a spatial resolution of 0.072 degrees (~8km). Errors in NDVI introduced from orbital drift were largely (~90%) eliminated in the most recent GIMMS version (Tucker *et al.*, 2005). The transitions between platforms may cause some discontinuities in the data (de Beurs & Henebry, 2005b), but these are expected not to affect trend slopes (i.e. gradual changes) in the vegetation index (Kaufmann *et al.*, 2000). A maximum value compositing (MVC) technique (Holben, 1986) was used to minimize cloud contamination during GIMMS processing and the risk of detecting trend changes caused by persistent cloud cover was further reduced by the configuration of the trend-break algorithm (see Section 5.2.3). Image acquisition started in July 1981, but we excluded 1981 in order to use only full one-year periods in the analysis. In this way, the 27-year time series (1982–2008) for each pixel consists of 648 NDVI measurements with a frequency of 24 scenes per year.

NDVI values lower than 0.2 are sparsely vegetated or not vegetated at all (Carlson & Ripley, 1997; Sobrino *et al.*, 2001), but to include sparsely vegetated areas in the analysis we masked pixels with yearly mean values below 0.1. The resulting dataset consists of 2,256,962 unmasked pixels (~86% of all terrestrial pixels excluding Antarctica). The NDVI signal in tropical evergreen forests is likely to saturate, causing low signal to noise ratios (Huete *et al.*, 1997). These regions were not omitted from the analysis, because abrupt changes might well be detectable. However, results for these regions were interpreted with caution.

5.2.2 Land cover classification

Detected vegetation changes were summarized per land cover class – which is also referred to as biome – because each might respond differently to climate change and to land-use change (Chapin *et al.*, 2000; Verburg *et al.*, 2011). In the International Geosphere and Biosphere Programme (IGBP), a 1km AVHRR-based land cover product (DISCover) intended for remote sensing of global change was developed (Loveland *et al.*, 2000). The dataset consists of 17 general land-cover types, based on the climate-independent vegetation-classification logic of Running *et al.* (1994), but extended to provide, where possible, land-use implications and to represent landscape mosaics. For definitions of each category the reader is referred to Appendix 1 in Loveland & Belward (1997) and to Loveland *et al.* (2000) for an elaborated description of the dataset and comparison with other land-cover datasets. The classification scheme, among few others, was later adopted within the MODIS land-cover products. These products provide yearly land-cover maps at 500m spatial resolution. In this study, the 2009 MOD12C1 product was used, as it provides land cover at an aggregated 0.05 degree spatial resolution, which closely resembles the GIMMS spatial resolution. The MOD12C1 dataset was resampled to 0.072deg resolution using a majority method, which best preserves the spatial structure of major land cover classes at the cost of minor classes (Dendoncker *et al.*, 2008; Verburg *et al.*, 2011). For this reason, the class 'urban and built-up' had few pixels and was omitted from the summary statistics. The classes 'snow/ice', 'barren' and 'water bodies' are not represented in the analysis due to the masking procedure described in Section 5.2.1.

5.2.3 Detecting trend changes within time series

Depending on biome, NDVI time series may contain a strong seasonal component linked with the growing seasons of vegetation being monitored. Most existing change detection techniques are unable to account for seasonal variation and analyze time series by aggregating the measurements by season or calendar year or they compare specific periods between years (Coppin *et al.*, 2004). A more generic change detection method was proposed by Verbesselt *et al.* (2010a,b). This method for detecting Breaks For Additive Seasonal and Trend (BFAST) accounts for seasonality and enables the detection of trend change within the time series. The methods are available in the BFAST package for R (R Development Core Team, 2011). Here, we explain the key concepts of BFAST and apply a modified version. The full motivation for the procedure is given in afore-mentioned publications, where also a validation is provided using both simulated time series and MODIS NDVI data for Australian environments.

The basic principle of the BFAST algorithm is the combination of time series decomposition into seasonal, trend, and remainder components with methods for

detecting structural changes in both the trend and seasonal components. In this study we focused on breaks in the trend component. It was assumed that non-linearity can be approximated by a piecewise linear model and, as such, linearity was assumed in the individual trend segments. An additive decomposition approach was used to iteratively fit the piecewise linear regression model and a seasonal model (Haywood & Randall, 2008). The general model is of the form:

$$Y_t = T_t + S_t + e_t \ : \ t \in \{1...n\} \tag{5.1}$$

where, at time t in the time series {1 … n}, Y_t is the observed NDVI value, T_t is the trend component, S_t the seasonal component en e_t the remainder component which contains the variation beyond what is explained by T_t and S_t.

The iteration is initialized with an estimate $\hat{S}_t$ of the seasonal component using a non-parametric season-trend decomposition (STL) method (Cleveland *et al.*, 1990). Subsequently, the estimates of S_t and T_t and their changes are determined by iterating through the following steps until the number and position of the detected breakpoints remain unchanged:

(step 1a) Test whether breakpoints are occurring in the seasonally adjusted data (Y_t–S_t), using the MOving SUM (MOSUM) approach (Zeileis & Kleiber, 2005). If the test indicates significant change ($\alpha = 0.05$), the breakpoints are estimated using the method of Bai & Perron (2003), as implemented by Zeileis *et al.* (2002). This method minimizes the Bayesian information criterion (BIC) (Schwarz, 1978) to determine the optimal number of breaks m and uses an iterative procedure – minimizing the residual sum of squares – to estimate the optimal break positions and accompanying 95% confidence intervals. For the MOSUM test to hold the nominal significance level, the error terms after decomposition should not be serially correlated.

(step 1b) The trend component $\hat{T}$ for each segment is estimated using robust linear regression (Venables & Ripley, 2002). As such, the trend component is described by a robust piecewise linear model, which allows the trend to exhibit changes. The positions in time of these trend changes are indicated by the individual breakpoints. The trend within each segment j is assumed to be linear with intercept α_j and slope β_j:

$$T_t = \alpha_j + \beta_j \cdot t \ : \ j \in \{1...m\} \tag{5.2}$$

where m equals the number of abrupt trend changes so that m+1 equals the number of segments.

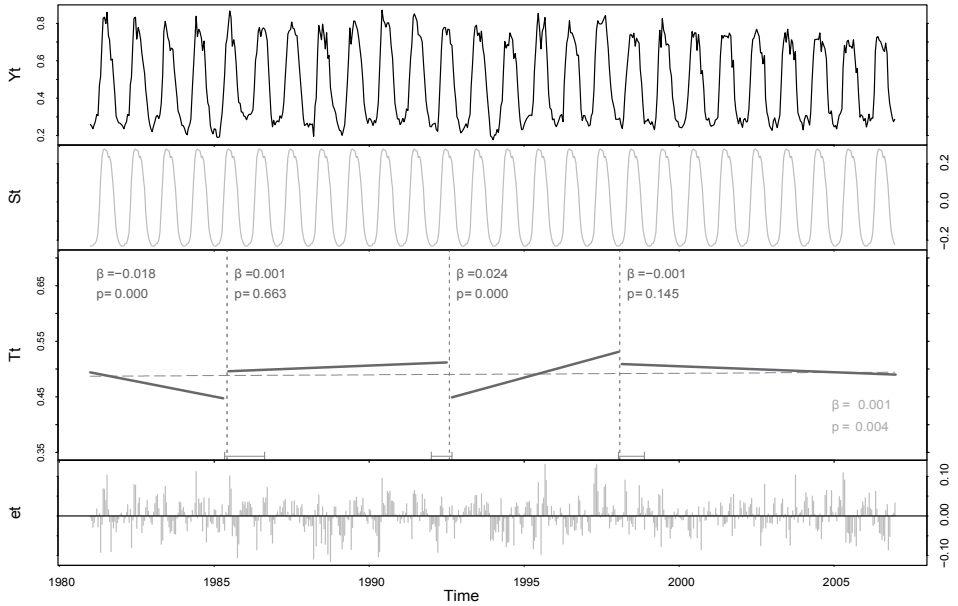

Figure 5.1 Example of decomposition and trend break analysis for a location in China (35.913ºN, 108.513ºE). The top panel shows the GIMMS NDVI data (Y_t), while the other 3 panels depict the individual components after decomposition. The seasonal (S_t) and remainder (e_t) components have zero mean while the trend component (T_t) shows the temporal trend in NDVI: a period of browning between 1982 and 1986 and a period of greening between 1994 and 1998. The slope coefficients (β) of the other two segments are not significant ($p > 0.05$). The dashed line (T_t panel) shows the equivalent linear model for the full time series.

(step 2) Detrended data ($Y_t - T_t$) are used to refit the seasonal term S_t using a harmonic model with 3 components, i.e. periods of 12, 6 and 3 months.

(step 3) The number and position of breakpoints are compared to the previous iteration and the fitting procedure is finalized if they remain unchanged.

BFAST can be generically applied to VI time series independent of the land-cover type, reference periods or specific change trajectory. The only parameterization required is the maximum number of breakpoints m_{max} or the minimum time between breakpoints. The minimum time between breakpoints needs to coincide with the typical length scale of the monitored processes. In line with Verbesselt *et al.* (2010a) and following the recommendations of Bai & Perron (2003), we used a minimum of 4 years (corresponding to ~15% of the 27-year data span) between successive breakpoints. In case of several changes within a 4 year segment, only the most statistically significant is detected. This configuration also reduced the effect of

persistently clouded areas, as clouds were found to be captured by the remainder component (e_t). For illustration, Figure 5.1 shows the decomposition and breakpoint detection for a GIMMS pixel in China. The trend component (T_t) consists of 4 segments with gradual changes, separated by 3 breakpoints at which abrupt changes were detected. For comparison, the T_t panel also shows the linear model for the full time series, together with the slope coefficient and the corresponding significance value (p). The latter is based on generalized least squares (GLS) to account for remaining short-lag serial autocorrelation.

5.2.4 Analysis of NDVI changes

The BFAST procedure was extended to analyze the significance of the detected slopes in T_t against the null hypothesis that slope $\beta_j = 0$ at $\alpha = 0.05$ (degrees of freedom equals the number of observations in the segment minus 2). Only significant slopes were adopted as indicators for greening ($\beta_j > 0$) or browning ($\beta_j < 0$). Subsequently, the *duration* of the significant greening and browning segments and the *magnitude of change in NDVI* were calculated. The first is the sum of length of individual segments with significant slopes and the latter is a combination of gradual magnitude within segments and abrupt magnitude at the breakpoints between consecutive segments. Results were summarized at global, hemisphere and biome scales. Abrupt changes shortly after the Mt Pinatubo eruption (Jun 1991 – Dec 1992) were extracted separately for mapping possible effects of this eruption on NDVI trends. All described analyses were performed using R statistical software (R Development Core Team, 2011) on a high performance computing facility.

5.3 Results

5.3.1 Duration of gradual changes

Figure 5.2 illustrates the detected duration of both gradual greening and gradual browning, without showing the associated slope or absolute changes in NDVI values. The most conspicuous region in terms of long greening periods is the eastern part of Europe. Also regions in North America, most tundra regions, the savanna between the Sahara desert and the equator and parts of India exhibited a greening trend for 20 years or longer. Most of these areas are in the Northern Hemisphere while long browning periods were mainly found in the Southern Hemisphere, conspicuously in parts of Argentina and Australia. In the Northern Hemisphere, on the other hand, browning was mainly found in the Kazakh steppe and in the boreal forests in parts of Siberia, Alaska and Canada.

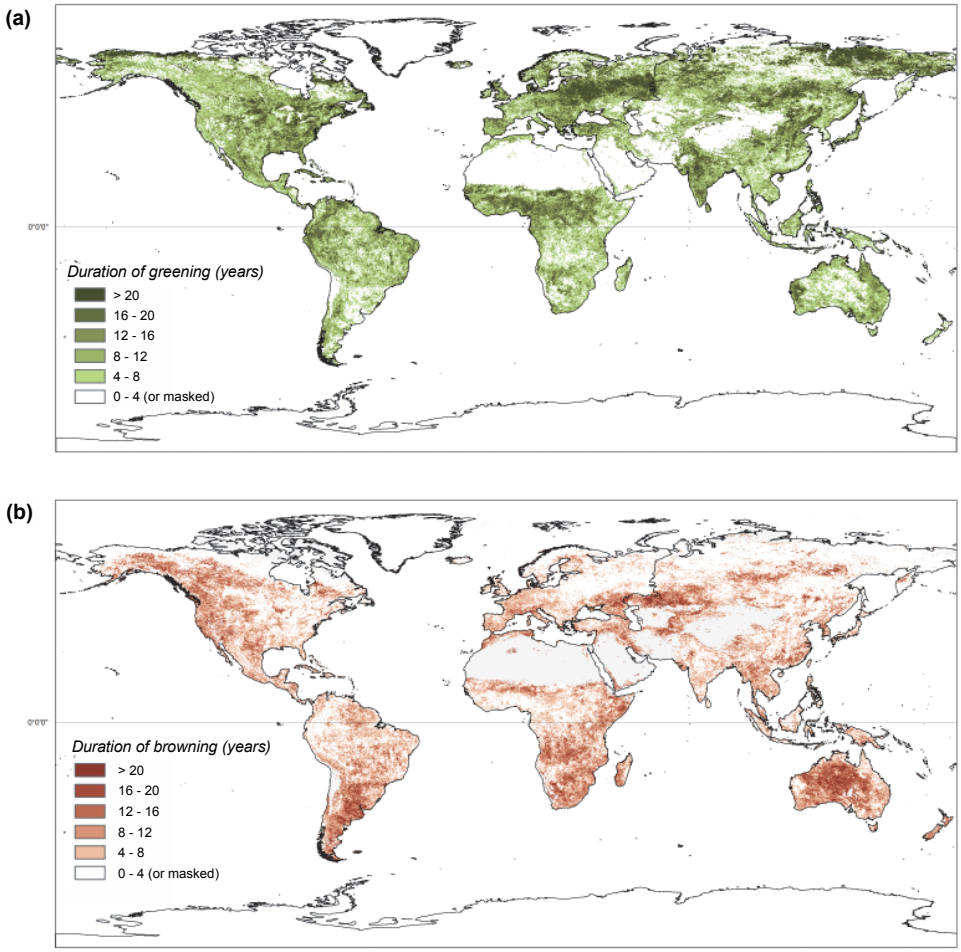

Figure 5.2 Duration of change by means of number of years in which a significant ($\alpha = 0.05$) NDVI trend was found. (a) positive trend, or greening and (b) negative trend, or browning. White areas were masked out (see sections *Data* and *Methods*) or showed short or insignificant trends.

A distinct difference was found between both hemispheres regarding the duration of greening and browning. Gradual greening trends lasted longer than equivalent browning trends in all biomes in the Northern Hemisphere, while the opposite holds for most biomes in the Southern Hemisphere (Table 5.1). The global figure is mainly determined by the Northern Hemisphere – due to the north-heavy arrangements of the continents – and therefore greening trends lasted longer in all biomes, although most conspicuously in mixed forests, croplands and cropland / vegetation mosaics. The longest gradual browning trends were found in grasslands. On average, the detected

duration of gradual changes varied roughly between 3 and 6 years for NH browning and between 9 and 14 years for NH greening. The SH durations varied between 7 and 9 years for greening and between 7 and 12 years for browning.

5.3.2 Trend breaks

Following the described approach, large parts of the global surface experienced NDVI trend changes during the 1982–2008 period. From the unmasked area, 32.9% shows zero, 27.2% one, 22.7% two and 17.2% more trend changes. Most of these were detected in Australia, Argentina, south-west Texas (USA) / north-east Mexico, Botswana and western South Africa (Figure 5.3). The higher northern latitudes and the tropics seem least affected by trend discontinuities, although some were detected in the North American boreal forests. For the better part, the detected breakpoints separate segments with significant slopes from segments with insignificant slopes. However, for 14.5% of the total land surface the slope coefficient swapped sign, which indicates that both a period of significant greening and a period of significant browning occurred at the same location between 1982 and 2008. Many of these shifts between greening and browning were found in semi-arid climate regions, but also in temperate climate regions in Europe and North America. The majority of this area corresponded to open and closed shrubland, while grassland takes a second place.

Table 5.1 Total duration of gradual NDVI change in years. Lengths of individual significant segments were summed and averaged over all pixels within the land-cover class for the Northern Hemisphere (*NH*), the Southern Hemisphere (*SH*) and globally (*G*). Land-cover classes (number and name) correspond to the IGBP classification (Loveland *et al.*, 2000).

		Positive change (greening)			Negative change (browning)		
Land-cover class / biome		*NH*	*SH*	*G*	*NH*	*SH*	*G*
1	Evergreen Needleleaf Forest	10.41		10.41	6.14		6.14
2	Evergreen Broadleaf Forest	9.51	9.48	9.51	5.24	7.34	5.05
3	Deciduous Needleleaf Forest	7.84		7.84	4.21		4.21
4	Deciduous Broadleaf Forest	13.08	6.56	11.10	4.25	9.76	6.00
5	Mixed Forests	13.57		13.57	4.04		4.04
6	Closed Shrublands	10.32	9.70	10.13	6.21	9.67	7.55
7	Open Shrublands	11.93	7.58	10.75	2.93	12.44	5.43
8	Woody Savannas	9.83	7.14	9.16	4.76	8.87	5.81
9	Savannas	14.98	9.18	10.34	3.92	7.54	6.83
10	Grasslands	10.77	7.59	10.18	7.85	10.55	8.34
11	Permant Wetlands	12.10	7.70	11.38	3.02	8.27	3.74
12	Croplands	13.49	8.10	12.86	5.09	10.23	5.66
14	Cropland / Vegetation Mosaic	13.31	8.68	12.60	4.46	6.70	4.78

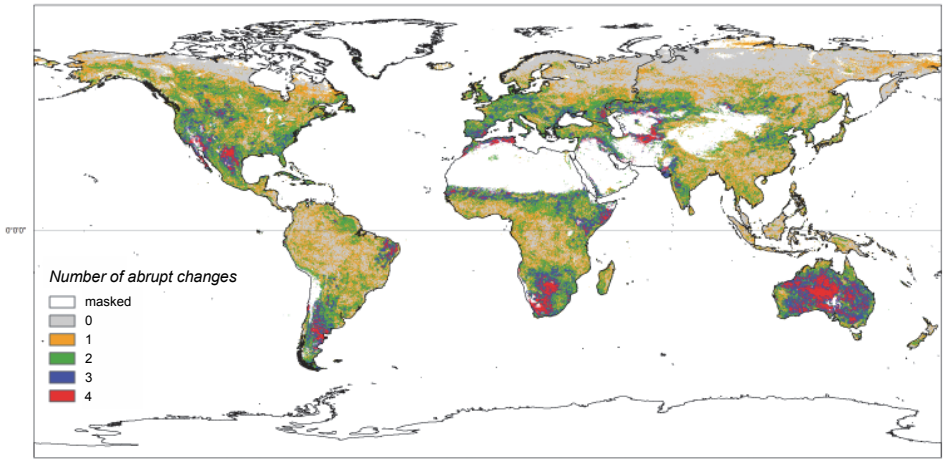

Figure 5.3 Number of detected abrupt changes, or breakpoints, irrespective of the magnitude of the changes. Areas with a yearly mean NDVI < 0.10 were masked.

5.3.3 Magnitude of NDVI changes

Global greening and browning patterns were divided into gradual and abrupt changes in NDVI and are shown in Figure 5.4*a,b*. Gradual changes – which were calculated from the detected duration of change and the corresponding slope coefficients – are shown in green and brown colors respectively and abrupt changes at breakpoints are, partially transparent, shown in blue. The magnitude of each of these components varies between 0 and ~0.15 (absolute NDVI units). Greening was found in many parts of the world and most conspicuously in the Northern Hemisphere, which is in line with the longer change trajectories of greening found there (Table 5.1). Abrupt greening was mainly found in areas with relatively sparse vegetation cover (e.g. Australian rangelands, African open shrublands and the Sahel region), mostly in combination with gradual browning, whereas abrupt browning was mainly detected in more densely vegetated regions (e.g. broadleaf forest in Europe and North America) and in humid grasslands. The sum of all significant change components provides the net change in NDVI (Figure 5.4*c*), with magnitudes up to ~0.04 (absolute NDVI units).

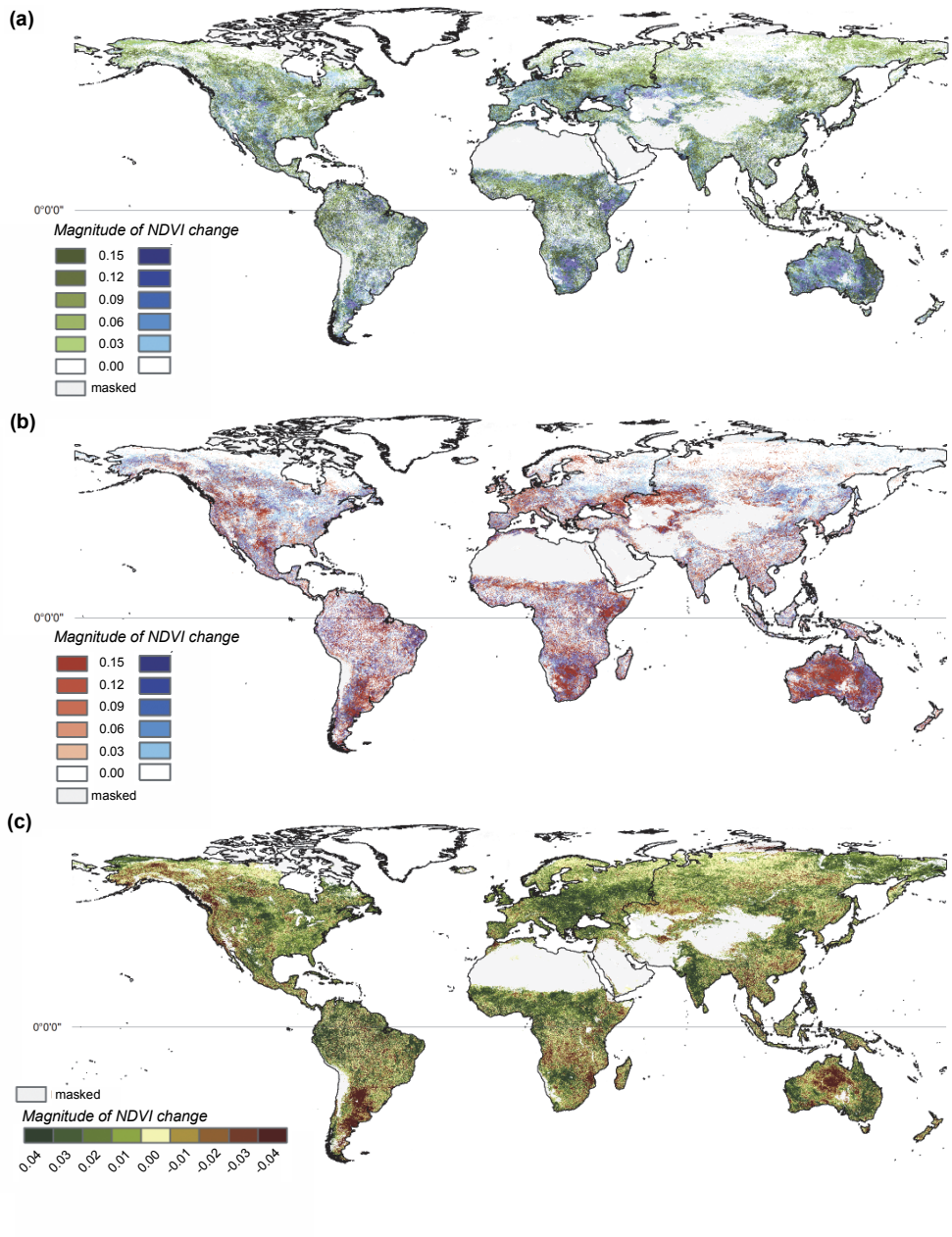

Figure 5.4 Global greening and browning in terms of NDVI changes between 1982 and 2008: (a) positive changes, both gradual (green) and abrupt (blue); (b) negative changes, both gradual (red) and abrupt (blue); (c) sum of the four components of figures a and b.

Table 5.2 summarizes the detected changes in NDVI per biome and hemisphere. At global scale, net greening is most conspicuous in cropland regions (net change 0.034), followed by evergreen broadleaf and mixed forests. In the Northern Hemisphere, savannas show the strongest indication for greening (0.050). Net greening was found in all biomes except for few minor net browning changes in the

Table 5.2 Changes in NDVI for the time span of the GIMMS dataset (1982–2008), subdivided into abrupt and gradual changes for the Northern Hemisphere (*NH*), the Southern Hemisphere (*SH*) and globally (*G*). For easier numerical representation, values were multiplied by 100. Land-cover classes (number and name) correspond to the IGBP classification (Loveland *et al.*, 2000). Classes 1 to 5 represent forest types.

		Gradual change			Abrupt change			Net result		
Land cover class / biome		*NH*	*SH*	*G*	*NH*	*SH*	*G*	*NH*	*SH*	*G*
greening										
1	Evergreen Needleleaf	5.80		5.92	2.91		2.91	0.68		**0.81**
2	Evergreen Broadleaf	9.23	9.24	9.25	5.87	5.99	5.94	2.25	2.65	**2.50**
3	Deciduous Needleleaf	3.10		3.10	1.18		1.18	0.81		**0.82**
4	Deciduous Broadleaf	7.38	7.62	7.56	3.59	6.29	4.46	2.56		**1.53**
5	Mixed Forests	5.89		6.05	2.58		2.58	2.45		**2.61**
6	Closed Shrublands	7.74	12.10	9.60	6.61	11.97	8.75	2.02	0.28	**1.42**
7	Open Shrublands	3.71	7.47	4.67	2.39	13.17	5.22	1.90	0.02	**1.39**
8	Woody Savannas	5.09	9.08	6.13	2.79	6.25	3.67	1.39	0.44	**1.16**
9	Savannas	9.84	10.84	10.65	5.68	6.81	6.59	5.03	1.67	**2.33**
10	Grasslands	6.00	8.03	6.32	6.40	9.58	6.96	2.04		**1.55**
11	Permant Wetlands	4.39	7.94	4.77	2.68	5.68	3.05	2.34	0.43	**2.07**
12	Croplands	7.84	10.84	8.14	4.62	8.06	5.01	3.79	0.36	**3.40**
14	Cropland Mosaic	7.09	7.23	7.10	3.73	4.66	3.85	2.87	1.08	**2.62**
browning										
1	Evergreen Needleleaf	-3.75		-3.74	-4.28		-4.28			
2	Evergreen Broadleaf	-6.42	-6.55	-6.48	-6.43	-6.03	-6.21			
3	Deciduous Needleleaf	-1.42		-1.42	-2.04		-2.04			
4	Deciduous Broadleaf	-3.34	-8.36	-4.98	-5.08	-6.33	-5.51		-0.79	
5	Mixed Forests	-2.53		-2.53	-3.49		-3.49			
6	Closed Shrublands	-6.84	-14.69	-9.94	-5.50	-9.09	-6.99			
7	Open Shrublands	-2.32	-14.79	-5.60	-1.88	-5.83	-2.90			
8	Woody Savannas	-3.03	-7.56	-4.19	-3.47	-7.33	-4.46			
9	Savannas	-4.99	-7.48	-6.99	-5.50	-8.50	-7.91			
10	Grasslands	-6.49	-11.67	-7.41	-3.87	-6.52	-4.32		-0.58	
11	Permant Wetlands	-2.22	-7.20	-2.83	-2.52	-5.99	-2.92			
12	Croplands	-4.12	-10.41	-4.81	-4.55	-8.14	-4.93			
14	Cropland Mosaic	-3.59	-5.55	-3.85	-4.36	-5.25	-4.48			

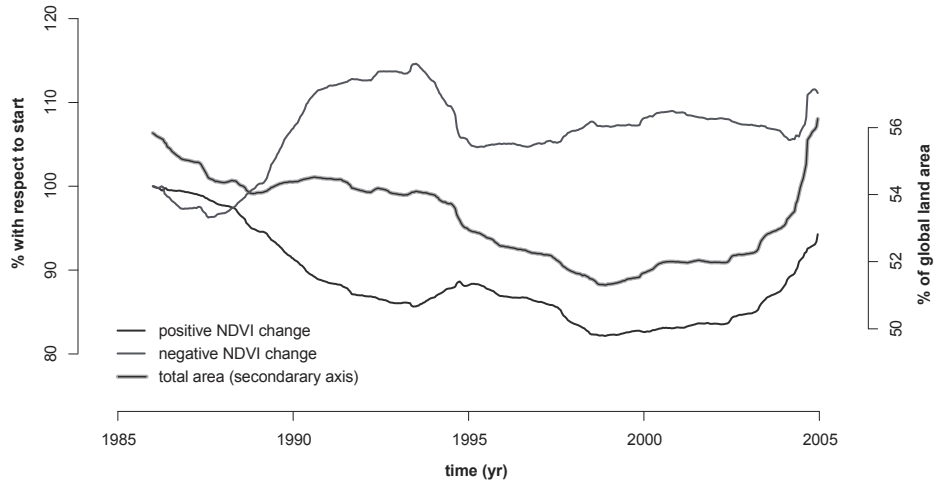

Figure 5.5 Primary axis: area with positive gradual trends in NDVI (*greening*) and negative gradual trends (*browning*) over time. The area was indexed with respect to the first four years (minimal segment length) of the time series. Secondary axis: percentage of total land area with significant greening or browning trend.

Southern Hemisphere. In general, the Northern Hemisphere showed less variation (in terms of absolute greening and browning per biome), but higher net NDVI changes compared to the Southern Hemisphere. In the latter, the highest variation was detected in shrublands and grasslands (e.g. parts of the Australian rangelands, Andean puna and Patagonian steppe / Monte semi-desert). The lowest variation was found in needleleaf forest and open shrublands in the Northern Hemisphere (e.g. boreal forest and tundra).

The detected NDVI trends do not only vary in space, but also in time. Figure 5.5 illustrates how gradual greening and browning trends were found to evolve across the time series by means of globally aggregated area per fortnightly time-step (with respect to the first four years in which no trend changes occurred by design). It appeared that the area which showed gradual greening decreased to 83% (with respect to the start of the time series) between 1986 and 2002, after which it increased to 92%. The browning area quickly increased to 118% in 1994, after which is decreased and stabilized around 110%. The total land area which experienced gradual changes was found to vary between 51% and 56% (blue line) with the minimum around the year 2000.

5.4 Discussion

The presented methodology, based on the BFAST algorithm, enabled detection of short-term greening or browning periods within a longer time series of satellite data. This approach is, in this sense, more flexible than previous global assessments of

vegetation activity (Bai *et al.*, 2008; de Jong *et al.*, 2011a). There is general agreement with respect to the afore-mentioned global assessments regarding the spatial pattern of net changes in NDVI (Figure 5.4*c*). However, the results showed different spatial patterns for gradual and abrupt NDVI changes (Figure 5.*4a,b*) and indicated that gradual trends generally last for periods shorter than the full length of the time series (Figure 5.2). The change rates for these shorter periods were, by definition, greater than those found using monotonic analysis and resulted in higher absolute NDVI changes within the 1982–2008 time span (Table 5.2). Considered over all pixels used in this study, greening rates were found to be around 4 to 5 times greater with respect to monotonic analysis with a fixed change duration of 26 years (Bai *et al.*, 2008). Browning rates were also greater, which may be accountable to shrubland biomes. This indicates that, especially in these regions, short-term greening and browning effects averaged out using monotonic analysis. This was found to occur in approximately 15% of the global land area, which showed both gradual browning and gradual greening trends between 1982 and 2008. The net global figure of NDVI change was positive for all land-cover classes, but slightly lower than estimated in mentioned monotonic studies. A plausible explanation for this effect is that monotonic methods are likely to overestimate changes in periods which were considered stable in this study. For example, in Figure 5.1 the entire time span was considered significant in case of the monotonic method ($p = 0.004$), while only ~9 out of 27 years were considered significant using the BFAST method.

5.4.1 Possible drivers of NDVI trends and trend changes

Terrestrial vegetation productivity is influenced by many cyclical and abrupt events which might cause trends in vegetation productivity to change (Gobron *et al.*, 2010). These events include climatic and oceanic oscillations, of which the El Niño / La Niña - Southern Oscillation (ENSO) with a period of 4-7 years is the best known (Woodward *et al.*, 2008), but also volcanic eruptions and anomalously warm and dry years (e.g. the European drought of 2003: Ciais *et al.*, 2005). Aside from biophysical drivers, the observation record might be contaminated with measurement errors originating from sensor changes, orbital drift of satellites or atmospheric effects. Most measurement errors can be well corrected for, but other drivers are likely to cause actual changes in vegetation response in some biomes or regions (e.g. volcanic eruptions and oceanic oscillations). Some of these effects are discussed here.

The GIMMS dataset has been corrected for aerosols injected into atmosphere by volcanic eruptions, i.e. the El Chichon eruption in April 1982 and the Mount Pinatubo eruption in June 1991 (Slayback *et al.*, 2003). Still, discontinuities might result from actual vegetation response to temporary global cooling. Effects of El Chicon are not likely to be found in the GIMMS data, because the eruption date is close to the start of the dataset and therefore the initial status is unknown. After the Mt Pinatubo eruption, however, a higher representation of breakpoints was found (de

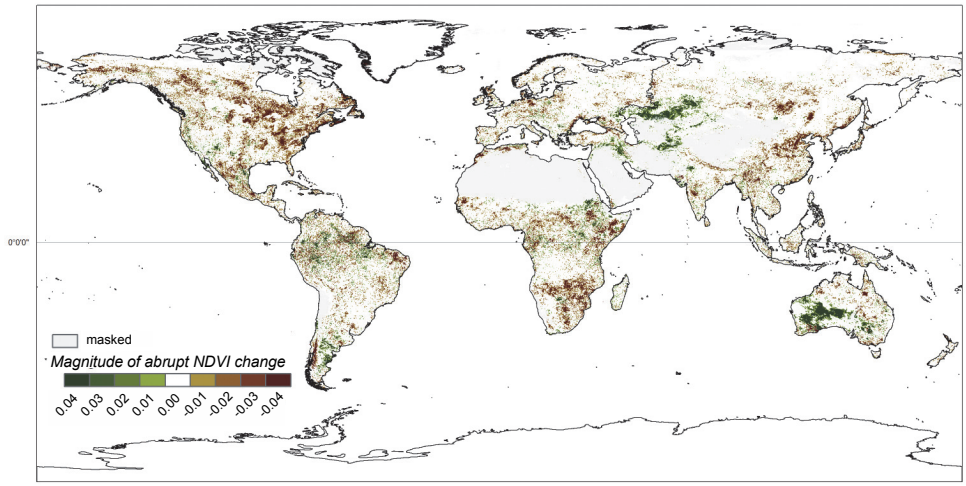

Figure 5.6 Magnitude of abrupt NDVI changes detected shortly after the Mt Pinatubo eruption (Jun 1991 – Dec 1992). Green colours indicate positive changes and brown colours negative changes.

Jong *et al.*, 2011b) and cooling effects attributable to the eruption have been reported around the world (Lucht *et al.*, 2002; Soden *et al.*, 2002; Angert *et al.*, 2004). This provides a candidate explanation for the high occurrence of abrupt trend changes around this time. Figure 5.6 shows that abrupt changes in NDVI were detected in many regions in the world between June 1991 and December 1992. Browning was most conspicuous in North America, Southern Africa and Eastern Asia. This corresponds with negative NDVI changes found in the higher northern latitudes between 1991 and 1992 (Slayback *et al.*, 2003). Two large regions showed positive changes (abrupt greening): Kazakhstan and the states of Western and South Australia. In Kazakhstan this might be explained by a sharp decline in precipitation in the years before the eruption (Pilifosova *et al.*, 1997). A weak El Niño event caused warming and higher precipitation in certain regions shortly after the eruption date (Woodward *et al.*, 2008). This might have counterbalanced some Pinatubo effects and caused the abrupt greening in Australia.

The Sahel experienced climatic extremes in terms of drought. During the last 30 years of the 20th century, nearly all years have been anomalously dry (Nicholson, 2000), which is likely related to the Atlantic multi-decadal oscillations (AMO) (Zhang & Delworth, 2006). In water-limited ecosystems like these, such rainfall trends are expected to induce browning trends, possibly amplified by a positive feedback due to increasing albedo (Zhang & Delworth, 2006). However, greening trends were found in the Sahel, especially in the southern parts. These trends are strongest in the 1980s and were found to change into browning trends in the northern Sahel. The net result for 1982–2008 showed greening (Figure 5.4*c*), which is

probably the result of recovery from the droughts which were most severe around the start of the GIMMS dataset. It will be a complex exercise to disentangle all sea-atmosphere-land interactions which drive the gradual and abrupt changes in vegetation productivity here, but there seems to be a general agreement that the Sahel vegetation is heavily influenced by natural processes, more than by men (Fensholt & Rasmussen, 2011). In these and other shrubland biomes – especially in the Southern Hemisphere – it was found that the greening changes are generally abrupt, followed by gradual browning (Figure 5.4 and Table 5.2, classes 6 and 7). Relatively wet years might lead to extensive germination of short-lived plants, which is followed by browning in successive drier years. The total variation in NDVI change is also highest in these regions (together with grasslands), which is likely explained by strong reactions to climatic fluctuations like ENSO cycles. A large number of abrupt changes was found in Australia – which is particularly prone to ENSO fluctuations – around the strong 1997/98 El Niño (Wolter & Timlin, 1998) and following La Niña events. These fluctuations are much smaller in the Northern Hemisphere figures for the same biomes, owing to the stable tundra regions, which form – in the IGBP DISCover classification – part of the (open) shrublands and due to the reduced ENSO influences. Other climatic oscillations which act at (sub-)decadal time scale and which have larger effects in the Northern Hemisphere include the Pacific Decadal Oscillation (PDO) and the North Atlantic Oscillation (NAO). Both have mainly been in positive phases during the GIMMS time span, which leads to relatively high temperatures some regions (Viles & Goudie, 2003), but not likely to trend breaks in NDVI.

Relatively long periods of browning were detected in boreal forests in Canada and Siberia (Figure 5.2). This boreal browning is in line with results from previous studies (Bunn *et al.*, 2007), in which drought and, accordingly, vapor pressure deficits (VPD) were documented as possible drivers. In North America, large forested areas experienced a decline in productivity without significant changes in growing season length, indicating impacts of late summer drought (Zhang *et al.*, 2009; Goetz *et al.*, 2011). This is in agreement with several trend analyses performed on the GIMMS dataset indicating that boreal browning is mainly attributable to stress within the growing season, rather than to changes in length of growing season (Goetz *et al.*, 2005; de Jong *et al.*, 2011a) and supported by tree ring studies (Lloyd & Bunn, 2007). Net NDVI increase was found for all land cover classes, but Table 2 shows that the lowest increases were found for needleleaf forest – which is most abundant in the boreal regions. Arctic coastal tundra ecosystems, on the other hand, mostly show a stable greening trend which is likely related to decreasing sea ice concentrations and associated higher land surface temperatures (Goetz *et al.*, 2011). Aside from boreal regions, long periods of browning were also found in Kazakhstan. These have been attributed to drought conditions, at least towards the end of the time series, when negative precipitation trends were found from both station observations

and gridded precipitation data (de Beurs *et al.*, 2009). The same research showed an increase in NDVI, using MODIS data from 2000–2008, in a study area in the European part of Russia, which is in accordance with the long-term greening trends found in this study. These trends were attributed to land abandonment and an increase in agricultural productivity (de Beurs *et al.*, 2009). Agricultural expansion plays an important role in Argentina as well (Viglizzo *et al.*, 2011), which is likely one of the drivers of the negative NDVI trends found there. On the other hand, the strongest indication for greening is also found in cropland regions (Table 5.2), which is likely attributable to improved agricultural techniques. Urban expansion might have caused local NDVI decline around several cities. In the global statistics this effect is not captured as a result of the resampling scheme used for the land cover data. For such purposes it is recommended to run the BFAST algorithm on MODIS (or equivalent) data. This recommendation also holds for other purposes where processes act beyond the spatial resolution of GIMMS, for instance most deforestation studies.

Many regions, other than discussed above, show significant NDVI trends and for most of these regions ample studies relate the trends to possible drivers. Few studies, however, assessed trends and drivers at continental or larger scale. In the Northern Hemisphere, greening patterns were found and related to increasing temperature and precipitation (Zhou *et al.*, 2001), but recently trends in certain regions were also found to have stalled or even inversed (Wang *et al.*, 2011). Globally, the terrestrial net primary productivity (NPP) was found to have reduced during the past decade, attributable to large-scale warming-associated droughts in the Southern Hemisphere (Zhao & Running, 2010) and a likely soil moisture deficit (Jung *et al.*, 2010). This is in line with the browning patterns (Table 5.2) and the increasing area with browning trends (Figure 5.5) found in this study, although the strongest increase was found before 1994. The sharp increase in 2004 might be partly explained by a decrease in vegetation productivity in Europe following the anomalous warm year of 2003 (Ciais *et al.*, 2005). Overall, the past decade showed an increase in greening trends, but our analysis period for trend changes was limited to 2005.

5.4.2 Limits and artifacts

The presented approach proved capable of detecting trend changes in global NDVI time series and reduced the limitation of a commonly assumed fixed change trajectory. Common trend analysis methods may average out the temporal signal for time series which consist of several different change periods. Accordingly, areas might be labeled stable while in reality changes occurred over periods of several years or – the other way around – stable periods are included in a significant long-term trend. The longer a time series is, the more likely that this effect conceals actual short-term trends, which might be closer related to driving processes than long-term trends. Information on greening versus browning sign changes, for instance, is

crucial for monitoring the effect of land-management changes or the influence of meteorological conditions on vegetation status. This information can be provided using the presented approach, keeping in mind some constraints.

Several NOAA satellites have been used to generate the GIMMS dataset. Although the data has been thoroughly corrected (Tucker *et al.*, 2005), this potentially causes trend breaks within the time series (Cracknell, 1997; de Beurs & Henebry, 2004). Table 5.3 lists the platform changes and the corresponding dates. We analyzed the frequency distribution of the detected break points, from which it appeared that few sensor changes (between NOAA platforms 9, 11 and 14) coincide with periods with a higher than average number of breakpoints (de Jong *et al.*, 2011b) but a causal relationship could not be established. The likeliness of these transitions influencing the timing of detected breaks is highest in low-latitude biomes, especially in case of sparse vegetation cover and relatively light-colored soils, but even then it is likely not to affect the detected trend slopes (Kaufmann *et al.*, 2000).

NDVI is a one dimensional measure with a multi-dimensional biophysical origin, which – despite the improved time series analysis techniques – urges caution in the interpretation of trends. Given that the data is free of measurement errors, it still does not directly measure the amount of standing biomass nor the vegetation productivity, but is also influenced by canopy structure and soil parameters, among others (Baret & Guyot, 1991; Myneni *et al.*, 1995). It is therefore not straightforward to relate NDVI changes to ecosystem changes, which in itself are often multi-actor issues and subject to change over time (Nelson *et al.*, 2006). Expressing productivity change in terms of Net Primary Productivity (NPP) – using empirical relationships with NDVI or production efficiency models – yields an indicator which is closer related to biophysical processes and better amenable to economic analysis. The relationship between the two, however, is not always strong and not over the entire range linear (Paruelo *et al.*, 1997), although a large part of interannual variation in NPP (30% up to 90%, depending on biome) can be explained by NDVI (Potter *et al.*, 1999). The application of trend break analysis of satellite records in combination with production efficiency models needs further investigation.

AVHRR platforms	Date
NOAA-7 > NOAA-9	Feb 10, 1985
NOAA-9 > NOAA-11	Nov 9, 1988
NOAA-11 > NOAA-9d	Sep 20, 1994
NOAA-9d > NOAA-14	Jan 19, 1995
NOAA-14 > NOAA-16	Nov 1, 2000
NOAA-16 > NOAA-17	Jan 1, 2004

Table 5.3 Sensor changes within the time span of the GIMMS dataset. Due to malfunction of NOAA-11 and failure of NOAA-13 to achieve orbit, NOAA-9 descending node data was used in the period Sep 20, 1994 until Jan 19, 1995 (Tucker *et al.*, 2005).

5.5 Conclusions

Temporal decomposition of trends in vegetation activity inferred from NDVI revealed an alternating pattern of short-term greening and browning trends for large parts of the terrestrial surface. For almost 15% of this area, both periods with an increase and with a decrease in vegetation activity were found between 1982 and 2008. The ENSO-prone shrubland and grassland regions, mainly in the Southern Hemisphere, appeared specifically prone to reversing trends. Many trend changes were detected for certain regions after the strong ENSO event of 1997/98 and globally after the Mt Pinatubo eruption of June 1991.

Different spatial patterns were found for abrupt and gradual changes. Abrupt greening prevailed in semi-arid regions, probably due to their strong reactions to climatic variations. These abrupt greening events were often followed by periods of gradual browning. In general, greening prevailed in all land cover classes and as a result the global figure indicates greening between 1982 and 2008, strongest in croplands and weakest in needleleaf forests. Greening trends were also found to be weaker in the Southern Hemisphere, compared to the Northern Hemisphere. Globally, the area which experienced gradual greening trends was found to decrease over time, while browning increased. This might indicate an overall reduction in global terrestrial vegetation activity, although an increasing trend was found in recent years.

The results from this study show that linear trend analysis over a time series of arbitrary length may obscure significant trend changes appearing within shorter duration, while particularly the latter can be linked to large scale drivers. As such, automatic detection of trend changes provides a new step in the analysis of trends in global vegetation activity, specifically in (semi-arid) shrub- and grassland biomes.

Acknowledgements

We are grateful to Molly Brown and the GIMMS group for providing their latest dataset and to the ESG-HPC people of Wageningen University for facilitating model calculations. We acknowledge in particular Wietse Franssen for his assistance. We would like to thank Achim Zeileis for his answers to our questions about structural change and three anonymous reviewers and the editor of Global Change Biology for their constructive comments, which helped to improve the manuscript.

Chapter 6

Spatial relationship between climatologies and changes in global vegetation activity

Rogier de Jong, Michael E. Schaepman, Reinhard Furrer, Sytze de Bruin

"When we look about us towards external objects, and consider the operation of causes, we are never able, in a single instance, to discover any power or necessary connexion; any quality, which binds the effect to the cause, and renders the one an infallible consequence of the other."

David Hume (1737)
Enquiries Concerning The Human Understanding and Concerning The Principles of Morals

This chapter is to be submitted to Global Change Biology

Abstract

Vegetation, the main component of the terrestrial biosphere, is often used as a proxy in studies addressing land degradation and climate change. Several studies have reported on temporal trends in time series of satellite data. There is, however, little known about the processes underlying changes in vegetation activity at large spatial scales. In this study, we aimed at quantifying the spatial relationship between potential climatic influence (i.e. temperature, precipitation and incident radiation) and human-induced change in vegetation activity as a step towards establishing links between plant growth, climate change, and human-induced land change. A spatial additive model was used in combination with regression models representing both, deterministic or fixed-effects and a spatially correlated random field representing a random component. Little over 50% of the variance could be explained with changes related to climatologies; the remainder may contain large-scale human interventions or residual climate effects (likely hidden in negative feedbacks). The strongest relationship between climate and vegetation activity was found in forests. Large-scale vegetation changes which could not be related to climate variables were found in sub-equatorial Africa, mainly in Tanzania and Zimbabwe. The novelty of this study is the combination of a spatial modeling approach with long-term climate and vegetation records, which showed plausible associations between limiting climate variables and vegetation activity in many regions, as well as locations where these associations were less pronounced.

6.1 Introduction

Vegetation is the main component of the terrestrial biosphere and remotely sensed vegetation indices (VI) are often used in climate change studies as a proxy for vegetation amount and photosynthetic capacity (Myneni *et al.*, 1995). Today, VI time series are available at large spatial scales and dense time intervals. Studying the available satellite imagery at global scale involves the analysis of large quantities of data, which is usually done on a per-pixel basis. Temporal VI changes have been quantified using several approaches, including parametric linear models on data aggregated on a yearly basis (Bai *et al.*, 2008), on a seasonal basis (Eklundh & Olsson, 2003), non-parametric models on the full time series (Pouliot *et al.*, 2009) or seasonal-trend decomposition algorithms (de Jong *et al.*, 2012). The general pattern of the detected changes is mostly the same: increases in VI over time (*greening*) have been found in many areas of the world, for instance in Europe, the Sahel and India. Decrease (*browning*), on the other hand, has been identified mainly in the Southern Hemisphere (e.g. South America), but also in boreal forests (de Jong *et al.*, 2012). These results indicate temporal change in vegetation activity over the past decades, but leave the relation with underlying processes open.

Changes in vegetation activity – as we use to refer to changes in vegetation index, following Zhou *et al.* (2001) – form a complex system of biotic and abiotic interactions, which differ between land-cover classes and may evolve over time themselves (Nelson *et al.*, 2006). Changes may be induced by natural processes, anthropogenic processes or, often, by a combination of both (Evans & Geerken, 2004). For these reasons, disentangling all drivers of changes in vegetation activity at large spatial scales remains an unsolved issue. Typical spatial resolutions ranging from 0.05 – 0.5 degrees complicate the issue as they involve mixed pixels, consisting of several vegetation types and other land-use/land-cover types. Many local-scale processes may influence vegetation at sub-pixel level, including changes in land management, human-induced land degradation, changes in soil background and local diseases or fires. Climate change, on the other hand, is more likely to act at much larger spatial scales. In global datasets with relatively large pixel size, local-scale effects may be expected to be randomly distributed (in space), while climatic effects may express as a spatially correlated field (Zhou *et al.*, 2001).

Climate observations (temperature, precipitation, cloudiness, amongst others) are available as global gridded data with monthly intervals since the beginning of the previous century (Mitchell & Jones, 2005). Variations in vegetation activity have been inferred from satellite data at global scale since the early 1980s (Tucker *et al.*, 2005). The normalized difference vegetation index (NDVI) is currently the most widely applied spectral index for quantification of trends in vegetation activity. It directly correlates to the fraction of absorbed photosynthetically active radiation

(fPAR) and can – in combination with an efficiency conversion factor and the amount of incident PAR – be used to quantify gross primary productivity (GPP) (Running *et al.*, 2004). Comparisons between climate change and changes in NDVI can be made for the last decades using statistically derived trends over time.

In this study, the described temporal and spatial components were combined into an additive model where the observed changes in vegetation activity are modelled as the additive combination of fixed (climate) effects, spatially dependent random effects and independent residuals. First, we used a land-cover specific deterministic model and a regression-tree approach to explain variation in vegetation activity from climate changes. Covariates for these models were selected based on the assumption that plant growth is limited by either one or a combination of three climatological constraints: water availability, temperature and incident radiation (Field *et al.*, 1995). This assumption was found to hold for most parts of the world, except for some regions (e.g. tropics) where other environmental controls – including nutrient availability or biological constraints like multi-layer canopies – constrain plant growth (Churkina & Running, 1998). Changes in global vegetation activity cannot be solely accounted to changes in the described climate parameters. Other factors which tend to occur over large geographic areas might have contributed to the observed changes in vegetation activity, for instance temporal variations in permafrost or other climate responses. Such factors are likely to cause spatial autocorrelation, even at coarse spatial resolution. For this reason we added a spatially smooth field to model random effects originating from other actors than captured by the fixed-effects model. A Gaussian random field (GRF) model was used for this purpose.

With this work, we aim at quantifying spatial relationships between climatic constraints and temporal VI trends. We are interested in trends beyond the pixel-level and associations with possible drivers that can be made using historical data and without a-priori information. The associated spatial patterns help the interpretation of relationships between vegetation activity, climate change, and human-induced land-use / land-cover changes.

6.2 Data

6.2.1 NDVI data

The National Oceanographic and Atmospheric Administration (NOAA) acquired the longest series of data using advanced very-high resolution radiometer (AVHRR) sensors. We used the most recent GIMMS version G datasets (Tucker *et al.*, 2004), consisting of 28 years of NDVI data from 1981 through 2008, aggregated to fortnightly scenes at 8km spatial resolution (see Section 1.2.3). These fortnightly scenes were derived from daily 4km global area coverage (GAC) data (Tucker *et al.*, 2005), applying a maximum value compositing (MVC) technique to remove bias

caused by atmospheric conditions (Holben, 1986). This, however, is not an atmospheric-correction method and some inaccuracy remains, especially in hazy and cloudy conditions (Nagol *et al.*, 2009). For this reason, we applied a harmonic interpolation algorithm (Roerink *et al.*, 2000; de Jong *et al.*, 2011a) to remove remaining noise in areas with frequent cloud cover. Areas with very sparse or no vegetation cover (median NDVI < 0.1) were masked out, as well as regions at higher than 72 degrees northern latitude. As such, we excluded the northernmost regions of Russia and Canada. In these regions, NDVI signals have been found to be distorted by high solar zenith angles and by snow and ice (Brown *et al.*, 2006). Orbital decay and changes in NOAA satellites are known to affect AVHRR data but processed NDVI data have been found free of trends introduced from these effects (Kaufmann *et al.*, 2000). Discussions on the GIMMS data quality and derived trends are, among others, provided by Zhou *et al.* (2001), Baldi *et al.* (2008) and Alcaraz-Segura *et al.* (2010).

6.2.2 Climate data

High resolution gridded datasets with global coverage were obtained from the Climatic Research Unit (CRU). The most recent TS 3.1 datasets (Mitchell & Jones, 2005) were released in April 2011 and provide time series for a range of parameters (Table 6.1). The dataset spans 1901–2009, but only the subset matching the time span of GIMMS data was used. Daily observations were aggregated into monthly mean values with 0.5 degree spatial resolution. As such, each time step consists of a 720 columns and 360 rows image. Non-terrestrial pixels were masked, resulting in approximately 65 000 observations per time step.

Table 6.1 Climate parameters provided by the Climate Research Unit (CRU) TS 3.1 dataset as high resolution monthly grids (spatial resolution 0.5 degree) for the time span 1901–2009.

Label	Parameter	Unit
CLD	cloud cover	%
DTR	diurnal temperature range	degree C
FRS	frost day frequency	Days
PRE	Precipitation	Mm
TMP	daily mean temperature	degree C
TMN	daily minimum temperature	degree C
TMX	daily maximum temperature	degree C
VAP	vapour pressure	hecta-Pascal
WET	wet day frequency	Days
PET	potential evapotranspiration	Mm

Covariates were selected based on the assumption that plant growth is limited by water availability, temperature and/or incident radiation (Field *et al.*, 1995). Changes in either of these parameters might induce changes in vegetation productivity and in the proxy NDVI signal. For most regions, water availability is determined by the amount of precipitation, although snowmelt should be accounted as well for high northern latitudes and in mountainous regions. In this study, this parameter was confined to precipitation as the mentioned regions are temperature-limited rather than water-limited (Nemani *et al.*, 2003). Time series of incident PAR are not globally available, but the amount of PAR is to a large extent determined by the intensity and duration of cloud overcast (Zhuravleva *et al.*, 2006). Therefore, trends in temperature (TMP), precipitation (PRE), cloud cover (CLD) were selected as covariates for the deterministic prediction of NDVI trends. Potential Evapotranspiration (PET) is a reflection of the energy available to evaporate water given that ample water is available. It may reflect growth-limitation by radiation, for which it was incorporated as additional covariate. PET was calculated as reference value for grass according to the method used by the United Nations Food and Agricultural Organization (Ekström *et al.*, 2007) – which is a variant of the Penman-Monteith method (Allen *et al.*, 1994). The gridded TMP, TMN, TMX, VAP and CLD (Table 6.1) were used as input for this method. PET units are mm/day and were multiplied by the number of days in each month to obtain mm/month. The ratio PRE/PET is known as the aridity index (AI) (Middleton & Thomas, 1997) and was additionally used as indicator of water-limiting conditions for plant growth.

6.2.3 Land-cover data

Land cover was considered because biomes may respond differently to climate change and to land-use change (Chapin *et al.*, 2000; Verburg *et al.*, 2011). In the International Geosphere and Biosphere Programme (IGBP), a 1km AVHRR-based land-cover product (DISCover), intended for remote sensing of global change, was developed. The dataset consists of 17 general land cover types, based on an extended climate-independent vegetation classification logic of Running *et al.* (1994). For definitions of each category the reader is referred to Appendix 1 in Loveland & Belward (1997) and to Loveland *et al.* (2000) for an elaborated description of the dataset and comparison with other land cover datasets. The classification scheme was later adopted within the moderate resolution imaging spectrometer (MODIS) land cover products (Friedl *et al.*, 2002), which provide yearly land cover maps at 500m spatial resolution. In this study, the MCD12C1 product was used, as it provides land cover at an aggregated 0.05 degree spatial resolution together with the sub-pixel frequency of each class. These land cover classes were used to develop biome-specific regression models on a subset of homogeneous pixels. Both GIMMS and MCD12C1 datasets provide higher spatial resolutions than CRU data and needed to

be resampled to 0.5 degree resolution. The aggregation scheme used for this purpose is described in the Methods section.

6.3 Methods

6.3.1 Spatial aggregation of NDVI and LCC data

The native spatial resolution of the CRU TS 3.1 climate data is 0.5 degree, whereas the land cover data from the MCD12C1 product and the GIMMS NDVI data have spatial resolutions of 0.05 degree (~5.6km) and 0.073 degree (~8km) respectively. Therefore, both the land cover data and the temporal NDVI trends needed to be resampled to 0.5 degree spatial resolution. With regard to the discrete land-cover data, the spatial aggregation scheme determines the area and the spatial coherence of each land cover class within the aggregated product (Dendoncker *et al.*, 2008; Verburg *et al.*, 2011). For this reason, careful selection of the aggregation scheme is crucial. A central pixel approach best preserves the relative area of the individual classes, especially the minor classes. A majority approach, on the other hand, provides the best result in terms of spatial structure of the major classes. In this study, we adopted the majority scheme to assign the prevailing land cover class (Figure 6.1*a*) and we used the sub-pixel frequency (Figure 6.1*b*) to select relatively homogeneous pixels for fitting the regression models. The raw GIMMS data was used for determination of temporal trends in NDVI between 1982 and 2008 at 0.072 degrees (~8km) spatial resolution. The resulting dataset was aggregated to 0.5 degrees resolution using the areal mean.

6.3.2 Temporal changes in vegetation activity and climatologies

The total amount of change was determined for both NDVI and climate time series using linear regression after correction for seasonality. The latter was described by additive harmonic functions with periods of 12, 6 and 3 months respectively. The seasonal component was subtracted from the original data before fitting the linear model. The slope coefficient of the fitted model was multiplied by the length of the time series to obtain the magnitude of change. For the GIMMS data, trend analysis was applied before the spatial resampling procedure. The resulting change maps (Figure 6.2) were used for the additive model that is described in the next section. Significance of the slope coefficients was assessed using generalized least squares (GLS). In this way, possible short-lag temporal autocorrelation, which remains after subtracting the seasonal component, is accounted for in the calculation of the *p*-values. All trends at 0.05-confidence level were retained; other slope coefficients were neglected (and appear as zero in Figure 6.2).

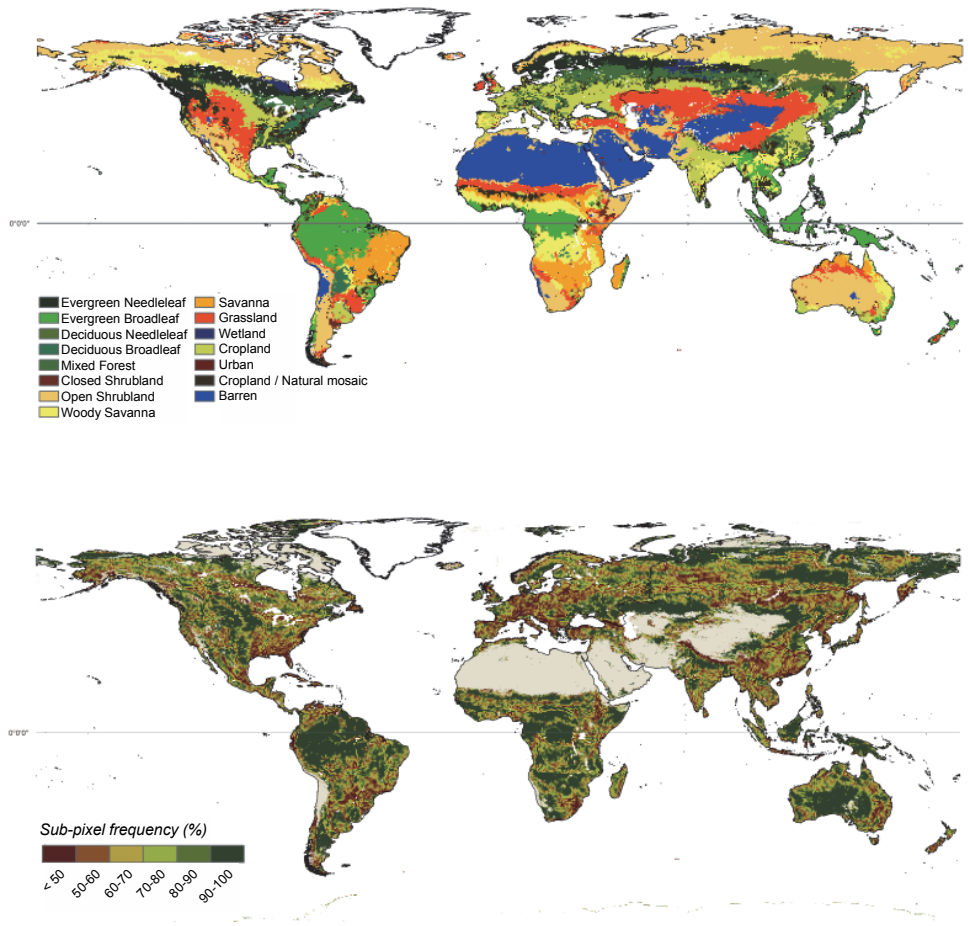

Figure 6.1 (*a*) Major land cover class based on the MODIS MCD12C1 product and the International Geosphere-Biosphere Programme classification scheme (Loveland *et al.*, 2000). The data were resampled to 0.5 degree spatial resolution using a majority resampling approach. (*b*) sub-pixel frequency of the major land-cover class (%).

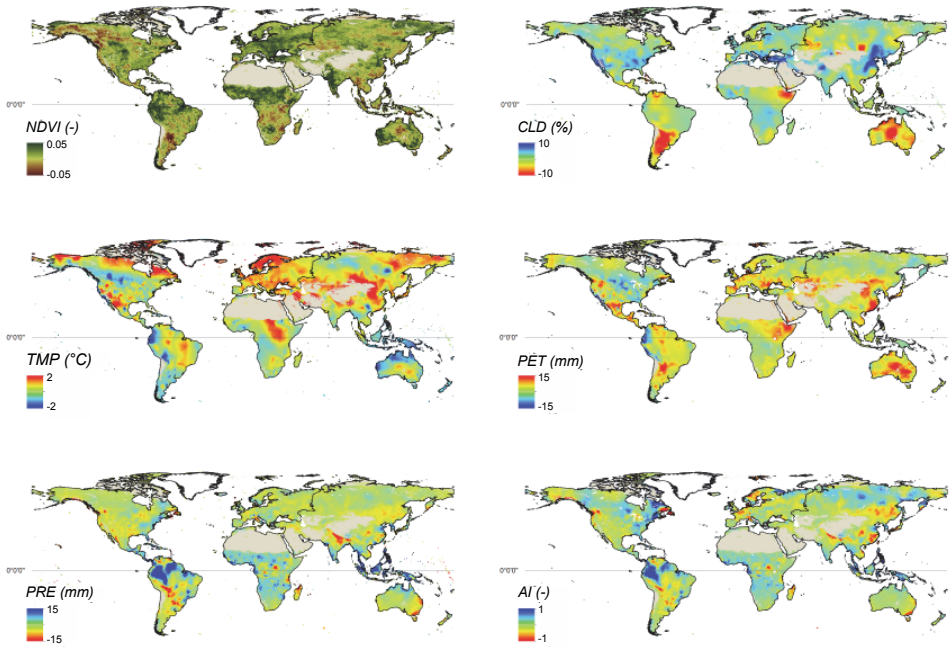

Figure 6.2 Temporal changes in vegetation activity and Climate Research Unit (CRU) parameters (1982 – 2008). Left, top to bottom: vegetation activity (NDVI), temperature (TMP), precipitation (PRE). Right, top to bottom: cloudiness (CLD), potential evapotranspiration (PET) and aridity index (AI). Changes in climate parameters were derived with linear models, after seasonal decomposition, on monthly gridded data (CRU TS 3.1) (Mitchell & Jones, 2005).

6.3.3 Additive model for observed NDVI changes

An additive model was used for describing the observed temporal changes in NDVI (observation matrix **Y**). The model consists of a deterministic part where **Y** depends on a set of covariates **X** with their coefficients β (fixed effects), a spatial process h and a residual noise component ε (Eq. 6.1).

$$\mathbf{Y} = \mathbf{X}\beta + h + \varepsilon \tag{6.1}$$

The individual components were modelled using a backfitting approach, consisting of an iterative estimation of the fixed effects β (regression step) and the spatial field h (kriging step). Initially, $\mathbf{X}\hat{\beta}$ was estimated using a regression tree model on the input data **Y**. The initial spatial field $\hat{h}$ was fitted on the residuals of this model. Initial values for the parameters of the spatial model were estimated by the method-of-moments, which is affected by both the random variation and the

variation represented by the fixed effects (Lark *et al.*, 2006); the backfitting approach pursues optimal parameter estimation in this situation of mutual model dependency. The procedure is schematized in Method 6.1.

Method 6.1

[1] Put $i = 0$; let $\hat{\beta}^{(0)}$ be an initial fit of $\mathbf{Y}$ on $\mathbf{X}$

[2] Let $\hat{h}^{(0)}$ be an initial fit on $\mathbf{Y} - \mathbf{X}\hat{\beta}^{(0)}$ (see Method 6.2)

[3] Put $i = i + 1$

[4] Estimate $\hat{\beta}^{(i)}$ from $\mathbf{Y} - \hat{h}^{(i-1)}$

[5] Estimate $\hat{h}^{(i)}$ from $\mathbf{Y} - \hat{\beta}^{(i)}$

[6] Repeat steps 3 to 5 until convergence

[7] $\epsilon = \mathbf{Y} - \mathbf{X}\hat{\beta}^{(i)} - \hat{h}^{(i)}$

The deterministic approach (steps 1 and 4) and the spatial model (steps 2 and 5) are described in the following sections.

Deterministic model (fixed effects)

Climatic limitations on vegetation activity can be described by any combination of three drivers and their interactions: temperature, precipitation and incident PAR (Field *et al.*, 1995). As such, changes in these climate parameters may induce changes in vegetation activity as inferred by NDVI. Two approaches were used to model changes in NDVI from changes in limiting climate parameters, where CLD and PET were used as proxies for PAR. Different land cover classes (or biomes) are likely to respond different to changes in climatic conditions (Chapin *et al.*, 2000). For this reason, a model that directly relates climate changes to changes in vegetation activity (e.g. using multiple regression) is likely to be inaccurate in certain regions. At global scale we therefore used a more flexible regression tree model. Such a model is built by recursive partitioning of the sample (= *root node*) into more homogeneous nodes, or *children* (Breiman *et al.*, 1984). Each split is based on one predictor and is selected according to a splitting criterion which minimizes the total sum of squared deviations from node centres. The tree is grown until no splits can be made anymore due to lack of data and subsequently reduced in a process of *pruning* where least important splits, based upon the cost-complexity measure (Steinberg, 2009), are removed. We used cross-validation to derive the optimal complexity parameter. Using this, the 54601 grid cells (root node) were classified into 867 terminal nodes. All climate parameters were selected in approximately equal amounts in the splits. The resulting model was used to predict the change in vegetation activity by following the path from the root node down to the appropriate terminal node of the tree. This provided the fixed-effects term of the additive model in Eq. 6.1. A minus of this approach is the limited transparency of the predictor importance compared with linear regression models. Several methods can be used to estimate

variable importance, but their robustness is debated and even if successfully applied they have been limited to non-spatial estimates. Complementary to this approach we therefore applied multivariate linear regression (Eq. 6.2) for a better insight in contribution of the predictors in specific land cover regions.

$$\mathbf{Y} - h = \beta_0 + \begin{bmatrix} \Delta TMP \\ \Delta PRE \\ \Delta CLD \\ \Delta PET \end{bmatrix} \times [\beta_1 \quad \dots \quad \beta_4] \tag{6.2}$$

In Eq. 6.2, β are regression coefficients and the other vector contains changes in the CRU parameters (Table 1) as covariates (**X** in Eq. 6.1). The latter were determined for the same time span as the NDVI data using seasonal decomposition and a linear trend model. For the seasonal decomposition we used the smooth harmonic curve derived using the harmonic analysis of NDVI time series (HANTS) algorithm (Roerink *et al.*, 2000; de Jong *et al.*, 2011a). For the reasons mentioned above, the regression models were specifically parameterized for each land-cover class based on the MODIS land cover product (relying on the IGBP classification scheme). At 0.5 degree spatial resolution, land cover is in most cases a composite of smaller patches. The sub-pixel frequency (Figure 6.1*b*) of each class was used to quantify this effect. The highest threshold was selected such that each land cover class retained a sufficient number of pixels for training the regression models of Eq. 6.2. Above the threshold of 80%, the smaller land cover classes (deciduous broadleaf forest and closed shrubland) retained too few pixels for model training and significance tests. At the 80% level, permanent wetlands – the major land cover class in 514 grid cells (< 1%) – formed the only vegetated land cover class that could not be incorporated in the model. For all other classes, the coefficient of determination (R^2) and correlation coefficients between changes in climatologies and vegetation activity were listed (Table 6.2). The correlation between changes in aridity index and precipitation was high (0.71) and in the regression models the latter appeared stronger as a predictor. For that reason, the aridity index was omitted from the model.

Clusters of pixels in large homogeneous regions (Siberia, Amazon, Great Plains, etc.) may cause spatial dependency in the training data. Therefore, a bootstrapping method was applied for estimation of the model coefficients to avoid spatial autocorrelation. The number of bootstrap resamples was set to 1,000 for each land cover class. The output was used to calculate 95% confidence intervals and, based on these, to exclude parameters for which the regression coefficient appeared insignificantly different from zero.

Spatial field model (random effects)

The deterministic model is a per-pixel approach which does not account for spatial dependence, other than by land-cover interaction. Spatial dependence can be imposed by modeling h as a stationary Gaussian random field (GRF). A GRF is specified by its mean value function and its covariance function. Therefore, the main assumption underlying h is a normal distribution with, in this case, zero mean and covariance matrix $\sum(\Theta)$. The model parameters Θ (i.e. sill, nugget and range parameter δ) fully characterize the random field, which is to say

$$h|\Theta \sim N(0, \sum(\Theta)) \tag{6.3}$$

The covariance matrices need to be symmetric and positive definite. They were specified using a spherical covariance function which satisfies these conditions. The size of each covariance matrix (i.e. square of the number of observations) may lead to serious computational issues for datasets of the size used here (Furrer & Sain, 2009). We used two measures to deal with this. First, a spherical function was selected because observations beyond the maximum range δ can be considered spatially uncorrelated. We determined δ using a negative 2 log-likelihood, or -2ln(L), curve while estimating $\hat{h}^{(0)}$ (Method 6.2), but for larger datasets δ might be imposed by memory limits. Second, recognizing the sparse nature of the covariance matrices, only non-zero entries were stored and used for estimation of Θ. For this part of the analysis we used the R package *spam* (Furrer & Sain, 2010). Subsequently, given that $\sum(\Theta)$ is a symmetric positive definite matrix, Cholesky decomposition was used to construct a lower triangular matrix **L**, such that the product $\mathbf{L}\mathbf{L}^T$ returns the original matrix. Solving linear systems becomes computationally more efficient using this manipulation (Higham, 2009), which we used to our advantage when estimating Θ and $\hat{h}$ as seen in Method 6.2.

Method 6.2

[0a] Let $\hat{\beta}^{(i)}$ be a fit from **Y** (fixed effects)
[0b] Estimate Θ_0 from $\mathbf{Y} - \hat{\beta}^{(i)}$ by method-of-moments
[0c*] Put $\delta = 0$ (unit: degrees)
[1*] Put $\delta = \delta + 1$
[2] Calculate distance matrix using δ and great-circle distance (unit: km)
[3] Apply spherical covariance function using Θ and δ
[4] Optimize Θ using MLE
[5*] Repeat steps 1 to 4 until minimum in -2ln(L) function
[6] Fix δ *, calculate $\hat{h}^{(i)}$ (Eq. 4) and continue with Algorithm 6.1

Initial values for Θ_0 used in the MLE were obtained by the method-of-moments using *gstat* (Pebesma & Wesseling, 1998). The spatial field $\hat{h}$ was then calculated from the estimated Θ (Eq. 6.4) and used for backfitting of β (Method 6.1 step 5). The procedure of the spatial field model is summarized in Method 6.2, where steps marked with an asterisk were only applied in the first iteration, i.e. when predicting $\hat{h}^{(0)}$ (Method 6.1 step 2). Methods 6.1 and 6.2 provide the best empirical linear unbiased prediction (EBLUP) of the spatial field (Henderson, 1975) and are, under the intrinsic assumption of Eq. 6.3, analogous to kriging approaches in geostatistics (Lark *et al.*, 2006). More specifically, given that the fixed-effect term is some linear combination of predictors, as in our case, then the EBLUP is equivalent to universal kriging or regression kriging.

$$\hat{h} = \widehat{\sum_h} \cdot \left(\widehat{\sum_h} + \widehat{\sum_\varepsilon}\right)^{-1} \cdot \left(\mathbf{Y} - \hat{\beta}\mathbf{X}\right) \tag{6.4}$$

Where $\sum_h$ is essentially identical to $\sum(\Theta)$, but without nugget variance ($\sum_\varepsilon$). The nugget variance is equivalent to $\hat{\sigma}^2 I$.

In summary, the spatial field is described by a spherical model based on the range, (partial) sill and nugget parameters. The optimal range δ was estimated during the first model iteration (Method 6.1 step 2). In terms of log-likelihood, the optimum was found around 900km (Figure 6.3*a*), with the most substantial decrease in -2ln(L) below ~500km. We used the most conservative range of δ = 897km (~8deg) for estimation of the other model parameters. This resulted in a covariance-matrix density of 3%, equivalent to 89.5 million nonzero elements for 54601 observations. The other parameters were estimated using this fixed range and the resulting spherical covariance function is shown in Figure 6.3*b*.

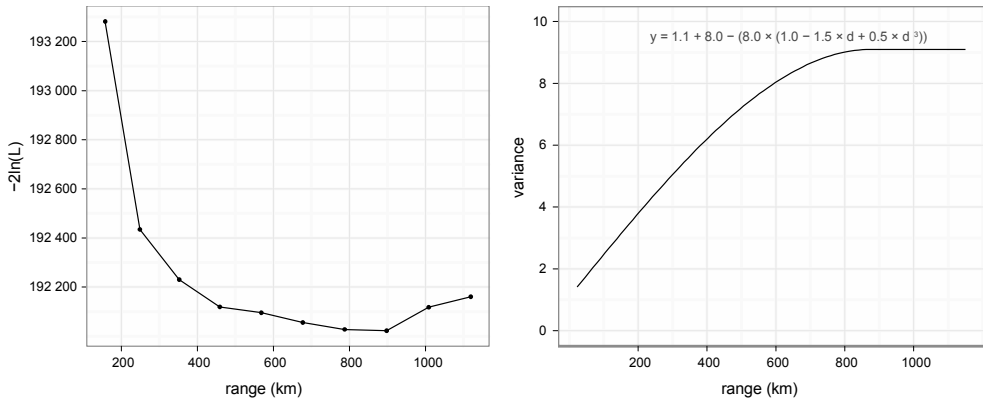

Figure 6.3 (a) Maximum likelihood estimation (MLE) of spatial model parameters as a function of range δ (x-axis). The y-axis shows the negative 2 log-likelihood, or -2ln(L). (b) the optimal spherical covariance function obtained from the MLE and used for the Gaussian Random Field (GRF).

Residual component

A pure-nugget effect (variogram not shown) indicated that the pixel values in the residual component are spatially uncorrelated. This implies that the combination of fixed effects and random effects captured all spatial variance at 0.5 degree resolution. As previously mentioned, the within-pixel variation, i.e. due to processes which act beyond 0.5deg scale, remains unexplained.

6.4 Results and discussion

6.4.1 Model predictions

Figure 6.4 shows the decomposition of the changes in vegetation activity into the fields described by the fixed effects, the spatial process and the residual error process, which includes local-scale effects. At global scale, the regression tree model was used to represent the variation in vegetation activity which can be associated to climatologies. The prediction based on the optimal model fit (in terms of lowest cross-validation error) explained 54% of the variation and is shown in the second panel of Figure 4. Bootstrapped regression models provided insight in land-cover specific associations between vegetation activity and growth-limiting climate

Table 6.2 Results of the bootstrapped linear regression model. For each land cover class (following Loveland *et al.*, 2000), the table lists the number of 0.5 degree grid cells in which the corresponding land cover dominates (Cells), the coefficient of determination of the fitted model (R^2) and the Pearson correlation coefficients between the change in NDVI and the parameters in the model. Homogeneous grid cells (sub-pixel frequency > 80%) were used for model training and climate parameters that did not significantly ($\alpha = 0.05$) contribute to the model were not included.

				Correlation coefficients			
	Land cover class	**Cells**	**R^2**	**TMP**	**PRE**	**CLD**	**PET**
Forest	Evergreen Needleleaf Forest	3474	0.43	0.65			0.25
	Evergeen Broadleaf Forest	4773	0.22		0.17		-0.16
	Deciduous Needleleaf Forest	1431	0.54	-0.57	-0.26		-0.32
	Deciduous Broadleaf Forest	663	0.68	-0.23		0.79	
	Mixed Forest	3441	0.25	0.14			-0.14
Non-Forest	Closed Shrubland	505	0.59	0.09	0.67	0.17	0.36
	Open Shrubland	11391	0.08	0.12	0.05	0.25	-0.17
	Woody Savanna	5557	0.20	0.38		-0.37	0.32
	Savanna	3119	0.10	0.16	0.06	-0.12	0.10
	Grassland	6211	0.22		0.14	0.30	-0.20
	Cropland	5327	0.13	0.07		0.28	0.05
	Cropland / Natural Mosaic	2392	0.20			0.30	

parameters. The performance, in terms of coefficient of determination (R^2), varied between land cover classes. There appeared to be a difference between forest and non-forest areas when it comes to the strength of association. In general, the strongest relationships were found in forests (Table 6.2), with the highest R^2 in deciduous classes and the lowest R^2 in the (tropical) evergreen broadleaf class. The latter was anticipated for a number of reasons: the use of NDVI is disputed in this class (Huete *et al.*, 1997), the density of climatological observations is low (Zhao & Running, 2011) and vegetation growth may not be limited by the included climatologies (Churkina & Running, 1998). Outside of the forests, the strongest relationship was found for closed shrubland (e.g. parts of the Sahel region) while the weakest relationship was found for open shrubland. The likely explanation for the latter is the heterogeneous distribution of this land cover class over the globe (Figure 6.1*a*). It includes, among other regions, the tundra, large parts of the Horn of Africa, southern Africa, central Australia and Argentina, each of which can be expected to react differently to climate changes (Chapin *et al.*, 2000, Chapter 2). For such reasons, the regression tree approach was adopted for global prediction (shown in Figure 6.4*b*).

Table 6.2 suggests that the relationship between cloudiness, which was used as proxy for incident radiation, and vegetation activity is more conspicuous for non-forest than for forest classes. A positive relationship between cloudiness and vegetation activity was found for all classes but savanna, which suggests that a reduction in incident radiation has a positive impact on vegetation activity in, among others, grasslands and croplands. For a proper explanation of this relationship it is important to understand the influence of direct and diffuse components of incoming global radiation and the PAR fraction in special (Spitters *et al.*, 1986). Clouds do not act as on/off switch for incident radiation, but determine the ratio between direct and diffuse radiation. For this reason, the efficiency of photosynthesis under overcast skies may be underestimated (Roderick *et al.*, 2001; Gu *et al.*, 2002) which would be a candidate explanation for the observed relationship. For other land cover systems, the combination of higher temperatures and reduced cloudiness may increase the potential evapotranspiration, but limit vegetation activity, as observed for savannas. These ecosystems are predominantly water limited, rather than temperature limited (Nemani *et al.*, 2003). In addition to the increased photosynthetic efficiency, the observed cloudiness associations may be related to changes in global radiative forcing. A reduction, or global *dimming*, has been suggested for the 1960s until late 1980s, but it was suggested that the trend inversed towards global *brightening* afterwards (Wild *et al.*, 2005). The latter was found to have raised the diffuse fraction of solar radiation which, in turn, may have boosted photosynthetic efficiency. Conversely, less direct radiation reduced evapotranspiration in some semi-arid regions (Oliveira *et al.*, 2011). In forest ecosystems, associations between cloudiness and vegetation activity were only found in the deciduous broadleaf class.

The (boreal) needleleaf classes show the strongest associations with temperature, which is in line with the expected limiting factor (Nemani *et al.*, 2003), although the deciduous needleleaf forests (Russia) show reduced vegetation activity despite the warming trend (Figure 6.2, Table 6.2). This case of *boreal browning* has been called the *divergence problem* and underlying processes remain unknown. Suggested causes include drought stress, pollution, global dimming, direct temperature stress and, likely, a combination of these (Goetz *et al.*, 2011). Drought stress would be in line with field observations in relatively dense forests (Goetz *et al.*, 2011) and radiation-related causes may be expected in other cases, although in this study only found through association with potential evapotranspiration. Radiation-hydrology feedback mechanisms may further complicate this issue (Oliveira *et al.*, 2011).

The strongest association with precipitation was found in closed shrublands, including parts of the Sahel. This region is known for its long anomalously dry period since the early 1970s (Nicholson, 2000), probably related to multidecadal oceanic oscillations (Zhang & Delworth, 2006). The record-low years were the early 1980s and since then a positive trend in both precipitation and vegetation activity was found (Fensholt & Rasmussen, 2011) which likely underlies the detected association.

In Figure 6.4, the general pattern of changes in vegetation activity is well captured by the fixed-effects model, although the greening patterns seem better represented than some of the browning patterns (e.g. in sub-equatorial Africa). These large-scale browning patterns were picked up by the spatially correlated field, which implies that they could not be directly related to the regarded climate changes, but the underlying processes are likely to act at large spatial scales. In Africa, two regions stand out: south / east of Lake Victoria (mainly Tanzania) and Zimbabwe / southern Mozambique. In the former, the changes might be partly related to human activities, since the fixed-effect model predicted small increases in vegetation activity rather than decreases. In recent decades, population increased and agriculture intensified accordingly. Although small parts of the area are in protected national parks (e.g. Serengeti), the browning hotspots are in unprotected woodland and grassland, parts of which were previously marked as degraded (Pelkey *et al.*, 2000). Wind erosion and overgrazing have been mentioned as causes for degradation in these regions (Dregne, 2002).

Figure 6.4 (next page) Decomposition of (*a*) the observed changes in vegetation activity (Figure 6.1*a*) into (*b*) fixed effects based on coefficients β and CRU climate parameters $\mathbf{X}$ as represented by the regression tree(CART) model, (*c*) random effects (smooth spatial field) h based on a Gaussian random field (GRF) and (*d*) residual term ε. The four insets in the right column illustrate the spatial structure of each model component at pixel level for the example of southern Africa. For few grid cells, fixed effects could not be estimated and, as a result, the spatial field not predicted, due to masking of water bodies and permanent wetlands (e.g. Lake Malawi in the insets).

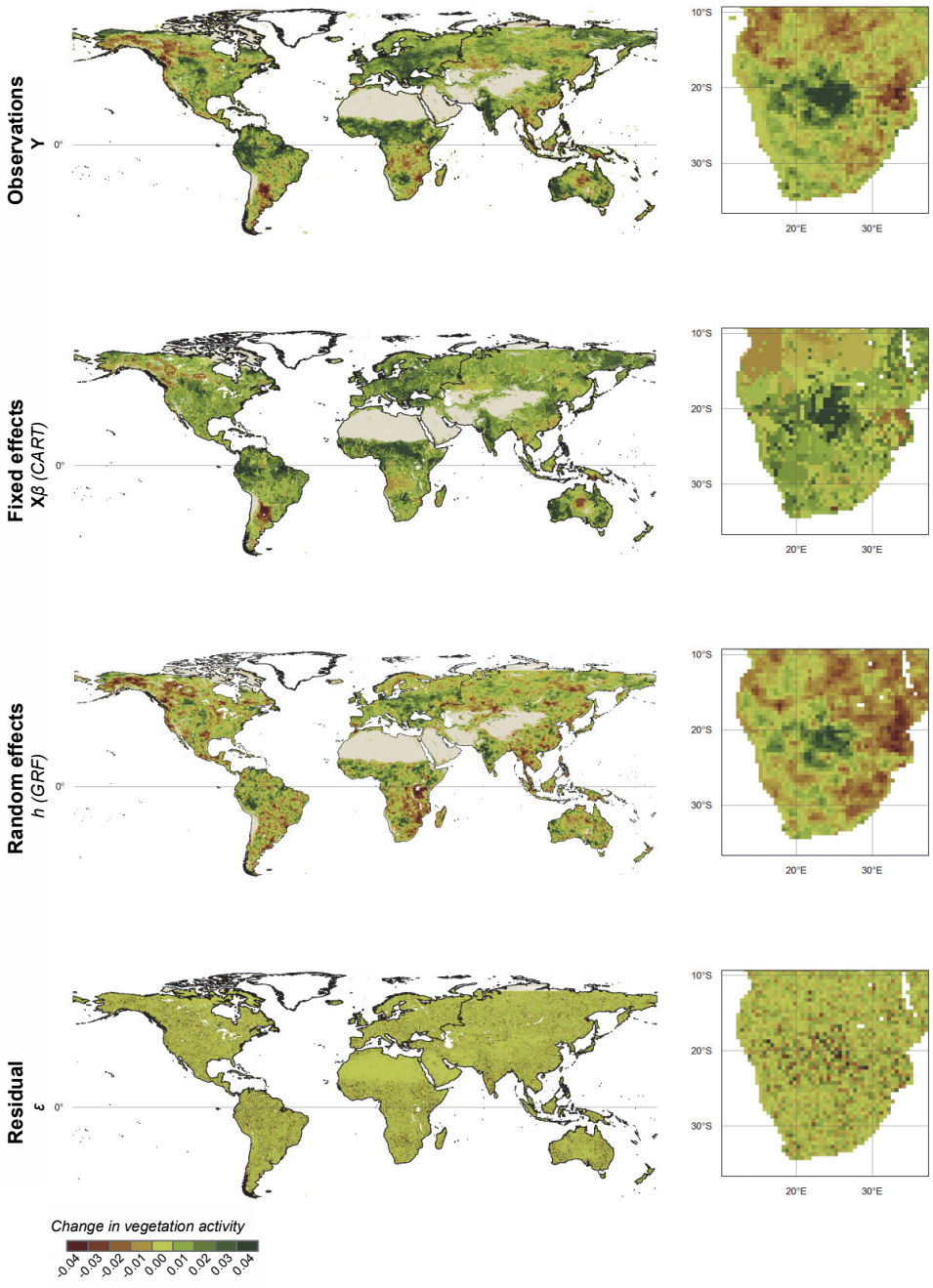
Observations
Y
Fixed effects
Xβ (CART)
Random effects
h (GRF)
Residual
ε
0°
10°S
20°S
30°S
20°E
30°E
Change in vegetation activity
-0.04
-0.03
-0.02
-0.01
0.00
0.01
0.02
0.03
0.04

Severe degradation was also found in Zimbabwe and attributed to human land use, concentrated in communal areas (Prince *et al.*, 2009). While relating potential productivity to actual productivity in this region, Prince *et al.* (2009) could establish no relationship between productivity declines and climatic factors, which is in line with our results. Other conspicuous regions include large parts of the needleleaf forests in Alaska, Canada and Russia. For these regions, the complicated relationship with climate and other abiotic factors was discussed before.

The remainder component in Figure 6.4*d* is spatially uncorrelated. This component may contain small-scale human interventions, indirect climate effects (likely hidden in uncaptured feedback mechanisms) or measurement error (Zhou *et al.*, 2001). It should be noted, however, that a substantial part of the local variation caused by small-scale processes was averaged out in the spatial aggregation procedure. Climatological observations at higher spatial resolution would be needed to further disentangle these processes.

6.4.2 Limitations and outlook

The results from the presented model showed plausible associations between limiting climate variables and vegetation activity. However, it also seems appropriate to reflect on the limitations and on future steps to be taken. First of all, we are aware that correlation, on which this study relied, does not mean causation. The presented statistical methods form no atmosphere-vegetation interaction model and there are many climatological processes that cannot be resolved while being of influence at the regarded spatial scale. Sophisticated modeling of the deterministic component, including mentioned climate-vegetation feedback mechanisms, might be achieved with full spatial-temporal models, but comes with challenges. For example, estimation of many model parameters, given only NDVI as response variable, is likely to run into an ill-posed scenario. Furthermore, dynamic temporal lags between some climatic predictors and vegetation response need to be accounted for. The latter is neither simple nor straightforward at large spatial and temporal extents (Eklundh, 1998).

The predictive power of the gridded climate data at hand is limited for reasons of spatial interpolation, i.e. the effective number of observations is lower than the number of 0.5 degree grid cells. This lack of predictive power currently gives more weight to the random components of the model. A denser climate observation network would increase the predictive power, especially in remote areas, although great value of the CRU dataset resides in its time span. As regards the cloudiness data, station-based observations have been augmented with sunshine records (Mitchell & Jones, 2005) and few observations are available outside Europe, North America and Asia. Both may bias the prediction and render radiation the component where improvement is most needed.

6.5 Conclusions

In this study we applied a decomposition of spatial patterns in vegetation-activity changes in an attempt to contribute to the quest of disentangling various climate and human effects. As a step towards this goal, we aimed at quantifying spatial relationships between temporal trends in potentially growth-constraining climatologies (i.e. temperature, precipitation and radiation) and vegetation activity, inferred from normalized difference vegetation index (NDVI) data. The deterministic, or fixed-effects, component established a global relationship which explained about 54% of the spatial variation. The remainder was described using a spatially correlated field as well as spatially uncorrelated residuals. This demonstrated that associations between vegetation-activity trends and possible drivers can be made using historical satellite data. Land-cover specific regression models, in combination with spatial patterns from the random-effect component, demonstrated that the strongest relationships were found in forests, while weak relationships were found for more heterogeneously distributed land-cover classes like open shrubland. For many classes, inverse relationships with cloudiness may indicate that, also at large scales, vegetation activity is positively influenced by a higher proportion of diffuse light. Strongest relationships with temperature, both positive and negative, were found in needleleaf forest. A negative relationship is, in this case, indicative of reduced vegetation activity under warming conditions: an effect which is, for boreal forests, known as the divergence problem. Strong positive relationships between precipitation and vegetation activity were found in closed shrublands, including the Sahel. For other sub-Saharan regions, including Tanzania and Zimbabwe, browning trends could not be related to climate variables. In these regions, negative changes in vegetation activity may need to be explained by human activities.

Acknowledgements

We are grateful to Molly Brown and the GIMMS group for providing their latest dataset and to Rama Nemani for sharing the source data of Figure 1a in (Nemani *et al.*, 2003). We acknowledge Peter Verburg for the discussions about spatial aggregation issues. Funding was provided by ISRIC – World Soil Information.

Chapter 7

Synthesis

7.1 Main results

Seven billion people, directly or indirectly, depend on Earth's capacity to let plants grow. Slight changes in this capacity may have dire environmental and societal consequences. It is therefore a valuable effort to closely monitor fluctuations in vegetation activity and to detect changes. This information lies at the heart of land degradation monitoring. To recall, this work addressed four main research questions, as they were listed in Section 1.3. In answering these questions, this work aimed at advanced understanding of dynamics and trends in global vegetation activity, in relation to climate variability, for use in land resource applications, including land degradation assessments. The four research questions are individually addressed below, followed by general conclusions and an outlook for future research efforts.

1: What is the current state-of-art in large-scale quantitative land degradation assessment and what are knowledge gaps, key ecological indicators and successful methods that have not yet been exploited to their full potential?

Land degradation is recognised as a global environmental and development issue on a par with climate change, but due to its complex nature there is until today no consensus on its causes, severity and extent. Among the most urgent demands is the separation of human-induced from climate-induced degradation, irrespective of the question to what extent the latter is caused by human interventions. In the case of direct human actors, e.g. land-use changes or overexploitation of land resources, mitigation might be targeted by different land-use practises, while climate-induced changes can, most likely, not be counteracted at this scale. In such cases, a way of adaptation to these developments is required. For making such decisions and associated policy, it is not sufficient to rely on anecdotal and qualitative information. Quantified, explicit information is needed to determine the nature and seriousness of the situation. This requires consistent monitoring of key indicators at a range of scales. Key indicators, however, can only be selected if an unambiguous definition of land degradation is adopted. This is hardly possible at global scale, since the term land degradation can be very specific to prevailing environmental conditions and is often subject to interpretation and perception (Section 2.1). Despite this contentiousness, a main characteristic can be distilled from the many existing definitions: reduction or loss of ecosystem services, notably the primary production service (Adeel *et al.*, 2005). Loss of vegetation activity and/or cover have therefore been widely used as key indicator, also because of the availability of long-term VI time series. The first quantitative global assessment of land degradation and improvement (GLADA) used linear trends over yearly averaged NDVI measurements

and translated these into NPP (Bai *et al.*, 2008). There is, however, still criticism and steps towards improvement included (*I*) advancement of the change detection techniques, (*II*) the use of spatial-contextual information in the interpretation of detected changes, (*III*) integration of state assessments using model-based links to driving processes and (*IV*) validation using regional assessments (Section 2.5).

The more thorough use of the temporal and spatial dimensions of the available VI datasets was adopted as research line for the technical work of this thesis. This targets the first two identified steps for improvement of land degradation monitoring. The temporal dimension provided the initial focus and the second research question, around which we elaborated several enhanced change detection methods. A conventional approach for change detection involves yearly aggregation of VI measurements, which inherently eliminates useful intra-annual information. The reduction of the information content also obstructs the possibilities of detecting trend reversals or possible (catastrophic) shifts in the greening or browning regime. We know that such shifts have occurred in the past decades (Schimel *et al.*, 2001; Slayback *et al.*, 2003; Angert *et al.*, 2005; Wang *et al.*, 2011), but quantitative information is lacking at the global scale. This knowledge gap provided our third research question. Finally, the interpretation of detected changes beyond the per-pixel level using spatial-contextual approaches was targeted by our final research question.

In following the described research line, the main focus was on spectral vegetation indices. However, VIs are not exclusive as key indicator for land degradation. In previous studies they have, for instance, been complemented with climate parameters and, at smaller spatial scales, with yield statistics or demographic measures. Conspicuously, precipitation changes have been adopted in a range of land degradation studies in the form of the rain use efficiency (RUE) concept (Le Houérou, 1984; Prince *et al.*, 1998; Symeonakis & Drake, 2004; Bai *et al.*, 2008). This concept was developed for use in arid and semi-arid environments and assumes that water availability is limiting for plant growth – i.e. RUE is the ratio of NPP to precipitation. In the most prominent study area for land degradation, the Sahel, this resulted in a debate about the way RUE should be interpreted. At least, the relationship with trends in precipitation itself should be carefully considered. If this is done properly, temporally *invariant* RUE measurements might then still indicate human-induced degradation (Hein & de Ridder, 2006). This conclusion was later disputed for reasons of the uncertainty in RUE close to zero rainfall and for methodological issues in derivation of temporal trends (Prince *et al.*, 2007). A follow-up then concluded that uncertainties do indeed exist and may be attributed to non-linearity in the NPP–RUE relationship and to cross-scale effects, i.e. feedback mechanisms at site-scale may differ from spatially integrated observations (Hein *et*

al., 2011). At least, it can be concluded that the concept strongly correlates with the use of precipitation trends and that it is not globally applicable.

Finally, both the start and the extent of the time series leave ample space for uncertainty about degradation trends. The presented work demonstrates advancements in monitoring of *long-term* vegetation activity on our globe. Long-term, in this context, coincides with the few decades for which satellite imagery is available: slightly more than one human generation. This is a short and seemingly arbitrary time span in the Earth's system – with climate cycles acting at time scales of thousands of years and beyond – and may raise questions about the relevance of the efforts. At the same time, it covers the period in which the human population grew from 4.5 billion to 7 billion and, as a consequence, the period in which relatively small changes in vegetation productivity can be of large environmental and societal importance. These changes may need adaptation to new conditions, including humanitarian aid in regions which see land resources degrading in present time. On the other hand, it urges to weigh the lack of initial-state information in the interpretation of changes.

2: Can we use the full temporal dimension offered by satellite records for detection of vegetation-activity trends and what is then the influence of land-surface phenology?

Change detection using yearly integrals of NDVI measurements is a robust approach for most parts of the world, as we demonstrated in Chapter 4, but it eliminates intra-annual information. The latter is useful for the interpretation of changes and might provide clues towards driving processes. Also, the way data is aggregated influences the change detection. This issue is well-known for the spatial domain as the modifiable areal unit problem (MAUP), but it also affects the temporal domain: the detected magnitude of change is, in part, determined by the way in which data is aggregated.

As an alternative to reducing the temporal resolution, we investigated the use of harmonic analyses and non-parametric trend tests. The first may serve several purposes, including the detection of clouds as large negative deviations from the expected VI value. It can also be applied to describe the seasonal component of the observed VI signal. Greening and browning trends were quantified using a linear model on observations from which the seasonal component was subtracted. Furthermore, a seasonal non-parametric model was tested on raw GIMMS data. Both approaches preserve the full temporal resolution, but with each arise other issues. In case of the linear model, the observations are not truly independent since anomalies are likely to persist for longer than two weeks. This increases the risk of detecting false-positives: statistically significant trends which do not exist in reality. It might

then become problematic to distill what is practically meaningful from what is statistically meaningful. In this work, this effect was reduced by modifying the confidence intervals accordingly using generalized instead of ordinary least squares. The non-parametric tests are not affected by this issue. However, this type of tests compares observations in time based on the associated calendar dates and, as such, they rely on the intrinsic assumption that the growing seasons are invariant over time. This assumption does, for various reasons, not hold for global monitoring. Therefore, phenological shifts and variation in length of growing season were accounted for by adjusting the timing of the observations to the growing season. In this way, the observations represent vegetation development stages rather than calendar days. The resulting trend provides a measure of within-season *growing intensity* rather than accumulated vegetation productivity. A reduction in growing intensity might indicate degradation due to nutrient or water stress, since changes in length of growing season due to temperature are not regarded. Harmonic functions were used to determine phenological parameters, although these are mainly suited for single growing seasons in regions with sufficiently high seasonal amplitude. The development of a globally comprehensive method which accounts for all growing regimes is an urgent issue which has been adopted by the research community (Geerken, 2009; Stöckli *et al.*, 2011).

Conspicuous greening and browning hotspots were previously identified in literature (see Table 2.2) and Chapter 3, about monotonic trends, seconded most of these conclusions. The non-parametric models demonstrated the significant influence of variations in land-surface phenology and provided the option of including intra-annual variation within the analysis. The results were adequate for use in our next steps: detection of trend reversals and interpretation of spatial patterns.

3: Can we detect trend reversals within the time series and what is the implication of these reversals for global vegetation activity trends?

For detection of temporal trends in long-term time series of VI data, the signal-to-noise ratio is small. That is to say, the magnitude of change is typically several orders of magnitude smaller than seasonal variation and may, in some cases, be of the same magnitude as artifacts like sensor degradation. Furthermore, with time series becoming longer, trends become more likely to be obscured by alternation between positive and negative changes. Underlying this logic is the important question about the specific duration of phenomena under consideration: how long should a trend last in order to qualify as indicator for land degradation or improvement? An exact answer cannot be given, but provided that food crises like the 2011 Somalia and Kenya example can be caused by few anomalous years, it is at

least substantially shorter than the time span of the VI data. As a logical result, changes in vegetation activity over time can be regarded as a sequence of greening and/or browning periods, separated by abrupt changes with varying magnitude. This can be further illustrated by trend reversals which have been found and debated in recent publications. For example, the core message of a recent paper in *Science* – which caused a polemic between various scientist – was a detected reversal, around the year 2000, turning global greening into global browning (Zhao & Running, 2010). The negative trends in MODIS-based modelled vegetation productivity expressed strongly in the Southern Hemisphere and were mainly attributed to drought effects. In response, it was argued that the influence of temperature on other model parameters could have caused artificial trends (Medlyn, 2011; Samanta *et al.*, 2011) and that the occurrence of short-term trends should not be interpreted as long-term change (Samanta *et al.*, 2011). These arguments were largely rebutted (Zhao & Running, 2011): sensitivity tests showed that temperature-dependence may have influenced the magnitude, but not the sign of the NPP changes and short-term changes were attributed to differences between field-based and satellite-based NPP measurements. The latter may imply scale-dependent (or: *cross-scale*) effects, which are discussed in Section 7.3. The discussion, however, emphasizes the importance of including short-term trends in the analysis as well as establishing a sound relationship with climatological constraints.

Various studies acknowledged the occurrence of trend reversals, but the timing is commonly imposed (Slayback *et al.*, 2003; Angert *et al.*, 2005) or a single turning point is regarded (Wang *et al.*, 2011). For above-mentioned reasons, there is an urgent need for a data-driven technique which detects and quantifies trend changes without a-priori knowledge on timing or location. Based on this need, the study presented in Chapter 5 aimed at detection of trend changes and decomposition of long-term vegetation-activity trends into short-term variation which is closer related to the typical length scale of driving processes. This is an important step towards a better understanding and explanation of trends in vegetation activity at the sub-decadal scale. We did not argue the validity and existence of monotonic trends, but we added another step to the analysis of the temporal domain.

Seasonally-adjusted VI data from Chapter 3 were used as input and piece-wise linear models revealed the magnitude of abrupt and gradual changes. Trend changes were detected in large parts of the world, especially in (semi-arid) shrubland and grassland biomes where abrupt greening was often followed by gradual browning. An example of this effect was found in the Sahel, which might contribute to the previously-mentioned debate about human vs. climatic drivers of land degradation in this region. Many abrupt changes were found around large-scale natural influences like the Mt Pinatubo eruption in 1991 and the strong 1997/98 El Niño event. Analysis of the detected timing of the trend breaks indicated that the area with browning trends increased over time while the area with greening trends decreased. This

supports the earlier-mentioned greening-to-browning reversal (Zhao & Running, 2010), although greening regained area in the early 2000s. The Southern Hemisphere showed the strongest evidence of browning, again in correspondence with the modelled NPP trends. For 15% of the global land area, trends were found to reverse between greening and browning within the analysis period. This demonstrated the importance of accounting for trend changes when analyzing long-term NDVI time series. The research question can therefore be positively answered and the main implications for the vegetation-activity trends are the increased interpretability in terms of closer relationships to sub-decadal actors like the El Niño southern oscillation (ENSO).

4: What are the spatial relationships between potential climatic growth constraints and trends in vegetation activity?

So far, this thesis aimed at enhancing change detection techniques, but trends were detected irrespective of their driving processes. Chapter 2, however, highlighted the difficulties in interpretation, even if trends are detected with the highest achievable accuracy. This partly resides in the limited information content of VI data. Vegetation indices provide a proxy for vegetation activity, in terms of photosynthetic capacity and amount of standing biomass, but the functioning of terrestrial vegetation systems is so complex that it inherently renders studies which are exclusively based on VI data ill-conditioned for disentangling driving processes. This begs for other data to be included in any analysis of causality. Given the aimed separation between human and climatic actors, the climate component is best suited for quantitative analysis. Subsequently, under the assumption *expressio unius est exclusion alterius*, the attribution of certain trends to climatic drivers leave unexplained trends for interpretation as possibly human-induced. As such, quantification of spatial relationships between trends in vegetation activity and climate variables might provide a step towards establishing links between climate change, human-induced land changes and vegetation activity.

The basic principle underlying the study presented in Chapter 6 is that plant growth is constrained by either one or a combination of three climate parameters: temperature, precipitation or radiation. This holds for almost all regions of the world, with the exception of dense tropical forests where vegetation structure might be limiting (Field *et al.*, 1995; Churkina & Running, 1998). Nemani *et al.* (2003) showed the global distribution of the various constraints (Figure 7.1). Time series of monthly measurements or proxies of these constraints were used to develop an additive spatial model describing fixed effects (associated to climate) and random effects (non-associated). The first accounted for 54% of the spatial variation, which demonstrated that a substantial part of the detected vegetation-activity trends can be

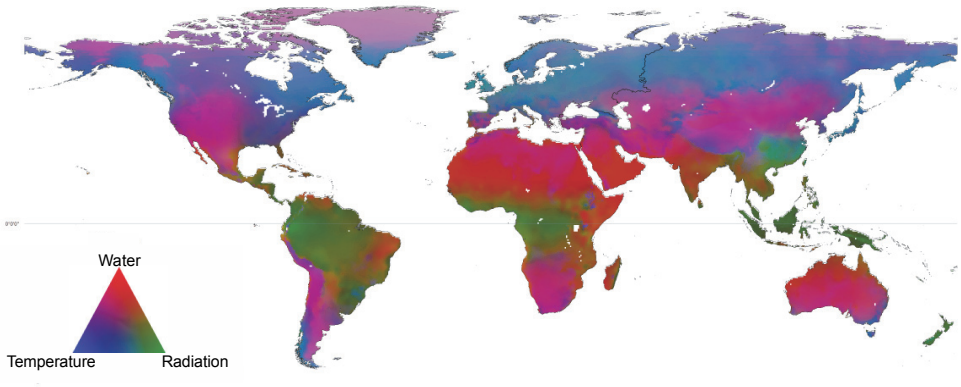

Figure 7.1 Geographic distribution of potential climatic constraints to plant growth, derived from long-term climate statistics. Modified after Nemani *et al.* (2003, Figure 1*a*), using original data.

associated to climate change. In some extensive sub-Saharan regions, including Tanzania and Zimbabwe, browning trends could not be related to climate variables. In these regions, drivers may need to be found in human activities. With this study the spatial context of the detected monotonic trends was used for interpretation of the changes and association to climate changes as follow-up to one of the identified improvements in Chapter 2. We realize that this only entails a first step towards a comprehensive methodology, as discussed in Section 7.3.

7.2 General conclusions

Large-scale monitoring of land resources and influences of climatic changes and human interventions is inherently complicated and involves multitudinous actors and feedback systems. The main contribution of this work towards this quest is (*I*) the identification of research lines and knowledge gaps for large-scale quantitative assessments of greening and browning, (*II*) the use of the full temporal dimension and phenological changes in the trend detection, (*III*) the decomposition of long-term trends into shorter-term variation for a closer description of the system dynamics, (*IV*) the quantification of spatial relationships between climate changes and changes in vegetation activity. The main conclusions from these studies are as follows.

- Land degradation, in common definitions, involves a long-term decline in vegetation productivity. Vegetation activity, inferred from NDVI, can serve as a proxy, but interpretation of detected trends requires either auxiliary information or expert knowledge, as negative trends cannot always be associated to land degradation and *vice versa*. An urgent and currently

unsolved issue in global assessments is the separation of degradation due to (direct) human actors from climate-driven changes.

- Linear trends which are based on yearly NDVI aggregates provide accurate estimates of the magnitude of change, but eliminate the option of using intra-annual variation for assignment of candidate drivers. A decrease in *photosynthetic intensity* within the growing season may indicate nutrient or water stress, while changes in phenology are commonly temperature-induced.

- At global scale, phenological shifts and variation in length of growing season render comparisons of NDVI values by calendar date unsatisfactory. At the same time, an imposed change trajectory, e.g. by the arbitrary length of the time series, urges careful interpretation. Temporal decomposition revealed an alternating pattern of short-term greening and browning trends for large parts of the terrestrial surface. The ENSO-prone shrubland and grassland regions, mainly in the Southern Hemisphere, appeared specifically prone to trend reversals.

- Different spatial patterns were found for abrupt and gradual changes. Abrupt greening prevailed in semi-arid regions, probably due to their strong reactions to climatic variations. These abrupt greening events were often followed by periods of gradual browning. In general, greening prevails in all land cover classes and as a result the global figure indicates an increase in vegetation activity in recent decades.

- Spatial relationships between changes in climatic growth constraints (temperature, precipitation and radiation) and vegetation activity provide insight in the potential actors and feedback systems. Using the deterministic component of an additive spatial model, more than 50% of the variation in vegetation activity could be associated to climatic changes. For specific regions, browning trends could not be related to climate variables. Here, drivers may need to be found in human activities.

7.3 Reflection and outlook

The research line of this thesis has sought to amalgamate the contemporary problem of degrading land resources and the existing long-term satellite records which have the potential of capturing this phenomenon. The scientific contribution of this thesis herein is a combination of a fundamental and an applied part: (*I*) the tailoring of techniques adopted from other scientific fields, including econometrics and spatial statistics, for use with historical satellite records and (*II*) the application and

interpretation of these techniques at global scale. Land degradation, however, is a contentious issue; the complexity which attends monitoring efforts was set out in the previous section and in Chapter 2. Many limitations to the presented studies could be listed, but they boil down to a few core issues.

- Land degradation exists in many documented forms, e.g. Lal *et al.* (1989) lists 12 processes and 9 (human) factors and Zucca *et al.* (2012) list a wide range of indicators and global issues. For this reason, the current assessment can by design not attribute a degradation form or driver to a detected trend.

- The historical vegetation records and scant climate observations in many regions exceed the spatial scale at which many driving processes act. Cross-scale effects may confuse feedbacks between climate and vegetation activity, resulting in omission of small-scale feedback mechanisms. Direct human land-use effects are also likely to act beyond the analysis scale of this work.

These issues implicate two research lines in which future developments may reside: (*I*) the development and application of physically-based process models for establishing cause-and-effect relationships, and (*II*) regionalization of the analysis without compromising on the consistency. Both research lines are briefly discussed below. Third is a data-driven perspective, which is a very nature of remote-sensing science. The number of environmental and climatological processes which can be captured, including processes at decadal time scales, will increase owing to the lengthening VI records. For example, the relationship between vegetation-activity trends and different oceanic oscillations will become more transparent. Knowledge of this natural background variation is crucial as a baseline for detection of non-natural disturbances. Advances in satellite-based remote sensing will improve measurement but, as indicated, further development of physical process models is needed to establish cause-and-effect relationships.

(I) Physical, process models

Soil degradation research started out with a focus on driving processes. The re-focus on topical subjects like sustainability of the 1980s and 1990s have put soil degradation on the global agenda, but shifted the process-driven approach towards an indicator-driven approach (de Jong, 2010). Effects were measured at broader and coarser spatial scales than before, but the relationships with driving processes could no longer be established easily. NDVI trends, in this sense, do provide a globally consistent yardstick, and they do highlight places where biologically significant change is happening, but they are not sophisticated measures of land degradation, let alone the driving processes.

This highlights the need for physical models which simulate detected changes based on underlying processes. In the simplified case of taking vegetation activity as proxy for land degradation, these models should focus on potential limiting factors for vegetation growth (Figure 7.1). Currently, vegetation-atmosphere feedback mechanisms are not fully understood or cannot be replicated from remotely sensed data. For instance, vertical differentiation of atmospheric and near-surface fluxes (carbon, water, oxygen) is an issue, as is the quantification of nutrient availability. Remote-sensing based production efficiency models (PEMs) use meteorological estimates for modeling NPP as a more direct measurement than a VI. New concepts which need to be introduced in such modeling efforts include the differentiation of direct and diffuse radiation for assessment of issues like the boreal divergence problem (Section 6.5.1) and possibly the integration of trend reversals by means of different model parameterization for greening and browning segments. The difference in parameterization, in turn, might provide a better understanding of growth-limiting factors. The detection of trend reversals may be combined with the application of ecological theories – e.g. catastrophic shifts and hysteresis effects in soil-vegetation-atmosphere interactions (Scheffer & Carpenter, 2003; Janssen *et al.*, 2008). The advancements in deriving soil properties from spectral data (Mulder *et al.*, 2011) and the development of remote-sensing based soil erosion models (Symeonakis & Drake, 2010) may complement the modeling efforts with a soil component. Validation of model results requires measurements of vegetation productivity. From a remote-sensing perspective, this can only be approximated using fluorescence-based techniques (Section 1.2.1) and, for the time being, at regional scales.

(II) Regionalization

The results of global studies are often disputed because they differ from traditional expert assessments and they are hard to validate in the field (Section 2.5). At the same time, new-generation sensors start to provide time series long enough to apply proposed change-detection techniques at finer spatial scales. Consistent inspection of detected hotspots has for yet not been undertaken, but moderate resolution imagery and afore mentioned modeling approaches, will facilitate this. For future research on this topic, we can therefore expect a shift in various scales, not the least in spatial scale.

In Chapter 6, steps were made towards establishing statistical relationships between climatic constraints on plant growth and vegetation-activity trends. For effective relationships, however, it is crucial to capture the typical spatial and temporal scales of the processes under consideration. We compromised on the spatial scale, in favour of the temporal domain. This may result in omission of processes and feedback systems at scales closer to land degradation as it is commonly understood. Also, processes that are being captured may seem influential at coarse scales, whilst

they are in reality not at finer scales. Such *cross-scale effects* need to be targeted with a scale-adaptive approach, in both temporal and spatial sense. This will be an essential step in bridging observations and understandings.

In conclusion, future remote-sensing based monitoring of the contemporary land degradation problem resides in a combination of thorough understanding of the physical radiation-interaction concepts (e.g. fluorescence and productivity measurements), model-based relationships between driving processes and vegetation response (e.g. influence of climatic constraints) and validated assessments at comprehensive spatial scales. Modeling at various regional scales – using time-series data from new-generation sensors like MODIS – will be mandatory to advance relationships to coarse scales for monitoring and policy making. At that scale, the AVHRR record will continue to be the most important source of quantitative information about status and trends in terrestrial vegetation activity. With respect to land degradation, there is new concern about feeding the world and food production has to compete for land with energy (biofuels) and feed (increased animal production). This has renewed global interest in soil science and agriculture (Hartemink & McBratney, 2008) and therefore, land degradation will remain a major issue as long as an ever increasing number of people depend on the same land resources.

References

Adeel Z, Safriel U, Niemeijer D, White RP (2005) Millennium Ecosystem Assessment: Desertification Synthesis. World Resources Institute, Washington, DC.

Adler ED (1985) Soil conservation in South Africa. In: *Department of Agriculture and Water Supply, Bulletin 406. Government Printers*. Pretoria, Republic of South Africa.

Alcaraz-Segura D, Chuvieco E, Epstein HE, Kasischke ES, Trishchenko A (2010) Debating the greening vs. browning of the North American boreal forest: differences between satellite datasets. *Global Change Biology,* **16**, 760-770.

Allen R, Smith M, Perrier A, Pereira L (1994) An update for the definition of reference evapotranspiration. *ICID bulletin,* **43**, 1-34.

Angert A, Biraud S, Bonfils C, Buermann W, Fung I (2004) CO2 seasonality indicates origins of post-Pinatubo sink. *Geophysical Research Letters,* **31**, L11103.

Angert A, Biraud S, Bonfils C *et al.* (2005) Drier summers cancel out the CO2 uptake enhancement induced by warmer springs. *Proceedings of the National Academy of Sciences of the United States of America,* **102**, 10823-10827.

Anyamba A, Tucker CJ (2005) Analysis of Sahelian vegetation dynamics using NOAA-AVHRR NDVI data from 1981-2003. *Journal of Arid Environments,* **63**, 596-614.

Asner GP, Heidebrecht KB (2003) Imaging spectroscopy for desertification studies: comparing AVIRIS and EO-1 Hyperion in Argentina drylands. *IEEE Transactions on Geoscience and Remote Sensing,* **41**, 1283-1296.

Asner GP, Nepstad D, Cardinot G, Ray D (2004) Drought stress and carbon uptake in an Amazon forest measured with spaceborne imaging spectroscopy. *Proceedings of the National Academy of Sciences of the United States of America,* **101**, 6039-6044.

Asner GP, Rudel TK, Aide TM, Defries R, Emerson R (2009) A contemporary assessment of change in humid tropical forests. *Conservation Biology,* **23**, 1386-1395.

Asrar G (1989) *Theory and Applications of Optical Remote Sensing,* New York, USA, John Wiley and Sons.

Aubreville A (1949) *Climats, Forêts et Desertification de l'Afrique Tropicale,* Paris, Societé d'Editions Geographiques, Maritimes et Coloniales.

Azzali S, Menenti M (1999) Mapping isogrowth zones on continental scale using temporal Fourier analysis of AVHRR-NDVI data. *International Journal of Applied Earth Observation and Geoinformation,* **1**, 9-20.

Baartman JEM, Van Lynden GWJ, Reed MS, Ritseman CJ, Hessel R (2007) Desertification and land degradation: origins, processes and solutions; Report 4: summary literature review. In: *DESIRE Report Series*. Wageningen, The Netherlands, ISRIC - World Soil Information.

Baghdadi N, Boyer N, Todoroff P, El Hajj M, Bégué A (2009) Potential of SAR sensors TerraSAR-X, ASAR/ENVISAT and PALSAR/ALOS for monitoring sugarcane crops on Reunion Island. *Remote Sensing of Environment,* **113**, 1724-1738.

Bai J, Perron P (2003) Computation and analysis of multiple structural change models. *Journal of Applied Econometrics,* **18**, 1-22.

Bai ZG, Dent DL (2007) GLADA partner country reports: Land Degradation and Improvement Identification by Remote Sensing. In: *ISRIC / FAO*. Wageningen, The Netherlands / Rome, Italy.

Bai ZG, Dent DL (2009) Recent Land Degradation and Improvement in China. *AMBIO: A Journal of the Human Environment,* **38**, 150-156.

Bai ZG, Dent DL, Olsson L, Schaepman ME (2008) Proxy global assessment of land degradation. *Soil Use and Management,* **24**, 223-234.

Baldi G, Nosetto M, Aragón R, Aversa F, Paruelo J, Jobbágy E (2008) Long-term Satellite NDVI Data Sets: Evaluating Their Ability to Detect Ecosystem Functional Changes in South America. *Sensors,* **8**, 5397-5425.

Baldocchi D, Falge E, Gu L *et al.* (2001) FLUXNET: A new tool to study the temporal and spatial variability of ecosystem–scale carbon dioxide, water vapor, and energy flux densities. *Bulletin of the American Meteorological Society,* **82**, 2415-2434.

Banwart S (2011) Save our soils. *Nature,* **474**, 151-152.

Barber VA, Juday GP, Finney BP (2000) Reduced growth of Alaskan white spruce in the twentieth century from temperature-induced drought stress. *Nature,* **405**, 668-673.

Baret F, Guyot G (1991) Potentials and limits of vegetation indices for LAI and APAR assessment. *Remote Sensing of Environment,* **35**, 161-173.

Baret F, Jacquemoud S, Hanocq JF (1993) The soil line concept in remote sensing. *Remote Sensing Reviews,* **7**, 65-82.

Bastin GN, Ludwig JA, Eager RW, Chewings VH, Liedloff AC (2001) Indicators of landscape function: comparing patchiness metrics using remotely-sensed data from rangelands. *Ecological Indicators,* **1**, 247-260.

Beck C, Grieser J, Rudolf B (2004) A New Monthly Precipitation Climatology for the Global Land Areas for the Period 1951 to 2000. In: *Climate Status Report 2004*. Offenbach, Germany, German Weather Service.

Beck HE, Mcvicar TR, Van Dijk AIJM, Schellekens J, De Jeu RaM, Bruijnzeel LA (2011) Global evaluation of four AVHRR–NDVI data sets: Intercomparison and assessment against Landsat imagery. *Remote Sensing of Environment,* **115**, 2547-2563.

Beck PSA, Atzberger C, Høgda KA, Johansen B, Skidmore AK (2006) Improved monitoring of vegetation dynamics at very high latitudes: A new method using MODIS NDVI. *Remote Sensing of Environment,* **100**, 321-334.

Ben-Dor E (2009) Review of Remote Sensing-based methods to Assess Soil Salinity. In: *Remote Sensing of Soil Salinization.* (eds Metternicht GI, Zinck JA), CRC Press, Taylor & Francis Group.

Bergkamp G (1996) Mediterranean geoecosystems: hierarchical organisation and degradation. PhD, University of Amsterdam, The Netherlands, 238 pp.

Bertiller MB, Ares JO, Bisigato A (2002) Multiscale Indicators of Land Degradation in the Patagonian Monte, Argentina. *Environmental Management,* **30**, 704-715.

Birkes D, Dodge Y (1993) Nonparametric Regression. In: *Alternative Methods of Regression*. Hoboken, NJ, USA, John Wiley & Sons, Inc.

Blaikie P (1985) *The Political Economy of Soil Erosion in Developing Countries*, Longman Development Studies, London, New York.

Boer MM (1999) Assessment of dryland degradation: linking theory and practice through site water balance modeling. PhD, Utrecht University, The Netherlands, 288 pp.

Boles SH, Verbyla DL (2000) Comparison of Three AVHRR-Based Fire Detection Algorithms for Interior Alaska. *Remote Sensing of Environment,* **72**, 1-16.

Bonan GB, Levis S, Sitch S, Vertenstein M, Oleson KW (2003) A dynamic global vegetation model for use with climate models: concepts and description of simulated vegetation dynamics. *Global Change Biology,* **9**, 1543-1566.

Boschetti M, Stroppiana D, Brivio PA, Bocchi S (2009) Multi-year monitoring of rice crop phenology through time series analysis of MODIS images. *International Journal of Remote Sensing,* **30**, 4643 - 4662.

Box EO, Holben BN, Kalb V (1989) Accuracy of the AVHRR Vegetation Index as a Predictor of Biomass, Primary Productivity and Net CO2 Flux. *Vegetatio,* **80**, 71-89.

Bradfield R (1960) Opportunities for soil scientists in freeing the world from hunger. In: *Seventh International Congress of Soil Science (ISSS).* Madison, WI.

Breiman L, Friedman JH, Olshen RA, Stone CJ (1984) *Classification and Regression Trees,* Wadsworth, Belmont, CA, Chapman and Hall / CRC Press.

Brown ME, Pinzon JE, Didan K, Morisette JT, Tucker CJ (2006) Evaluation of the consistency of long-term NDVI time series derived from AVHRR,SPOT-vegetation, SeaWiFS, MODIS, and Landsat ETM+ sensors. *IEEE Transactions on Geoscience and Remote Sensing,* **44**, 1787-1793.

Bunn AG, Goetz SJ, Kimball JS, Zhang K (2007) Northern high-latitude ecosystems respond to climate change. *Eos,* **88**, 333-340.

Cai XL, Sharma BR (2010) Integrating remote sensing, census and weather data for an assessment of rice yield, water consumption and water productivity in the Indo-Gangetic river basin. *Agricultural Water Management,* **97**, 309-316.

Cao M, Prince SD, Li K, Tao B, Small J, Shao X (2003) Response of terrestrial carbon uptake to climate interannual variability in China. *Global Change Biology,* **9**, 536-546.

Carlson TN, Ripley DA (1997) On the relation between NDVI, fractional vegetation cover, and leaf area index. *Remote Sensing of Environment,* **62**, 241-252.

Ceccato P (2001) Estimation of vegetation water content using remote sensing for the assessment of fire risk occurence and burning efficiency. PhD, University of Greenwich, UK, 168 pp.

Chamaille-Jammes S, Fritz H, Murindagomo F (2006) Spatial patterns of the NDVI-rainfall relationship at the seasonal and interannual time scales in an African savanna. *International Journal of Remote Sensing,* **27**, 5185-5200.

Champion HG, Seth SK (1968) *A revised survey of the forest types of India,* Delhi, India, Government of India Press.

Chape S, Blyth S, Fish L, Fox P, Spalding M (2003) United Nations list of protected areas. IUCN, Gland, Switzerland and UNEP-WCMC, Cambridge, UK.

Chapin FS, Matson PA, Vitousek PM (2011) *Principles of terrestrial ecosystem ecology,* London, UK, Springer.

Chapin FS, Zavaleta ES, Eviner VT *et al.* (2000) Consequences of changing biodiversity. *Nature,* **405**, 234-242.

Chen S, Rao P (2008) Land degradation monitoring using multi-temporal Landsat TM/ETM data in a transition zone between grassland and cropland of northeast China. *International Journal of Remote Sensing,* **29**, 2055-2073.

Chen Z, Li S, Ren J *et al.* (2008) Monitoring and Management of Agriculture with Remote Sensing. In: *Advances in Land Remote Sensing.* (ed Liang S), Springer Science.

Choudhury BJ, Ahmed NU, Idso SB, Reginato RJ, Daughtry CST (1994) Relations between evaporation coefficients and vegetation indices studied by model simulations. *Remote Sensing of Environment,* **50**, 1-17.

Churkina G, Running SW (1998) Contrasting climatic controls on the estimated productivity of global terrestrial biomes. *Ecosystems,* **1**, 206-215.

Cleland EE, Chuine I, Menzel A, Mooney HA, Schwartz MD (2007) Shifting plant phenology in response to global change. *Trends in Ecology & Evolution,* **22**, 357-365.

Cleveland RB, Cleveland WS, Mcrae JE, Terpenning I (1990) STL: A seasonal-trend decomposition procedure based on loess. *Journal of Official Statistics,* **6**, 3-73.

Cloudsley-Thompson JL (1974) The expanding Sahara. *Environmental conservation,* **1**, 5.

Çöltekin A, De Sabbata S, Willi C, Vontobel I, Pfister S, Kuhn M, Lacayo M (2011) Modifiable Temporal Unit Problem. In: *ISPRS/ICA workshop "Persistent problems in geographic visualization" (ICC2011).* Paris, France.

Cook KH (2008) Climate science: The mysteries of Sahel droughts. *Nature Geoscience,* **1**, 647-648.

Coppin P, Jonckheere I, Nackaerts K, Muys B, Lambin E (2004) Digital change detection methods in ecosystem monitoring: a review. *International Journal of Remote Sensing,* **25**, 1565-1596.

Cowpertwait PSP, Metcalfe AV (2009) Basic Stochastic Models. In: *Introductory Time Series with R.* (eds Gentleman R, Hornik K, Parmigiani G). Dordrecht, The Netherlands, Springer. 254p.

Cracknell A, Varotsos C (2007) The IPCC Fourth Assessment Report and the Fiftieth Anniversary of Sputnik. *Environmental Science and Pollution Research,* **14**, 384-387.

Cracknell AP (1997) *The advanced very high resolution radiometer (AVHRR),* London, Taylor & Francis.

Cracknell AP (2001) The exciting and totally unanticipated success of the AVHRR in applications for which it was never intended. *Advances in Space Research,* **28**, 233-240.

Crutzen PJ (2002) Geology of mankind. *Nature,* **415**, 23.

Dahlberg AC (2000) Interpretations of environmental change and diversity: a critical approach to indications of

degradation — the case of Kalakamate, northeast Botswana. *Land Degradation & Development,* **11**, 549-562.

Dakos V, Scheffer M, Van Nes EH, Brovkin V, Petroukhov V, Held H (2008) Slowing down as an early warning signal for abrupt climate change. *PNAS,* **105**, 14308-14312.

Dalal-Clayton BD, Dent DL (2001) *Knowledge of the land, land resources information and its use in rural development*, Oxford University Press.

Dark SJ, Bram D (2007) The modifiable areal unit problem (MAUP) in physical geography. *Progress in Physical Geography,* **31**, 471-479.

De Beurs KM, Henebry GM (2004) Trend analysis of the Pathfinder AVHRR Land (PAL) NDVI data for the deserts of central Asia. *IEEE Geoscience and Remote Sensing Letters,* **1**, 282-286.

De Beurs KM, Henebry GM (2005a) Land surface phenology and temperature variation in the International Geosphere-Biosphere Program high-latitude transects. *Global Change Biology,* **11**, 779-790.

De Beurs KM, Henebry GM (2005b) A statistical framework for the analysis of long image time series. *International Journal of Remote Sensing,* **26**, 1551-1573.

De Beurs KM, Wright CK, Henebry GM (2009) Dual scale trend analysis for evaluating climatic and anthropogenic effects on the vegetated land surface in Russia and Kazakhstan. *Environmental Research Letters,* **4**, 045012.

De Jong R (2010) The trend in soil degradation publications. *IUSS Bulletin,* **116**, 21-25.

De Jong R, De Bruin S, De Wit A, Schaepman ME, Dent DL (2011a) Analysis of monotonic greening and browning trends from global NDVI time-series. *Remote Sensing of Environment,* **115**, 692-702.

De Jong R, Verbesselt J, Schaepman ME, De Bruin S (2011b) Detection of Breakpoints in Global NDVI time series. In: *34th International Symposium on Remote Sensing of Environment (ISRSE).* 10-15 April 2011, Sydney, Australia.

De Jong R, Verbesselt J, Schaepman ME, De Bruin S (2012) Trend changes in global greening and browning: contribution of short-term trends to longer-term change. *Global Change Biology,* **18**, 642-655.

De Wit AJW, Su B (2005) Deriving phenological indicators from SPOT-VGT data using the HANTS algorithm. In: *2nd international SPOT-*

VEGETATION user conference. Antwerp, Belgium.

Dean WRJ, Hoffinan MT, Meadows ME, Milton SJ (1995) Desertification in the semi-arid Karoo, South Africa: review and reassessment. *Journal of Arid Environments,* **30**, 247-264.

Defries R, Achard F, Brown S, Herold M, Murdiyarso D, Schlamadinger B, De Souza Jr C (2007) Earth observations for estimating greenhouse gas emissions from deforestation in developing countries. *Environmental Science & Policy,* **10**, 385-394.

Defries R, Hansen M, Townshend J (1995) Global discrimination of land cover types from metrics derived from AVHRR pathfinder data. *Remote Sensing of Environment,* **54**, 209-222.

Del Valle HF, Blanco PD, Metternicht GI, Zinck JA (2010) Radar remote sensing of wind-driven land degradation processes in northeastern Patagonia. *Journal of Environmental Quality,* **39**, 62-75.

Demenocal PB (2008) Palaeoclimate: Africa on the edge. *Nature Geoscience,* **1**, 650-651.

Dendoncker N, Schmit C, Rounsevell M (2008) Exploring spatial data uncertainties in land-use change scenarios. *International Journal of Geographical Information Science,* **22**, 1013-1030.

Dent D, Asfary AF, Giri C *et al.* (2007) Land (Chapter 3). In: *UNEP Global Environment Outlook 4 (GEO4): environment for development.* (ed Kassas M). Valletta, Malta, Progress Press Ltd.

Dent D, Young A (1981) *Soil survey and land evaluation,* London, Geo Allen & Unwin.

Dent DL, Bai ZG, Schaepman ME, Olsson L (2009) Response to Wessels: Comments on 'Proxy global assessment of land degradation'. *Soil Use and Management,* **25**, 93-97.

Doktor D, Bondeau A, Koslowski D, Badeck F-W (2009) Influence of heterogeneous landscapes on computed green-up dates based on daily AVHRR NDVI observations. *Remote Sensing of Environment,* **113**, 2618-2632.

Domenikiotis C, Loukas A, Dalezios NR (2003) The use of NOAA/AVHRR satellite data for monitoring and assessment of forest fires and floods. *Natural Hazards and Earth System Sciences,* **3**, 115-128.

Donohue RJ, Mcvicar TR, Roderick ML (2009) Climate-related trends in Australian vegetation cover as inferred from satellite observations, 1981-2006. *Global Change Biology,* **15**, 1025-1039.

Dorigo WA, Zurita-Milla R, De Wit AJW, Brazile J, Singh R, Schaepman ME (2007) A review on reflective remote sensing and data assimilation techniques for enhanced agroecosystem modeling. *International Journal of Applied Earth Observation and Geoinformation,* **9**, 165-193.

Dregne HE (1986) Desertification of Arid Lands. In: *Physics of Desertification.* (eds El-Baz F, Hassan MHA). Dordrecht, The Netherlands, Martinus Nijhoff.

Dregne HE (2002) Land degradation in the drylands. *Arid Land Research Management,* **16**, 99-132.

E-Soter Website (2010) Official portal of the e-SOTER project, http://www.esoter.net.

Ehrlich PR (1968) *The Population Bomb,* New York, USA, Ballantine.

Eklundh L (1998) Estimating relations between AVHRR NDVI and rainfall in East Africa at 10-day and monthly time scales. *International Journal of Remote Sensing,* **19**, 563-570.

Eklundh L, Olsson L (2003) Vegetation index trends for the African Sahel 1982-1999. *Geophysical Research Letters,* **30**, 1430.

Ekström M, Jones PD, Fowler HJ, Lenderink G, Buishand TA, Conway D (2007) Regional climate model data used within the SWURVE project, 1: projected changes in seasonal patterns and estimation of PET. *Hydrology and Earth System Sciences,* **11**, 1069-1083.

El Hassan IM (2004) Desertification Monitoring Using Remote Sensing Technology. In: *International Conference on Water Resources & Arid Environment.* King Saud University.

Eswaran H, Lal R, Reich PF (2001) Land Degradation: an overview. In: *2nd International Conference on Land Degradation and Desertification.* Khon Kaen, Thailand, Oxford Press, New Delhi, Inda.

Evans J, Geerken R (2004) Discrimination between climate and human-induced dryland degradation. *Journal of Arid Environments,* **57**, 535-554.

Fao-Unesco (1988) Soil map of the world, revised legend (with corrections and updates). In: *Techical Paper 20.* Wageningen, The Netherlands, ISRIC - World Soil Information.

Fao (1976) A framework for land evaluation. In: *Soils bulletin 32.* Rome, Italy, Food and Agricultural Organization of the United Nations.

Fao (1979) A provisional methodology for soil degradation assessment. Rome, Food and Agricultural Organization of the United Nations.

Fensholt R, Rasmussen K (2011) Analysis of trends in the Sahelian 'rain-use efficiency' using GIMMS NDVI, RFE and GPCP rainfall data. *Remote Sensing of Environment,* **115**, 438-451.

Fensholt R, Rasmussen K, Nielsen TT, Mbow C (2009) Evaluation of earth observation based long term vegetation trends - Intercomparing NDVI time series trend analysis consistency of Sahel from AVHRR GIMMS, Terra MODIS and SPOT VGT data. *Remote Sensing of Environment,* **113**, 1242-1255.

Fensholt R, Sandholt I, Rasmussen MS (2004) Evaluation of MODIS LAI, fAPAR and the relation between fAPAR and NDVI in a semi-arid environment using in situ measurements. *Remote Sensing of Environment,* **91**, 490-507.

Feoli E, Vuerich LG, Zerihun W (2002) Evaluation of environmental degradation in northern Ethiopia using GIS to integrate vegetation, geomorphological, erosion and socio-economic factors. *Agriculture, Ecosystems & Environment,* **91**, 313-325.

Field CB, Randerson JT, Malmström CM (1995) Global net primary production: Combining ecology and remote sensing. *Remote Sensing of Environment,* **51**, 74-88.

Foley JA, Levis S, Costa MH, Cramer W, Pollard D (2000) Incorporating dynamic vegetation cover within global climate models. *Ecological Applications,* **10**, 1620-1632.

Friedl MA, Davis FW, Michaelsen J, Moritz MA (1995) Scaling and uncertainty in the relationship between the NDVI and land surface biophysical variables: An analysis using a scene simulation model and data from FIFE. *Remote Sensing of Environment,* **54**, 233-246.

Friedl MA, Mciver DK, Hodges JCF *et al.* (2002) Global land cover mapping from MODIS: algorithms and early results. *Remote Sensing of Environment,* **83**, 287-302.

Furrer R, Sain SR (2009) Spatial model fitting for large datasets with applications to climate and microarray problems. *Statistics and Computing,* **19**, 113-128.

Furrer R, Sain SR (2010) spam: A Sparse Matrix R Package with Emphasis on MCMC Methods for Gaussian Markov Random Fields. *Journal of Statistical Software,* **36**, 1-25.

Gallo KP, Daughtry CST, Bauer ME (1985) Spectral estimation of absorbed photosynthetically active radiation in corn canopies. *Remote Sensing of Environment,* **17**, 221-232.

Gamon JA, Serrano L, Surfus JS (1997) The photochemical reflectance index: an optical indicator of photosynthetic radiation use efficiency across species, functional types, and nutrient levels. *Oecologia,* **112**, 492-501.

Gardner W, Fawcett J, Fitzpatrick R, Norton R (2004) Chemical reduction causing land degradation. I Overview. *Plant and Soil,* **267**, 51-59.

Geerken RA (2009) An algorithm to classify and monitor seasonal variations in vegetation phenologies and their inter-annual change. *ISPRS Journal of Photogrammetry and Remote Sensing,* **64**, 422-431.

Glantz MH, Orlovsky NS (1983) Desertification: a review of the concept. *Desertification Control Bulletin,* **9**, 15-22.

Glenn EP, Huete AR, Nagler PL, Nelson SG (2008) Relationship Between Remotely-sensed Vegetation Indices, Canopy Attributes and Plant Physiological Processes: What Vegetation Indices Can and Cannot Tell Us About the Landscape. *Sensors,* **8**, 2136-2160.

Gobron N, Belward A, Pinty B, Knorr W (2010) Monitoring biosphere vegetation 1998-2009. *Geophysical Research Letters,* **37**, L15402.

Gobron N, Mélin F, Pinty B, Verstraete M, Widlowski J, Bucini G (2003) A global vegetation index for SeaWiFS: Design and applications. In: *Remote Sensing and Climate Modeling: Synergies and Limitations.* (eds Beniston M, Verstraete MM). Dordrecht, The Netherlands, Kluwer Academic Publishers.

Goetz SJ, Baccini A, Laporte NT *et al.* (2009) Mapping and monitoring carbon stocks with satellite observations: a comparison of methods. *Carbon Balance and Management,* **4**, 2.

Goetz SJ, Bunn AG, Fiske GJ, Houghton RA (2005) Satellite-observed photosynthetic trends across boreal North America associated with climate and fire disturbance. *Proceedings of the National Academy of Sciences of the United States of America,* **102**, 13521-13525.

Goetz SJ, Epstein HE, Bhatt US *et al.* (2011) Recent Changes in Arctic Vegetation: Satellite Observations and Simulation Model Predictions. In: *Eurasian Arctic Land Cover and Land Use in a Changing Climate.* (eds Gutman G, Reissell A). Amsterdam, Spring-Verlag.

Goetz SJ, Prince SD, Goward SN, Thawley MM, Small J (1999) Satellite remote sensing of primary production: an improved production efficiency modeling approach. *Ecological Modeling,* **122**, 239-255.

Goetz SJ, Prince SD, Small J, Gleason ACR, Thawley MM (2000) Interannual variability of global terrestrial primary production: results of a model driven with satellite observations. *Journal of Geophysical Research,* **105**, 20077-20091.

Goldshleger N, Ben-Dor E, Benyamini Y, Agassi M, Blumberg DG (2001) Characterization of soil's structural crust by spectral reflectance in the SWIR region. *Terra Nova,* **13**, 12-17.

Goulden ML, Munger JW, Fan S-M, Daube BC, Wofsy SC (1996) Exchange of Carbon Dioxide by a Deciduous Forest: Response to Interannual Climate Variability. *Science,* **271**, 1576-1578.

Govaerts Y, Lattanzio A (2008) Estimation of surface albedo increase during the eighties Sahel drought from Meteosat observations. *Global and Planetary Change,* **64**, 139-145.

Goward SN, Dye DG, Turner S, Yang J (1993) Objective assessment of the NOAA global

vegetation index data product. *International Journal of Remote Sensing,* **14**, 3365 - 3394.

Granger CWJ, Newbold P (1974) Spurious regressions in econometrics. *Journal of Econometrics,* **2**, 111-120.

Gu L, Baldocchi D, Verma SB, Black TA, Vesala T, Falge EM, Dowty PR (2002) Advantages of diffuse radiation for terrestrial ecosystem productivity. *J. Geophys. Res.,* **107**, 4050.

Haas EM, Bartholomé E, Combal B (2009) Time series analysis of optical remote sensing data for the mapping of temporary surface water bodies in sub-Saharan western Africa. *Journal of Hydrology,* **370**, 52-63.

Haberl H, Erb KH, Krausmann F *et al.* (2007) Quantifying and mapping the human appropriation of net primary production in earth's terrestrial ecosystems. *Proceedings of the National Academy of Sciences of the United States of America,* **104**, 12942-12947.

Hall F, Masek JG, Collatz GJ (2006) Evaluation of ISLSCP Initiative II FASIR and GIMMS NDVI products and implications for carbon cycle science. *Journal of Geophysical Research,* **111**, 1 - 15.

Hanafi A, Jauffret S (2007) Are long-term vegetation dynamics useful in monitoring and assessing desertification processes in the arid steppe, southern Tunisia. *Journal of Arid Environments,* **72**, 557-572.

Hansen J, Ruedy R, Sato M, Lo K (2010) Global surface temperature change. *Reviews of Geophysics,* **48**, RG4004, 4001-4029.

Hansen MC, Stehman SV, Potapov PV *et al.* (2008) Humid tropical forest clearing from 2000 to 2005 quantified by using multitemporal and multiresolution remotely sensed data. *Proceedings of the National Academy of Sciences of the United States of America,* **105**, 9439-9444.

Hartemink AE, Mcbratney A (2008) A soil science renaissance. *Geoderma,* **148**, 123-129.

Haywood J, Randall J (2008) Trending seasonal data with multiple structural breaks. NZ visitor arrivals and the minimal effects of 9/11. In: *Research report 08/10.* Victoria, New Zealand, University of Wellington.

Hein L, De Ridder N (2006) Desertification in the Sahel: a reinterpretation. *Global Change Biology,* **12**, 751 - 758.

Hein L, De Ridder N, Hiernaux P, Leemans R, De Wit A, Schaepman ME (2011) Desertification in the Sahel: Towards better accounting for ecosystem dynamics in the interpretation of remote sensing images. *Journal of Arid Environments,* **75**, 1164-1172.

Hellden U (1984) Drought impact monitoring. A remote sensing study of desertification in Kordofan, Sudan. In: *Rapporter och Notiser No. 61.* Lund, Sweden, Lunds Universitets Naturgeografiska Institution.

Helldén U (2008) A coupled human-environment model for desertification simulation and impact studies. *Global and Planetary Change,* **64**, 158-168.

Henderson CR (1975) Best Linear Unbiased Estimation and Prediction under a Selection Model. *Biometrics,* **31**, 423-447.

Herold M, Mayaux P, Woodcock CE, Baccini A, Schmullius C (2008) Some challenges in global land cover mapping: An assessment of agreement and accuracy in existing 1 km datasets. *Remote Sensing of Environment,* **112**, 2538-2556.

Herrmann SM, Anyamba A, Tucker CJ (2005) Recent trends in vegetation dynamics in the African Sahel and their relationship to climate. *Global Environmental Change Part A,* **15**, 394-404.

Heumann BW, Seaquist JW, Eklundh L, Jönsson P (2007) AVHRR derived phenological change in the Sahel and Soudan, Africa, 1982–2005. *Remote Sensing of Environment,* **108**, 385 - 392.

Higham NJ (2009) Cholesky factorization. *Wiley Interdisciplinary Reviews: Computational Statistics,* **1**, 251-254.

Hird JN, Mcdermid GJ (2009) Noise reduction of NDVI time series: An empirical comparison of selected techniques. *Remote Sensing of Environment,* **113**, 248-258.

Hirota M, Holmgren M, Van Nes EH, Scheffer M (2011) Global Resilience of Tropical Forest and Savanna to Critical Transitions. Science, 334, 232-235.

Hirsch RM, Slack JR (1984) A nonparametric trend test for seasonal data with serial dependence. *Water Resources Research,* **20**, 727-732.

Hirsch RM, Slack JR, Smith RA (1982) Techniques of trend analysis for monthly water quality data. *Water Resources Research,* **18**, 107-121.

Hockensmith RD, Steele JG (1949) Recent Trends in the Use of the Land-Capability Classification. *Proceedings Soil Science Society of America,* **14**, 383-388.

Hoffman MT, Simon T (2000) A National Review of Land Degradation in South Africa: The Influence of Biophysical and Socio-Economic Factors. *Journal of Southern African Studies,* **26**, 743-758.

Holben BN (1986) Characteristics of maximum-value composite images from temporal AVHRR data. *International Journal of Remote Sensing,* **7**, 1417-1434.

Holm AM, Cridland SW, Roderick ML (2003) The use of time-integrated NOAA NDVI data and rainfall to assess landscape degradation in the arid shrubland of Western Australia. *Remote Sensing of Environment,* **85**, 145-158.

Huang S, Siegert F (2006) Land cover classification optimized to detect areas at risk of desertification in North China based on SPOT VEGETATION imagery. *Journal of Arid Environments,* **67**, 308-327.

Huete A, Didan K, Miura T, Rodriguez EP, Gao X, Ferreira LG (2002a) Overview of the radiometric and biophysical performance of the MODIS vegetation indices. *Remote Sensing of Environment,* **83**, 195-213.

Huete A, Gao X, Kim HJ, Miura T, Borghi C, Ojeda R (2002b) Characterization of land degradation in Central Argentina with hyperspectral AVIRIS and EO-1 data. In: *Transactions of the 17th World Congress of Soil Science.* Bangkok, Thailand, IUSS (CD-ROM).

Huete A, Justice C, Liu H (1994) Development of vegetation and soil indices for MODIS-EOS. *Remote Sensing of Environment,* **49**, 224-234.

Huete AR (1988) A soil-adjusted vegetation index (SAVI). *Remote Sensing of Environment,* **25**, 295-309.

Huete AR, Huiqing L, Van Leeuwen WJD (1997) The use of vegetation indices in forested regions: issues of linearity and saturation. In: *Geoscience and Remote Sensing Symposium (IGARSS).* 3-8 Aug. 1997, Singapore, IEEE International.

Hussian M, Grimvall A, Burdakov O, Sysoev O (2005) Monotonic regression for the detection of temporal trends in environmental quality data. *Match,* **54**, 535-550.

Hüttich C, Herold M, Schmullius C, Egorov V, Bartalev SA (2007) Indicators of Northern Eurasia's land-cover change trends from SPOT-VEGETATION time-series analysis 1998-2005. *International Journal of Remote Sensing,* **28**, 4199-4206.

Imeson AC, Emmer I (1992) Implications of climatic change for land degradation in the Mediterranean. In: *Climatic change in the Mediterranean. Environmental and social impacts of climatic change and sealevel rise in the Mediterranean region.* (eds Jeftic L, Milliman JD, Sestini G)., Edward Arnold, London.

Inkpen R (2005) *Science, Philosophy and Physical Geography,* New York, USA, Routledge (Taylor & Francis Group).

IPCC (2007) Synthesis Report. In: *Fourth Assessment Report (AR4) of the Intergovernmental Panel on Climate Change.* (eds Pachauri RK, Reisinger A). Geneva, Switzerland, IPCC.

Jakubauskas ME, Legates DR, Kastens JH (2001) Harmonic Analysis of Time-Series AVHRR NDVI Data. *Photogrammetric Engineering & Remote Sensing,* **67**, 461-470.

James ME, Kalluri SNV (1994) The Pathfinder AVHRR land data set: An improved coarse resolution data set for terrestrial monitoring. *International Journal of Remote Sensing,* **15**, 3347-3363.

Janssen RHH, Meinders MBJ, Nes EHV, Scheffer M (2008) Microscale vegetation-soil feedback boosts hysteresis in a regional vegetation–climate system. *Global Change Biology,* **14**, 1-9.

Jones HG, Vaughan RA (2010) *Remote Sensing of Vegetation,* New York, Oxford University Press.

Jongschaap REE (2006) Integrating crop growth simulation and remote sensing to improve resource use efficiency in farming systems. PhD, Wageningen University, The Netherlands, 130 pp.

Jönsson P, Eklundh L (2002) Seasonality extraction by function fitting to time-series of satellite sensor data. *IEEE Transactions on Geoscience and Remote Sensing,* **40**, 1824-1832.

Julien Y, Sobrino JA (2009) The Yearly Land Cover Dynamics (YLCD) method: An analysis of global vegetation from NDVI and LST parameters. *Remote Sensing of Environment,* **113**, 329-334.

Julien Y, Sobrino JA (2010) Comparison of cloud-reconstruction methods for time series of composite NDVI data. *Remote Sensing of Environment,* **114**, 618-625.

Julien Y, Sobrino JA, Verhoef W (2006) Changes in land surface temperatures and NDVI values over Europe between 1982 and 1999. *Remote Sensing of Environment,* **103**, 43-55.

Jun W, Zhongbo S, Yaoming M (2004) Reconstruction of a Cloud-free Vegetation Index Time Series for the Tibetan Plateau. *Mountain Research and Development,* **24**, 348-353.

Jung M, Reichstein M, Ciais P *et al.* (2010) Recent decline in the global land evapotranspiration trend due to limited moisture supply. *Nature,* **467**, 951-954.

Justice CO, Townshend JRG, Holben BN, Tucker CJ (1985) Analysis of the phenology of global vegetation using meteorological satellite data. *International Journal of Remote Sensing,* **6**, 1271-1318.

Karlsen SR, Solheim I, Beck PSA, Høgda KA, Wielgolaski FE, Tommervik H (2007) Variability of the start of the growing season in Fennoscandia, 1982–2002. *International Journal of Biometeorology,* **51**, 513-524.

Kasischke ES, French NHF, Harrell P, Christensen Jr NL, Ustin SL, Barry D (1993) Monitoring of wildfires in Boreal Forests using large area AVHRR NDVI composite image data. *Remote Sensing of Environment,* **45**, 61-71.

Kasischke ES, Melack JM, Craig Dobson M (1997) The use of imaging radars for ecological applications - a review. *Remote Sensing of Environment,* **59**, 141-156.

Kassas M (1995) Desertification: a general review. *Journal of Arid Environments,* **30**, 115-128.

Kaufmann H, Segl K, Chabrillat S *et al.* (2006) EnMAP - A hyperspectral sensor for environmental mapping and analysis. In: *International Geoscience and Remote Sensing Symposium (IGARSS)*. 2006, Denver, USA, IEEE International.

Kaufmann HJ, Chabrillat S, Hill J, Langemann M, Muller A, Staenz K (2002) SAND - a hyperspectral sensor for the analysis of dryland degradation. In: *Geoscience and Remote Sensing Symposium (IGARSS)*. Toronto, Canada, IEEE International.

Kaufmann RK, Zhou L, Knyazikhin Y, Shabanov V, Myneni RB, Tucker CJ (2000) Effect of orbital drift and sensor changes on the time series of AVHRR vegetation index data. *IEEE Transactions on Geoscience and Remote Sensing,* **38**, 2584-2597.

Kéfi S, Rietkerk M, Alados CL, Pueyo Y, Papanastasis VP, Elaich A, De Ruiter PC (2007) Spatial vegetation patterns and imminent desertification in Mediterranean arid ecosystems. *Nature,* **449**, 213-217.

Kendall MG (1938) A New Measure of Rank Correlation. *Biometrika,* **30**, 81-93.

Kirkby MJ, Jones RJA, Irvine B *et al.* (2004) Pan-European soil erosion risk assessment: The PESERA Map, version 2003. In: *European Soil Bureau Research Report No. 16.* Luxembourg, Office for Official Publications of the European Communities.

Klingebiel AA, Montgomery PH (1961) Land-Capability Classification, Handbook 210. In: *US Dept Agriculture.* Washington DC.

Köhl M, Baldauf T, Plugge D, Krug J (2009) Reduced emissions from deforestation and forest degradation (REDD): A climate change mitigation strategy on a critical track. *Carbon Balance and Management,* **4**, 1750-1759.

Kokaly RF, Asner GP, Ollinger SV, Martin ME, Wessman CA (2009) Characterizing canopy biochemistry from imaging spectroscopy and its application to ecosystem studies. *Remote Sensing of Environment,* **113**, S78-S91.

Krumov A, Nikolova A, Vassilev V, Vassilev N (2008) Assessment of plant vitality detection through fluorescence and reflectance imagery. *Advances in Space Research,* **41**, 1870-1875.

Lal R, Hall GF, Miller FP (1989) Soil degradation: I. Basic processes. *Land Degradation and Development,* **1**, 51-69.

Lambin EF, Turner BL, Geist HJ *et al.* (2001) The causes of land-use and land-cover change: moving beyond the myths. *Global Environmental Change,* **11**, 261-269.

Lamprey HF (1988) Report on the desert encroachment reconnaissance in Northern Sudan: 21 October to 10 November 1975. *Desertification Control Bulletin,* **17**, 1-7.

Laneve G, Castronuovo MM (2005) Comparison between vegetation change analysis in Kenya based on AVHRR and SeaWiFS images. *International Journal of Remote Sensing,* **26**, 2549-2559.

Lark RM, Cullis BR, Welham SJ (2006) On spatial prediction of soil properties in the presence of a spatial trend: the empirical best linear unbiased predictor (E-BLUP) with REML. *European Journal of Soil Science,* **57**, 787-799.

Le Houérou HN (1984) Rain use efficiency: a unifying concept in arid-land ecology. *Journal of Arid Environments,* **7**, 213-247.

Liang L, Schwartz M (2009) Landscape phenology: an integrative approach to seasonal vegetation dynamics. *Landscape Ecology,* **24**, 465-472.

Liu JG, Mason P, Hilton F, Lee H (2004) Detection of rapid erosion in SE Spain: A GIS approach based on ERS SAR coherence imagery: InSAR Application. *Photogrammetric engineering and remote sensing,* **70**, 1179-1185.

Lloyd AH, Bunn AG (2007) Responses of the circumpolar boreal forest to 20th century climate variability. *Environmental Research Letters,* **2**, 045013.

Los SO (1998) Estimation of the ratio of sensor degradation between NOAA AVHRR channels 1 and 2 from monthly NDVI composites. *IEEE Transactions on Geoscience and Remote Sensing,* **36**, 206-213.

Los SO, Collatz GJ, Sellers PJ *et al.* (2000) A Global 9-yr Biophysical Land Surface Dataset from NOAA AVHRR Data. *Journal of Hydrometeorology,* **1**, 183-199.

Loveland TR, Belward AS (1997) The International Geosphere Biosphere Programme Data and Information System global land cover data set (DISCover). *Acta Astronautica,* **41**, 681-689.

Loveland TR, Reed BC, Brown JF, Ohlen DO, Zhu Z, Yang L, Merchant JW (2000) Development of a global land cover characteristics database and IGBP DISCover from 1 km AVHRR data. *International Journal of Remote Sensing,* **21**, 1303-1330.

Lucht W, Prentice IC, Myneni RB *et al.* (2002) Climatic control of the high-latitude vegetation greening trend and Pinatubo effect. *Science,* **296**, 1687-1689.

Ludwig JA, Bastin GN, Chewings VH, Eager RW, Liedloff AC (2007) Leakiness: A new index for monitoring the health of arid and semiarid landscapes using remotely sensed vegetation cover

and elevation data. *Ecological Indicators,* **7**, 442-454.

Lupo F, Linderman M, Vanacker V, Bartholomé E, Lambin EF (2007) Categorization of land-cover change processes based on phenological indicators extracted from time series of vegetation index data. *International Journal of Remote Sensing,* **28**, 2469-2483.

Lupo F, Reginster I, Lambin EF (2001) Monitoring land-cover changes in West Africa with SPOT Vegetation: impact of natural disasters in 1998-1999. *International Journal of Remote Sensing,* **22**, 2633 - 2639.

Luyssaert S, Inglima I, Jung M *et al.* (2007) CO2 balance of boreal, temperate, and tropical forests derived from a global database. *Global Change Biology,* **13**, 2509-2537.

Malthus TR (1798) An Essay on the Principle of Population, as it Affects the Future Improvement of Society. London, UK, Printed for J. Johnson, in St. Paul's Church-Yard.

Mann HB (1945) Nonparametric Tests Against Trend. *Econometrica,* **13**, 245-259.

Marceau DJ, Howarth PJ, Gratton DJ (1994) Remote sensing and the measurement of geographical entities in a forested environment. 1. The scale and spatial aggregation problem. *Remote Sensing of Environment,* **49**, 93-104.

Marzolff I, Poesen J (2009) The potential of 3D gully monitoring with GIS using high-resolution aerial photography and a digital photogrammetry system. *Geomorphology,* **111**, 48-60.

Mcbride GB, Loftis JC (1994) The most important statistical aspects. In: *Proceedings of the 1st international workshop Monitoring Tailor-Made (MTM): monitoring and assessment in water management.* Beekbergen, The Netherlands, RIZA, Lelystad (NL).

Meadows DH, Meadows DL, Randers J, Behrens WW (1972) *The limits to growth*, Universe Books New York.

Medlyn BE (2011) Comment on "Drought-Induced Reduction in Global Terrestrial Net Primary Production from 2000 Through 2009". *Science,* **333**, 1093.

Menzel A, Sparks TH, Estrella N *et al.* (2006) European phenological response to climate change matches the warming pattern. *Global Change Biology,* **12**, 1969-1976.

Metternicht G, Zinck JA, Blanco PD, Del Valle HF (2010) Remote sensing of land degradation: Experiences from Latin America and the Caribbean. *Journal of Environmental Quality,* **39**, 42-61.

Metternicht GI, Zinck JA (2003) Remote sensing of soil salinity: potentials and constraints. *Remote Sensing of Environment,* **85**, 1-20.

Metternicht GI, Zinck JA (2009) *Remote Sensing of Soil Salinization: Impact on Land Management*, CRC Press, Taylor & Francis Group.

Micklin PP (1988) Desiccation of the Aral Sea: a water management disaster in the Soviet Union. *Science,* **241**, 1170-1176.

Middleton N, Thomas D (1997) *World Atlas of Desertification, 2nd Ed.,* Nairobi, Kenya, United Nations Environmental Programme (UNEP).

Millenium Ecosystem Assessment (2005) Ecosystems and human well-being: synthesis. In: *Millennium Ecosystem Assessment.* Washington, DC., World Resources Institute / Island Press.

Mitchell TD, Jones PD (2005) An improved method of constructing a database of monthly climate observations and associated high-resolution grids. *International Journal of Climatology,* **25**, 693-712.

Monteith JL (1981) Climatic variation and the growth of crops. *Quarterly Journal of the Royal Meteorological Society,* **107**, 749-774.

Mougenot B, Pouget M, Epema G (1993) Remote sensing of salt-affected soils. *Remote Sensing Reviews,* **7**, 241-259.

Moulin S, Kergoat L, Viovy N, Dedieu G (1997) Global-Scale Assessment of Vegetation Phenology Using NOAA/AVHRR Satellite Measurements. *Journal of Climate,* **10**, 1154-1170.

Mueller AA, Kaufmann HJ, Briottet X, Pinet P, Hill J, Dech S (2001) Imaging spectrometer mission for the monitoring of desertification processes. *Sensors, Systems, and Next-Generation Satellites V,* **4540**, 82-87.

Mulder VL, De Bruin S, Schaepman ME, Mayr TR (2011) The use of remote sensing in soil and terrain mapping — a review. *Geoderma,* **162**, 1-19.

Myneni RB, Hall FG, Sellers PJ, Marshak AL (1995) The interpretation of spectral vegetation indexes. *IEEE Transactions on Geoscience and Remote Sensing,* **33**, 481-486.

Myneni RB, Hoffman S, Knyazikhin Y *et al.* (2002) Global products of vegetation leaf area and fraction absorbed PAR from year one of MODIS data. *Remote Sensing of Environment,* **83**, 214-231.

Myneni RB, Keeling CD, Tucker CJ, Asrar G, Nemani RR (1997) Increased plant growth in the northern high latitudes from 1981 to 1991. *Nature,* **386**, 698-702.

Nachtergaele F, Van Velthuizen H, Verelst L *et al.* (2008) Harmonized World Soil Database. FAO, Rome, Italy and IIASA, Laxenburg, Austria.

Nagol JR, Vermote EF, Prince SD (2009) Effects of atmospheric variation on AVHRR NDVI data. *Remote Sensing of Environment,* **113**, 392-397.

Neigh CSR, Tucker CJ, Townshend JRG (2008) North American vegetation dynamics observed with multi-resolution satellite data. *Remote Sensing of Environment,* **112**, 1749-1772.

Nelson GC, Bennett E, Berhe AA *et al.* (2006) Anthropogenic drivers of ecosystem change: an overview. *Ecology & Society,* **11**, 29.

Nemani RR, Keeling CD, Hashimoto H *et al.* (2003) Climate-Driven Increases in Global Terrestrial Net Primary Production from 1982 to 1999. *Science,* **300**, 1560-1563.

Nicholson S (2000) Land surface processes and Sahel climate. *Reviews of Geophysics,* **38**, 117–138.

Nicholson SE, Farrar TJ (1994) The influence of soil type on the relationships between NDVI, rainfall, and soil moisture in semiarid Botswana. I. NDVI response to rainfall. *Remote Sensing of Environment,* **50**, 107-120.

Niemi GJ, Mcdonald ME (2004) Application of Ecological Indicators. *Annu. Rev. Ecol. Evol. Syst.,* **35**, 89-111.

Okin GS, Murray B, Schlesinger WH (2001) Degradation of sandy arid shrubland environments: observations, process modeling, and management implications. *Journal of Arid Environments,* **47**, 123-144.

Oldeman LR, Hakkeling RTA, Sombroek WG (1990) World map of the status of human-induced soil degradation. Wageningen, The Netherlands, ISRIC - World Soil Information and Food and Agricultural Orginization of the United Nations.

Oldeman LR, Van Lynden GWJ (1997) Revisiting the GLASOD methodology. In: *Methods for Assessment of Soil Degradation.* (ed Lal R), CRC Press, Boca Raton.

Oliveira PJC, Davin EL, Levis S, Seneviratne SI (2011) Vegetation-mediated impacts of trends in global radiation on land hydrology: a global sensitivity study. *Global Change Biology,* **17**, 3453-3467.

Olsson L, Eklundh L, Ardö J (2005) A recent greening of the Sahel -- trends, patterns and potential causes. *Journal of Arid Environments,* **63**, 556-566.

Openshaw S, Taylor PJ (1979) A million or so correlation coefficients: three experiments on the modifiable areal unit problem. In: *Statistical applications in the spatial sciences.* (ed Wrigley N), Pion, London.

Paruelo JM, Epstein HE, Lauenroth WK, Burke IC (1997) ANPP estimates from NDVI for the central grassland region of the United States. *Ecology,* **78**, 953-958.

Paruelo JM, Garbulsky MF, Guerschman JP, Jobbágy EG (2004) Two decades of Normalized Difference Vegetation Index changes in South America: identifying the imprint of global change. *International Journal of Remote Sensing,* **25**, 2793-2806.

Pebesma EJ, Wesseling CG (1998) Gstat: a program for geostatistical modeling, prediction and simulation. *Computers & Geosciences,* **24**, 17-31.

Pelkey NW, Stoner CJ, Caro TM (2000) Vegetation in Tanzania: assessing long term trends and effects of protection using satellite imagery. *Biological Conservation,* **94**, 297-309.

Pettorelli N, Vik JO, Mysterud A, Gaillard J-M, Tucker CJ, Stenseth NC (2005) Using the satellite-derived NDVI to assess ecological responses to environmental change. *Trends in Ecology & Evolution,* **20**, 503-510.

Phillips LB, Hansen AJ, Flather CH (2008) Evaluating the species energy relationship with the newest measures of ecosystem energy: NDVI versus MODIS primary production. *Remote Sensing of Environment,* **112**, 4381-4392.

Phillips PCB (1986) Understanding spurious regressions in econometrics. *Journal of Econometrics,* **33**, 311-340.

Pilifosova O, Eserkepova I, Dolgih S (1997) Regional climate change scenarios under global warming in Kazakhstan. *Climatic Change,* **36**, 23-40.

Pinzon JE, Brown ME, Tucker CJ (2004) Monitoring Seasonal and interannual variations in Land-Surface Vegetation from 1981-2002 using GIMMS NDVI. Greenbelt, USA, NASA-Goddard Space Flight Center.

Pinzon JE, Brown ME, Tucker CJ (2005) EMD correction of orbital drift artifacts in satellite data stream. In: *Hilbert-Huang Transform and Its Applications.* (eds Huang NE, Shen SS). Singapore, World Scientific Publishing.

Potter CS, Klooster S, Brooks V (1999) Interannual Variability in Terrestrial Net Primary Production: Exploration of Trends and Controls on Regional to Global Scales. *Ecosystems,* **2**, 36-48.

Potter CS, Klooster SA (1997) Global model estimates of carbon and nitrogen storage in litter and soil pools: response to changes in vegetation quality and biomass allocation. *Tellus,* **49B**, 1-17.

Pouliot D, Latifovic R, Olthof I (2009) Trends in vegetation NDVI from 1 km AVHRR data over Canada for the period 1985-2006. *International Journal of Remote Sensing,* **30**, 149-168.

Prince SD, Becker-Reshef I, Rishmawi K (2009) Detection and mapping of long-term land degradation using local net production scaling: application to Zimbabwe. *Remote Sensing of Environment,* **113**, 1046-1057.

Prince SD, De Colstoun EB, Kravitz LL (1998) Evidence from rain-use efficiencies does not indicate extensive Sahelian desertification. *Global Change Biology,* **4**, 359-374.

Prince SD, Goward SN (1995) Global Primary Production: A Remote Sensing Approach. *Journal of Biogeography,* **22**, 815-835.

Prince SD, Tucker CJ (1986) Satellite remote sensing of rangelands in Botswana II. NOAA AVHRR and herbaceous vegetation. *International Journal of Remote Sensing,* **7**, 1555-1570.

Prince SD, Wessels KJ, Tucker CJ, Nicholson SE (2007) Desertification in the Sahel: a reinterpretation of a reinterpretation. *Global Change Biology,* **13**, 1308-1313.

Prospero JM, Lamb PJ (2003) African droughts and dust transport to the Caribbean: climate change implications. *Science,* **302**, 1024-1027.

Puigdefábregas J (1998) Ecological impacts of global change on drylands and their implications for desertification. *Land Degradation & Development,* **9**, 393-406.

R Development Core Team (2011) R: A language and environment for statistical computing. In: *R Foundation for Statistical Computing.* Vienna, Austria.

Rascher U, Gioli B, Miglietta F (2008) FLEX — Fluorescence Explorer: A Remote Sensing Approach to Quantify Spatio-Temporal Variations of Photosynthetic Efficiency from Space. In: *Photosynthesis. Energy from the Sun.* (eds Allen JF, Gantt E, Golbeck JH, Osmond B). Dordrecht, The Netherlands, Springer.

Rathmann R, Szklo A, Schaeffer R (2010) Land use competition for production of food and liquid biofuels: An analysis of the arguments in the current debate. *Renewable Energy,* **35**, 14-22.

Ravi S, Breshears DD, Huxman TE, D'odorico P (2010) Land degradation in drylands: Interactions among hydrologic-aeolian erosion and vegetation dynamics. *Geomorphology,* **116**, 236-245.

Reed BC, White M, Brown JF (2003) Remote sensing phenology. In: *Phenology: An Integrative Environmental Science.* (ed Schwartz MD). Dordrecht, The Netherlands, Kluwer Academic Publishing.

Reynolds JF, Stafford Smith MD, Lambin EF *et al.* (2007) Global Desertification: Building a Science for Dryland Development. *Science,* **316**, 847-851.

Riedler C, Jandl R (2002) Identification of degraded forest soils by means of a fuzzy-logic based model. *Journal of Plant Nutrition and Soil Science,* **165**, 320-325.

Rietkerk M, Dekker SC, De Ruiter PC, Van De Koppel J (2004) Self-Organized Patchiness and Catastrophic Shifts in Ecosystems. *Science,* **305**, 1926-1929.

Roderick M, Farquhar G, Berry S, Noble I (2001) On the direct effect of clouds and atmospheric particles on the productivity and structure of vegetation. *Oecologia,* **129**, 21-30.

Roerink GJ, Menenti M, Verhoef W (2000) Reconstructing cloudfree NDVI composites using Fourier analysis of time series. *International Journal of Remote Sensing,* **21**, 1911 - 1917.

Rosenzweig C, Casassa G, Karoly DJ *et al.* (2007) Assessment of observed changes and responses in natural and managed systems. In: *Climate Change 2007: Impacts, Adaptation and Vulnerability. Contribution of Working Group II to the Fourth Assessment Report of the Intergovernmental Panel on Climate Change.* (eds Parry ML, Canziani OF, Palutikof JP, Van Der Linden PJ, Hanson CE) Cambridge, UK, Cambridge University Press.

Ross JC (1963) Soil conservation in South Africa. (ed Department of Agriculture P, Republic of South Africa).

Rouse JW, Haas RH, Schell JA, Deering DW (1973) Monitoring vegetation systems in the Great Plains with ERTS. In: *Third Earth Resources Technology Satellite (ERTS) Symposium.* December 10, 1973, Washington DC, USA, NASA.

Running SW, Loveland TR, Pierce LL (1994) A vegetation classification logic based on remote sensing for use in global biogeochemical models. *Ambio,* **23**, 77-81.

Running SW, Nemani RR (1988) Relating seasonal patterns of the AVHRR vegetation index to simulated photosynthesis and transpiration of forests in different climates. *Remote Sensing of Environment,* **24**, 347-367.

Running SW, Nemani RR, Heinsch FA, Zhao M, Reeves M, Hashimoto H (2004) A Continuous Satellite-Derived Measure of Global Terrestrial Primary Production. *BioScience,* **54**, 547-560.

Saleska SR, Didan K, Huete AR, Da Rocha HR (2007) Amazon Forests Green-Up During 2005 Drought. *Science,* **318**, 612-.

Salomonson VV, Barnes WL, Maymon PW, Montgomery HE, Ostrow H (1989) MODIS: advanced facility instrument for studies of the Earth as a system. *IEEE Transactions on Geoscience and Remote Sensing,* **27**, 145-153.

Salvati L, Zitti M (2009) Assessing the impact of ecological and economic factors on land degradation vulnerability through multiway analysis. *Ecological Indicators,* **9**, 357-363.

Samanta A, Costa MH, Nunes EL, Vieira SA, Xu L, Myneni RB (2011) Comment on "Drought-Induced Reduction in Global Terrestrial Net Primary Production from 2000 Through 2009". *Science,* **333**, 1093.

Samanta A, Ganguly S, Hashimoto H *et al.* (2010) Amazon forests did not green-up during the 2005 drought. *Geophysical Research Letters,* **37**, L05401.

Sanchez PA, Ahamed S, Carre F *et al.* (2009) Digital Soil Map of the World. *Science,* **325**, 680-681.

Schaepman-Strub G, Schaepman ME, Painter TH, Dangel S, Martonchik JV (2006) Reflectance quantities in optical remote sensing - definitions and case studies. *Remote Sensing of Environment,* **103**, 27-42.

Schaepman ME (2007) Spectrodirectional remote sensing: From pixels to processes. *International Journal of Applied Earth Observation and Geoinformation,* **9**, 204-223.

Scheffer M, Carpenter S, Foley JA, Folke C, Walker B (2001) Catastrophic shifts in ecosystems. *Nature,* **413**, 591-596.

Scheffer M, Carpenter SR (2003) Catastrophic regime shifts in ecosystems: linking theory to observation. *Trends in Ecology & Evolution,* **18**, 648-656.

Schimel DS, House JI, Hibbard KA *et al.* (2001) Recent patterns and mechanisms of carbon exchange by terrestrial ecosystems. *Nature,* **414**, 169-172.

Schlesinger WH, Gramenopoulos N (1996) Archival photographs show no climate-induced changes in woody vegetation in the Sudan. *Global Change Biology,* **2**, 137-141.

Schlesinger WH, Reynolds JF, Cunningham GL, Huenneke LF, Jarrell WM, Virginia RA, Whitford WG (1990) Biological feedbacks in global desertification. *Science,* **247**, 1043-1048.

Schwarz G (1978) Estimating the Dimension of a Model. *The annals of statistics,* **6**, 461-464.

Seaquist JW, Hickler T, Eklundh L, Ardö J, Heumann BW (2008) Disentangling the effects of climate and people on Sahel vegetation dynamics. *Biogeosciences,* **6**, 469-477.

Seaquist JW, Olsson L, Ardö J (2003) A remote sensing-based primary production model for grassland biomes. *Ecological Modeling,* **169**, 131-155.

Sellers PJ, Berry JA, Collatz GJ, Field CB, Hall FG (1992) Canopy reflectance, photosynthesis, and transpiration. III. A reanalysis using improved leaf models and a new canopy integration scheme. *Remote Sensing of Environment,* **42**, 187-216.

Sellers PJ, Dickinson RE, Randall DA *et al.* (1997) Modeling the Exchanges of Energy, Water, and Carbon Between Continents and the Atmosphere. *Science,* **275**, 502-509.

Sims DA, Rahman AF, Cordova VD *et al.* (2008) A new model of gross primary productivity for North American ecosystems based solely on the enhanced vegetation index and land surface temperature from MODIS. *Remote Sensing of Environment,* **112**, 1633-1646.

Sjöström M, Ardö J, Arneth A *et al.* (2011) Exploring the potential of MODIS EVI for modeling gross primary production across African ecosystems. *Remote Sensing of Environment,* **115**, 1081-1089.

Slayback DA, Pinzon JE, Los SO, Tucker CJ (2003) Northern hemisphere photosynthetic trends 1982-99. *Global Change Biology,* **9**, 1-15.

Small EE, Giorgi F, Sloan LC, Hostetler S (2001) The effects of desiccation and climatic change on the hydrology of the Aral Sea. *Journal of Climate,* **14**, 300-322.

Sobrino JA, Raissouni N, Li Z-L (2001) A Comparative Study of Land Surface Emissivity Retrieval from NOAA Data. *Remote Sensing of Environment,* **75**, 256-266.

Soden BJ, Wetherald RT, Stenchikov GL, Robock A (2002) Global cooling after the eruption of Mount Pinatubo: A test of climate feedback by water vapor. *Science,* **296**, 727-730.

Sonneveld BGJS, Dent DL (2009) How good is GLASOD? *Journal of Environmental Management,* **90**, 274-283.

Soukupova J, Csefalvay L, Urban O, Kosvancova M, Marek M, Rascher U, Nedbal L (2008) Annual variation of the steady-state chlorophyll fluorescence emission of evergreen plants in temperate zone. *Functional Plant Biology,* **35**, 63-76.

Sparks TH, Aasa A, Huber K, Wadsworth R (2009) Changes and patterns in biologically relevant temperatures in Europe 1941-2000. *Climate Research,* **39**, 191-207.

Spitters CJT, Toussaint HaJM, Goudriaan J (1986) Separating the diffuse and direct component of global radiation and its implications for modeling canopy photosynthesis Part I. Components of incoming radiation. *Agricultural and Forest Meteorology,* **38**, 217-229.

Steinberg D (2009) CART: Classification and Regression Trees. In: *The Top Ten Algorithms in Data Mining.* (eds Wu X, Kumar V). Boca Raton, FL, USA, CRC Press (Taylor & Francis Group).

Stenchikov GL, Kirchner I, Robock A *et al.* (1998) Radiative forcing from the 1991 Mount Pinatubo volcanic eruption. *Journal of Geophysical Research,* **103**, 13837-13857.

Stöckli R, Rutishauser T, Baker I, Liniger MA, Denning AS (2011) A global reanalysis of vegetation phenology. *J. Geophys. Res.,* **116**, G03020.

Stöckli R, Rutishauser T, Dragoni D *et al.* (2008) Remote sensing data assimilation for a prognostic phenology model. *J. Geophys. Res,* **113**.

Stöckli R, Vidale PL (2004) European plant phenology and climate as seen in a 20-year AVHRR land-surface parameter dataset. *International Journal of Remote Sensing,* **25**, 3303 - 3330.

Stroppiana D, Boschetti M, Brivio PA, Carrara P, Bordogna G (2009) A fuzzy anomaly indicator for environmental monitoring at continental scale. *Ecological Indicators,* **9**, 92-106.

Summers D, Lewis M, Ostendorf B, Chittleborough D (2011) Visible near-infrared reflectance spectroscopy as a predictive indicator of soil properties. *Ecological Indicators,* **11**, 123-131.

Swinnen E, Veroustraete F (2008) Extending the SPOT-VEGETATION NDVI Time Series (1998–2006) Back in Time With NOAA-AVHRR Data (1985–1998) for Southern Africa. *IEEE Transactions on Geoscience and Remote Sensing,* **46**, 558-572.

Symeonakis E, Drake N (2004) Monitoring desertification and land degradation over sub-Saharan Africa. *International Journal of Remote Sensing,* **25**, 573-592.

Symeonakis E, Drake N (2010) 10-Daily soil erosion modeling over sub-Saharan Africa. *Environmental Monitoring and Assessment,* **161**, 369-387.

Tarnavsky E, Garrigues S, Brown ME (2008) Multiscale geostatistical analysis of AVHRR, SPOT-VGT, and MODIS global NDVI products. *Remote Sensing of Environment,* **112**, 535-549.

Tatem AJ, Goetz SJ, Hay SI (2008) Fifty years of earth-observation satellites. *American Scientist,* **96**, 390-398.

Taylor R (2010) Communities, Crime, and Reactions to Crime Multilevel Models: Accomplishments and Meta-Challenges. *Journal of Quantitative Criminology,* **26**, 455-466.

Tilman D, Socolow R, Foley JA *et al.* (2009) Beneficial biofuels - The food, energy, and environment trilemma. *Science,* **325**, 270-271.

Tottrup C, Rasmussen MS (2004) Mapping long-term changes in savannah crop productivity in Senegal through trend analysis of time series of remote sensing data. *Agriculture, Ecosystems & Environments,* **103**, 545-560.

Townshend JRG (1994) Global data sets for land applications from the Advanced Very High Resolution Radiometer: an introduction. *International Journal of Remote Sensing,* **15**, 3319 - 3332.

Townshend JRG, Justice CO (1988) Selecting the spatial resolution of satellite sensors required for global monitoring of land transformations. *International Journal of Remote Sensing,* **9**, 187-236.

Trenberth KE, Jones PD, Ambenje P *et al.* (2007) Climate Change 2007: The physical science basis, contribution of Working Group I. In: *Fourth assessment report of the Intergovernmental Panel on Climate Change.* (eds Solomon S, Qin D, Manning M, Chen Z, Marquis M, Averyt KB, Tignor M, Miller HL) Cambridge, UK, Cambridge University Press.

Tucker C, Pinzon J, Brown M *et al.* (2005) An extended AVHRR 8km NDVI dataset compatible with MODIS and SPOT vegetation NDVI data. *International Journal of Remote Sensing,* **26**, 4485-4498.

Tucker CJ (1979) Red and photographic infrared linear combinations for monitoring vegetation. *Remote Sensing of Environment,* **8**, 27-150.

Tucker CJ, Dregne HE, Newcomb WW (1991) Expansion and Contraction of the Sahara Desert from 1980 to 1990. *Science,* **253**, 299-301.

Tucker CJ, Holben BN, Elgin Jr JH, Mcmurtrey Iii JE (1981) Remote sensing of total dry-matter accumulation in winter wheat. *Remote Sensing of Environment,* **11**, 171-189.

Tucker CJ, Pinzon JE, Brown ME (2004) Global Inventory Modeling and Mapping Studies, NA94apr15b.n11-VIg, 2.0, Global Land Cover Facility, University of Maryland, College Park, Maryland.

Tucker CJ, Slayback DA, Pinzon JE, Los SO, Myneni RB, Taylor MG (2001) Higher northern latitude normalized difference vegetation index and growing season trends from 1982 to 1999. *International Journal of Biometeorology,* **45**, 184-190.

Tucker CJ, Vanpraet CL, Sharman MJ, Van Ittersum G (1985) Satellite remote sensing of total herbaceous biomass production in the senegalese sahel: 1980-1984. *Remote Sensing of Environment,* **17**, 233-249.

Turner BL, Lambin EF, Reenberg A (2007) The emergence of land change science for global environmental change and sustainability. *Proceedings of the National Academy of Sciences,* **104**, 20666-20671.

Turner DP, Ritts WD, Cohen WB *et al.* (2006) Evaluation of MODIS NPP and GPP products across multiple biomes. *Remote Sensing of Environment,* **102**, 282-292.

UNCCD (1994) Elaboration of an international convention to combat desertification in countries experiencing serious drought and/or desertification, particularly in Africa. Paris, France, General Assembly of the United Nations.

UNEP (2007) *Global Environment Outlook (GEO) 4,* Nairobi, Kenya.

United Nations Population Fund (UNPF) (2011) The state of world population 2011, people and possibilities in a world of 7 billion. New York, USA.

Vacca A, Loddo S, Ollesch G, Puddu R, Serra G, Tomasi D, Aru A (2000) Measurement of runoff and soil erosion in three areas under different land use in Sardinia (Italy). *CATENA,* **40**, 69-92.

Van Engelen VWP, Wen TT (1995) Global and National Soils and Terrain Digital Databases (SOTER); Procedures Manual. Wageningen, The Netherlands, ISRIC - World Soil Information.

Vargas RR, Omuto CT, Njeru L (2007) Land degradation assessment of a Selected Study Area in Somaliland: The application of LADA-WOCAT approach. In: *SWALIM L-10 Land Degradation Report.* Nairobi, Kenya, Food and Agricultural Organization of the United Nations.

Venables WN, Ripley BD (2002) *Modern Applied Statistics with S (4th ed.),* New York, USA, Springer.

Verbesselt J, Hyndman R, Newnham G, Culvenor D (2010a) Detecting trend and seasonal changes in satellite image time series. *Remote Sensing of Environment,* **114**, 106-115.

Verbesselt J, Hyndman R, Zeileis A, Culvenor D (2010b) Phenological change detection while accounting for abrupt and gradual trends in satellite image time series. *Remote Sensing of Environment,* **114**, 2970-2980.

Verburg PH, Neumann K, Nol L (2011) Challenges in using land use and land cover data for global change studies. *Global Change Biology,* **17**, 974-989.

Verhoef W, Menenti M, Azzali S (1996) A colour composite of NOAA-AVHRR-NDVI based on time series analysis (1981-1992). *International Journal of Remote Sensing,* **17**, 231-235.

Vermote E, Kaufman YJ (1995) Absolute calibration of AVHRR visible and near-infrared channels using ocean and cloud views. *International Journal of Remote Sensing,* **16**, 2317-2340.

Verrelst J (2010) Space-borne spectrodirectional estimation of forest properties. PhD, Wageningen University, The Netherlands, 153 pp.

Viglizzo EF, Frank FC, Carreno LV *et al.* (2011) Ecological and environmental footprint of 50 years of agricultural expansion in Argentina. *Global Change Biology,* **17**, 959-973.

Viles HA, Goudie AS (2003) Interannual, decadal and multidecadal scale climatic variability and geomorphology. *Earth-Science Reviews,* **61**, 105-131.

Vitousek PM, Mooney HA, Lubchenco J, Melillo JM (1997) Human Domination of Earth's Ecosystems. *Science,* **277**, 494-499.

Von Hardenberg J, Meron E, Shachak M, Zarmi Y (2001) Diversity of Vegetation Patterns and Desertification. *Physical Review Letters,* **87**, 198101.

Vrieling A (2006) Satellite remote sensing for water erosion assessment: A review. *CATENA,* **65**, 2-18.

Vrieling A (2007) Mapping Erosion from Space. Unpublished PhD PhD, Wageningen University, The Netherlands, 167 pp.

Walker JP, Houser PR, Willgoose GR (2004) Active microwave remote sensing for soil moisture measurement: a field evaluation using ERS-2. *Hydrological Processes,* **18**, 1975-1997.

Wang C, Qi J (2008) Biophysical estimation in tropical forests using JERS-1 SAR and VNIR imagery. II. Aboveground woody biomass. *International Journal of Remote Sensing,* **29**, 6827-6849.

Wang X, Piao S, Ciais P, Li J, Friedlingstein P, Koven C, Chen A (2011) Spring temperature change and its implication in the change of vegetation growth in North America from 1982 to 2006. *Proceedings of the National Academy of Sciences,* **108**, 1240-1245.

Wasson R (1987) Detection and measurement of land degradation processes. In: *Land degradation - Problems and policies.* (eds Chisholm A, Dumsday R), Cambridge University Press, UK.

Wessels KJ (2009) Letter to the Editor: comments on 'Proxy global assessment of land degradation'. *Soil Use and Management,* **25**, 91-92.

Wessels KJ, Prince SD, Malherbe J, Small J, Frost PE, Vanzyl D (2007) Can human-induced land degradation be distinguished from the effects of rainfall variability? A case study in South Africa. *Journal of Arid Environments,* **68**, 271 - 297.

Westerling AL, Hidalgo HG, Cayan DR, Swetnam TW (2006) Warming and Earlier Spring Increase Western U.S. Forest Wildfire Activity. *Science,* **313**, 940-943.

White MA, De Beurs KM, Didan K *et al.* (2009) Intercomparison, interpretation, and assessment of spring phenology in North America estimated from remote sensing for 1982–2006. *Global Change Biology,* **15**, 2335-2359.

White MA, Running SW, Thornton PE (1999) The impact of growing-season length variability on carbon assimilation and evapotranspiration over 88 years in the eastern US deciduous forest *International Journal of Biometeorology,* **42**, 139-145.

White MA, Thornton PE, Running SW (1997) A continental phenology model for monitoring vegetation responses to interannual climatic variability. *Global Biogeochemical Cycles,* **11**, 217-234.

Wickland DE (1989) Future directions for remote sensing in terrestrial ecological research. In: *Theory and Applications of Optical Remote Sensing.* (ed Asrar G). New York, USA, Wiley.

Wild M, Gilgen H, Roesch A *et al.* (2005) From Dimming to Brightening: Decadal Changes in Solar Radiation at Earth's Surface. *Science,* **308**, 847-850.

Wolter K, Timlin MS (1998) Measuring the strength of enso events: How does 1997/98 rank? *Weather,* **53**, 315-324.

Woodward FI, Lomas MR, Quaife T (2008) Global responses of terrestrial productivity to contemporary climatic oscillations. *Philosophical*

Transactions of the Royal Society B: Biological Sciences, **363**, 2779-2785.

Xin Z, Xu J, Zheng W (2008) Spatiotemporal variations of vegetation cover on the Chinese Loess Plateau (1981—2006): Impacts of climate changes and human activities. *Science in China Series D: Earth Sciences,* **51**, 67 - 78.

Yu D, Shi P, Shao H, Zhu W, Pan Y (2009) Modeling net primary productivity of terrestrial ecosystems in East Asia based on an improved CASA ecosystem model. *International Journal of Remote Sensing,* **30**, 4851-4866.

Zeileis A, Kleiber C (2005) Validating multiple structural change models-a case study. *Journal of Applied Econometrics,* **20**, 685-690.

Zeileis A, Leisch F, Hornik K, Kleiber C (2002) strucchange: An R package for testing for structural change in linear regression models. *Journal of Statistical Software,* **7**, 1-38.

Zeng N (2003) Drought in the Sahel. *Science,* **302**, 999-1000.

Zhang K, Kimball JS, Mu Q, Jones LA, Goetz SJ, Running SW (2009) Satellite based analysis of northern ET trends and associated changes in the regional water balance from 1983 to 2005. *Journal of Hydrology,* **379**, 92-110.

Zhang R, Delworth TL (2006) Impact of Atlantic multidecadal oscillations on India/Sahel rainfall and Atlantic hurricanes. *Geophysical Research Letters,* **33**, L17712.

Zhang X, Friedl MA, Schaaf CB *et al.* (2003) Monitoring vegetation phenology using MODIS. *Remote Sensing of Environment,* **84**, 471-475.

Zhao M, Running SW (2010) Drought-Induced Reduction in Global Terrestrial Net Primary Production from 2000 Through 2009. *Science,* **329**, 940-943.

Zhao M, Running SW (2011) Response to Comments on "Drought-Induced Reduction in Global Terrestrial Net Primary Production from 2000 Through 2009". *Science,* **333**, 1093.

Zhou L, Tucker CJ, Kaufmann RK, Slayback DA, Shabanov NV, Myneni RB (2001) Variations in northern vegetation activity inferred from satellite data of vegetation index during 1981 to 1999. *Journal of Geophysical Research,* **106**, 20269-20283.

Zhuravleva TB, Rublev AN, Udalova TA, Chesnokova TY (2006) On calculation of photosynthetically active radiation in estimation of carbon balance parameters of surface ecosystems. *Atmospheric and Oceanic Optics,* **19**, 57-59.

Zika M, Erb KH (2009) The global loss of net primary production resulting from human-induced soil degradation in drylands. *Ecological Economics,* **69**, 310-318.

Zucca C, Peruta RD, Salvia R, Sommer S, Cherlet M (2012) Towards a World Desertification Atlas; Relating and selecting indicators and data sets to represent complex issues. Ecological Indicators, 15, 157-170.

Summary

Land is synonym to 'terrestrial ecosystem' and *degradation* to 'a loss in its services', notably the supporting primary production service. As such, land degradation is a global issue on a par with climate change, but its extent and severity are only roughly known and there is little detail on the driving processes. Remote sensing is the only viable option for monitoring land resources at global scale and in a consistent and physical way by adopting vegetation activity and/or cover as proxies. A well-known spectral proxy is the normalized difference vegetation index (NDVI), which is available in high temporal-resolution time series since the early 1980s. There is a strong relationship between the index values, chlorophyll abundance and (photosyntethically active) solar energy absorption and hence the term *vegetation activity* can be used to refer to the state and dynamics of terrestrial ecosystems as inferred by NDVI. Changes in vegetation activity have in literature been referred to as *greening* and *browning* for positive and negative changes respectively. This thesis aimed at advancing the understanding of dynamics and trends in global vegetation activity, in relation to climate variability, for use in land resource applications, including land degradation assessments. Several change detection methods for long-term satellite records were developed and results were interpreted in a framework of global environmental change.

The main contribution of this work in the quest of monitoring global land degradation is: (*I*) the identification of research lines and knowledge gaps for large-scale quantitative assessments of greening and browning, (*II*) the use of the full temporal dimension and phenological changes in the trend detection, (*III*) the decomposition of long-term trends into shorter-term variation for a closer description of the system dynamics, (*IV*) the quantification of spatial relationships between climate changes and changes in vegetation activity.

A review of existing literature about vegetation-activity trends at global scale was presented in Chapter 2. Most recent studies indicate a general greening trend but combinations of greening and browning trends were also demonstrated. Improved understanding may be expected from data-driven and process-modeling approaches: new models, model-integration, enhanced statistical analysis and modern sensor imagery at medium spatial resolution should substantially improve the assessment of global land degradation. Two research lines were selected for further technical work: (*I*) advancement of the change detection techniques, (*II*) the use of spatial-contextual information in the interpretation of detected changes.

In Chapter 3, harmonic analyses and non-parametric trend tests were applied to the NDVI dataset at hand in order to detect and quantify greening and browning

without relying on temporal aggregation for seasonal adjustments. Monotonic trends (i.e. the direction of change is invariant over time) were found and it was demonstrated that phenological shifts and variations in length of growing season complicate the issue. Accounting for these variations, using vegetation development stages rather than calendar days, yielded insight in intra-annual variations. Detection of trends in *photosynthetic intensity* complemented the original analysis since they may be related to other drivers (e.g. nutrient or water stress) than yearly changes.

This approach did not rely on temporal aggregation, which might introduce artificial trends as we demonstrate in our chapter on the modifiable temporal unit problem (Chapter 4). Still, a major assumption underlying the analysis was that that trends were monotonic by nature. These monotonic trends, however, may consist of an alternating sequence of greening and/or browning periods. This effect and the contribution of short-term trends to longer term change was analyzed in Chapter 5 using a trend breaks analysis procedure. Both abrupt and gradual changes were detected in large parts of the world, especially in (semi-arid) shrubland and grassland. Many abrupt changes were found around large-scale natural influences like the Mt Pinatubo eruption in 1991 and the strong 1997/98 El Niño event. Temporal analysis indicated that the area with browning trends increased over time while the area with greening trends decreased. The Southern Hemisphere showed the strongest evidence of browning. Here, periods of gradual browning were generally longer than periods of gradual greening. In total, trend reversals were found for 15% of the global land area.

These new change detection techniques advance our understanding of vegetation variability at a multi-decadal scale, but do not provide links to driving processes. It will be very complex to disentangle all natural and human drivers and their interaction. As a first step, the spatial relationship between changes in potentially growth-constraining climatologies and changes in vegetation activity was addressed in Chapter 6. We applied a decomposition of spatial patterns into a deterministic, or fixed-effects, component and a spatially correlated, or random-effects, field. It appeared that a substantial proportion (54%) of the spatial variation in NDVI changes could be explained by changes in temperature, precipitation and incident radiation, especially in forest biomes. For other regions, including Tanzania and Zimbabwe, browning trends could not be related to climate variables. In these regions, negative changes in vegetation activity may need to be explained by human activities.

With these studies we demonstrated the value of global satellite records for monitoring land resources and we contributed to better interpretation, although we realize that many steps are still to be taken.

Samenvatting

Land is synoniem voor ‘terrestrisch ecosysteem’ en *degradatie* voor ‘een afname van zijn services’, in het bijzonder de ondersteunende primaire productieservice. Daarmee is landdegradatie een wereldwijd probleem – op gelijke voet met klimaatverandering – ondanks dat de omvang en impact maar globaal bekend zijn en er nauwelijks details bekend zijn over de onderliggende processen. Aardobservatie biedt de enige manier om het land en zijn bronnen op wereldwijde schaal consistent te monitoren door veranderingen in vegetatie-activiteit en -bedekking te meten. Een bekende spectrale proxy is de *normalized difference vegetation index* (NDVI), die sinds begin jaren 80 in hoge temporele resolutie beschikbaar is. Deze proxy vertoont sterke relaties met hoeveelheid chlorofyl en met absorptie van (fotosynthetisch actieve) zonnestraling en daarom kan de term vegetatie-activiteit worden gebruikt om te refereren aan de staat en dynamica van terrestrische ecosystemen zoals gemeten door de NDVI. Veranderingen hierin worden wel *vergroening* en *verbruining* genoemd voor respectievelijk toename en afname. Het doel van deze scriptie was om trends en dynamica in vegetatie-activiteit beter te begrijpen en te relateren aan klimaatveranderingen om ze toe te kunnen passen in landdegradatie-studies. Daarbij hoorde het ontwikkelen van diverse technieken om veranderingen te detecteren. De resultaten zijn vervolgens geïnterpreteerd in een landdegradatie-kader.

De belangrijkste bijdrage van dit werk aan de queeste naar het effectief monitoren van landdegradatie is: (*I*) het identificeren van onderzoekslijnen en kennishiaten voor grootschalige kwantitatieve studies naar vegetatie-activiteit, (*II*) het gebruik van de volledige temporele resolutie van beschikbare data in de trendstudies, (*III*) het vinden van korte-termijn trends die de dynamica van het systeem beter beschrijven, (*IV*) het kwantificeren van ruimtelijke relaties tussen veranderingen in vegetatie-activiteit en klimaatveranderingen.

Hoofdstuk 2 omvat een literatuurstudie naar trends in vegetatie-activiteit op wereldwijde schaal. Het bleek dat de meeste studies een globale toename (vergroening) vonden, maar combinaties met negatieve trends zijn ook aangetoond. Een beter inzicht kan worden verwacht via data-gedreven en proces-gedreven aanpakken: nieuwe modellen, integratie van diverse modellen, verbeterde statistische analyses en hogere ruimtelijke resolutie van nieuwe sensoren zullen hieraan bijdragen. Twee onderzoekslijnen zijn hier vastgesteld voor de opvolgende technische hoofdstukken: (*I*) verbetering van trenddetectie-technieken en (*II*) het gebruiken van ruimtelijk-contextuele informatie om de gedetecteerde veranderingen beter te interpreteren.

Harmonische en niet-parametrische analysetechnieken zijn in Hoofdstuk 4 op maat gemaakt voor en toegepast op NDVI tijdseries om zo trends in vegetatie-activiteit te kwantificeren zonder daarvoor de data per jaar te middelen. Monotone trends (i.e. teken van de richtingscoëfficient is onveranderlijk) zijn aangetoond, net als de complicatie die fenologie oplevert voor trenddetectie. Een aanpassing aan variaties in start en lengte van groeiseizoenen leverde een beter inzicht in intra-jaarlijkse variaties. Die variaties, samengevat als *fotosynthetische intensiteit*, vulde de oorspronkelijke analyse aan omdat het kan worden gerelateerd aan andere onderliggende processen (bv. nutriënt- of waterstress) dan jaarlijkse veranderingen.

De beschreven aanpak is niet afhankelijk van temporele aggregatie wat problemen kan veroorzaken zoals beschreven in het hoofdstuk over de *modifiable temporal unit problem* (Hoofdstuk 4). Desalniettemin, een belangrijke aanname was dat trends van nature monotoon zijn. Deze monotone trends kunnen echter bestaan uit een afwisseling van positieve en negatieve periodes. Dit effect en de invloed hiervan op lange-termijn trends zijn bestudeerd in Hoofdstuk 5. Met een trendbreuk-algoritme zijn abrupte en graduele veranderingen gevonden in grote delen van de wereld, in het bijzonder in (semi-aride) struik- en graslandschappen. Veel abrupte veranderingen zijn gevonden rondom grootschalige natuurinvloeden zoals de Mt Pinatubo-uitbarsting in 1991 en de sterke 1997/98 El Niño. Analyse van de trendveranderingen over tijd toonde aan dat een steeds groter deel van de aarde negatieve trends (verbruining) ging vertonen, ten koste van vergroening. Het zuidelijk halfrond vertoonde de sterkste verbruinings-signalen: deze perioden duurden stelselmatig langer dan de vergroenings-perioden. Trend-omkeringen (vergroening versus verbruining) konden voor ca. 15% van het aardoppervlak worden aangetoond.

Nieuwe detectietechnieken dragen bij aan een verbeterd inzicht in vegetatie-variabiliteit op een tijdschaal van meerdere decennia, maar ze verschaffen geen inzicht in de sturende processen. Het blijft zeer complex om alle natuurlijke en menselijke invloeden te ontrafelen, maar als eerste stap zijn diverse ruimtelijke relaties met klimaat bestudeerd in Hoofdstuk 6. Daar hebben we het ruimtelijke patroon in vegetatie-veranderingen ontbonden in een deterministische component die kan worden gerelateerd aan klimaatveranderingen en een overig ruimtelijk gecorreleerd patroon. Een substantieel deel (54%) van de NDVI-veranderingen, vooral in bosgebieden, kon worden verklaard vanuit veranderingen in temperatuur, neerslag en inkomende straling. In andere regio's, bv. Tanzania en Zimbabwe, negatieve trends konden niet worden gerelateerd aan klimaat. Hier zouden menselijke invloeden een rol kunnen spelen.

Met deze studies hebben we de waarde van historische satellietdata voor landdegradatie onderstreept en hebben we bijgedragen aan betere interpretatie, hoewel we ons realiseren dat er nog veel stappen genomen moeten worden.

Acknowledgements

Mutantur omnia, nos et mutamur in illis.
All things change and we too change, with them.

Time, its length and its nature play inherently crucial roles in discussions about these changes. They also play crucial roles in the course of a PhD, which, in itself, is a trajectory of change. The nature of time has been subject to interpretation by many philosophers and scholars in history, from which three main forms can be distilled: time as a line or a flow, time as a cycle and time as an arrow or a pulse. All three can be found in this thesis and also in its origin. In the course of a PhD one gradually grows from understanding to practitioning science: upstream and therefore sometimes with struggles. The starting point is the middle of the vast metaphorical ocean, heading for somewhere vaguely known. And working on terrestrial remote sensing, the middle of an ocean is obviously not the place to be. It takes a while to find a way and to come up with a first paper. It may take around ten draft versions and the fewer comments from your supervisors, the further you are from a publishable paper. Then, after submission, the next paper is waiting: the cycles of science. On the other hand, each acceptance notification from a journal gives a boost, a pulse towards this thesis. Then finally, although time doesn't end: *het is af!*

Many people have supported me during these years, for which I am very grateful. First of all, I would like to express my sincere thanks to my supervisors, *sine quibus non*, Michael Schaepman and Sytze de Bruin. During the introductory PhD weekend we were warned that the relationship with your supervisors has ups and downs and might dilute over time. Our relationship has been excellent throughout all years. Michael, thanks a lot for all discussions, your many helpful suggestions and for the support when necessary. Also thanks for introducing me to the Remote Sensing Laboratories in Zurich and for being faithful, also after finishing my PhD. Sytze, thank you for your open door; working with you as daily supervisor couldn't have been easier! Third in this row is David Dent. Thank you for the opportunity to work on 'your' project and for your thorough reviews of the several chapters in this thesis.

Physical geographers, like me, tend to know their way in a broad range of scientific fields, but usually they are specialist in none. Therefore, I would like to thank other people who have contributed to the work in this thesis. Allard de Wit, thank you for your support with IDL and the HANTS algorithm (Chapter 4). Jan Verbesselt, thanks for being very helpful with the trend-break analysis while you were still Down-Under and even more when you came to Wageningen. It resulted in one of the core chapters of this thesis (Chapter 6). Reinhard Furrer, thanks a lot for

the necessary math classes and for your patient support with the spatial statistics (Chapter 7).

And then there are all colleagues at ISRIC and CGI. You are too many to list individually, but you made Wageningen a great place to work for this Utrecht-guy. A few people I would like to mention in special: at ISRIC, Zhanguo Bai for the collaboration on the GLADA project and Alfred Hartemink for the discussions about (soil) science. Bob McMillan and Tom Hengl, thanks for all the excellent Wednesday barbeque and pasta lunches! At CGI, *the last of the Mohicans:* Titia Mulder and Valerie Laurent, but also 'new' colleagues Kim Calders and Hans Roelofsen. And Harm Bartholomeus: we talked often about our outdoor adventures, but somehow we (or I?) forgot that actions speak louder than words. So, see you in Switzerland?

Talking about Switzerland, I am grateful for having had the opportunity to work at the Remote Sensing Laboratories in Zurich. I would like to thank all colleagues for their hospitality and helpfulness. I am grateful to Jenneke, Paul, Steffi and Céline for the nice times and sleeping places in Zurich. In this respect, special thanks to Jan Blees and his roommates Regi and Marcel. I can't remember how many nights I stayed at your place, but it felt like coming home. Jan, also thanks for the skiing, flying, hiking, snow-shoeing, climbing, camping, …!

From the 'Peyne 2005 generation' of remote-sensing students in Utrecht, I am the last one to have finalized a PhD thesis. It must have been inspiring, thanks to Steven de Jong and Elisabeth Addink. Also, the Peyne catchment (Languedoc, France) was a great place for fieldwork (and for a cover photo). I am grateful to Wiebe Nijland for all the trips we made there together. And, to cite his own preface, for all the nice wine, the (near-infrared) photography, the many adventures with our Citroen BX, the discussions about remote sensing and, indeed, for more nice wine.

Every now and then your mind needs to be on something else than science. Maarten Leenders, thanks for the necessary distraction from the PhD work, for instance by the many concerts we visited and the trips we made. Also thanks, both Wiebe and Maarten, for your help with graphical design and for your support as *paranimfs*. I wrote large parts of Chapters 1 and 7 in a beautiful house on the Veluwe. Robert Voûte, thanks for that and for your support at Logica!

En dan als laatste, maar zeker niet als minste, wil ik mijn familie hartelijk bedanken. Zeker in het laatste jaar was ik regelmatig op zondag aan het werk in plaats van bij jullie langs te komen. Wouter, bedankt dat je toch hebt aangedrongen om er af en toe een dagje uit te gaan. Pa en ma, bedankt voor alle medeleven, ook toen ik aangaf na mijn PhD naar Zwitserland te willen verhuizen. En als allerlaatste Titia, wat een PhD naast de woeste wetenschap al kan brengen. Dankjewel! Thank you all!

Rogier
Elspeet, 24-12-2011

List of publications

Peer reviewed journals

de Jong, R., Schaepman, M.E., de Bruin, S. & Furrer, R. (in preparation). Spatial relationship between climatologies and changes in global vegetation activity. *Global Change Biology*

de Jong, R., Verbesselt, J., Schaepman, M.E., & de Bruin, S. (2012). Trend changes in global greening and browning: contribution of short-term trends to longer-term change. *Global Change Biology, 18*, 642-655

de Jong, R., & de Bruin, S. (2012). Linear trends in seasonal vegetation time series and the modifiable temporal unit problem. *Biogeosciences, 9*, 71-77

de Jong, R., de Bruin, S., de Wit, A., Schaepman, M.E., & Dent, D.L. (2011). Analysis of monotonic greening and browning trends from global NDVI time-series. *Remote Sensing of Environment, 115*, 692-702

de Jong, R., de Bruin, S., Schaepman, M.E., & Dent, D.L. (2011). Quantitative mapping of global land degradation using Earth observations. *International Journal of Remote Sensing, 32*, 6823-6853

Other scientific publications

de Jong, R., Verbesselt, J., Schaepman, M.E., & de Bruin, S. (2011). Detection of Breakpoints in Global NDVI time series. *34th International Symposium on Remote Sensing of Environment (ISRSE)*. Sydney, Australia

de Jong, R. (2011). Trendkaart voor landdegradatie. Kennis in Kaarten, atlas van Wagenings onderzoek naar onze groene leefomgeving (pp. 98-99). Environmental Science Group, Wageningen University, The Netherlands

Bai, Z.G., **de Jong, R.**, & van Lynden, G.W.J. (2010). An Update of GLADA - Global Assessment of Land Degradation and Improvement. ISRIC report 2010/08. ISRIC World Soil information and UN Food and Agricultural Organization, Wageningen, The Netherlands

Wilschut, L.I. (2010). Land use in the Upper Tana – technical report of a remote sensing based land use map. Green Water Credits Report 9 / ISRIC Report 2010/03 (Eds. MacMillan, B., Kauffman, S. & **de Jong, R.**). ISRIC – World Soil Information, Wageningen, The Netherlands

de Jong, R. (2010). The trend in soil degradation publications. *IUSS Bulletin, 116*, 21-25

Bindraban, P.S., Mantel, S., Bai, Z.G., & **de Jong, R.** (2010). Analytical tools for assessing land degradation and its impact on soil quality (EGU2010-14800). *Geophysical Research Abstracts, 12*

de Jong, R., Bai, Z.G., Dent, D.L., Schaepman, M.E., de Bruin, S., & de Wit, A. (2009). Enhanced assessment of global land degradation. *33th International Symposium on Remote Sensing of Environment (ISRSE)*. Stresa, Italy

de Jong, R., de Bruin, S., & Schaepman, M.E. (2008). Towards quantitative mapping of indicators of land degradation in drylands. *7th International Conference of the African Association of Remote Sensing of the Environment (AARSE)*. Accra, Ghana

Hiemstra, P., & **de Jong, R.** (2006). Estimating leaf water content in Mediterranean oak forests for forest fire models: a comparison between empirical and radiative transfer model inversion using hyperspectral imagery. *MSc thesis, Utrecht University*, 64p.

de Jong, R. (2006). Monitoring disturbances and regeneration of Eucalyptus forest in South-Western Australia using multi-temporal Landsat imagery. CSIRO & Landgate, Perth, Western Australia. *MSc thesis, Utrecht University*, 50p.

Short biography

Rogier de Jong was born in Nijmegen, The Netherlands, on January 4th 1983 and brought up in the close by village of Elst, where he attended primary school at *de Ark*. In 1995, he started high school at *Stedelijk Gymnasium Nijmegen (SGN)*. His spare time was dedicated to outdoor sports, including adventure races and skiing, and to the boy scouts. He still is an active member of *Laurentiusgroep* Bilthoven.

His career as geoscientist, as for many colleagues, started with collecting fossil ammonites and trilobites as well as the most beautiful minerals. He has special remembrances of the yellow-green Adamite and the deep-red Realgar crystals which contrasted beautifully against the white Dolomite substrate. All of these were collected – unhindered by any knowledge of geology or paleontology – in such a way that no context was described and that the resulting collection, which still resides in boxes somewhere, is useless to science, but nice a decoration. At that time, Rogier had the honor of taking part in the excellence track of *SGN,* as part of which he attended the biogeology lectures of Professor Bert van der Zwaan at the University of Nijmegen. It was then that he subscribed for the Earth Sciences curriculum at Utrecht University (starting 2001). In the first years he went back and forth between geology, biogeology and physical geography until he ultimately decided in favor of the latter. In the course of these studies, he took part in the renowned Berendsen-fieldwork (paleo-reconstruction of the Rhine-Meuse delta), the geomorphology-and-hydrology fieldwork in the French Alps and he specialized in environmental remote sensing during his MSc fieldwork and theses. Part of the latter was an internship at CSIRO and LandGate in Perth (Australia) about Eucalyptus forest regeneration from logging and wildfires. His MSc thesis was about quantification of vegetation water content using imaging spectroscopy and radiative-transfer models in the Peyne catchment in Languedoc, France.

After MSc graduation, Rogier started as business consultant in the geo/space IT domain at Logica NL. He worked on various topics, including asset tracking (transport division), remote sensing and military projects. In 2008, he got, supported by Logica NL, the opportunity to work on this PhD thesis. In the course of four years, he worked on the various topics presented in this thesis and he participated in various scientific conferences and MSc-level teaching. As part of the PhD-education program, he attended several summer-school courses on entrepreneurship, management and leadership. As of March 2012, Rogier moved to Zurich, Switzerland, to work as a postdoc with the Remote Sensing Laboratories at the University of Zurich. Here, he will continue on the presented work in the ‘Global Change and Biodiversity’ project and return to the spectroscopy domain in the ‘Apex’ / ‘Swiss Earth Observatory Network (SEON)’ project.

PE&RC PhD Education Certificate

With the educational activities listed below the PhD candidate has complied with the educational requirements set by the C.T. de Wit Graduate School for Production Ecology and Resource Conservation (PE&RC) which comprises of a minimum total of 32 ECTS (= 22 weeks of activities)

Review of literature (4.2 ECTS)
Quantitative mapping of global land degradation using Earth observations

Post-graduate courses (4.2 ECTS)
- Hyper I-net Summer School; GRS (2008)
- IDL Programming course; GRS (2008)
- Remote sensing of environment workshop; GRS (2008)

Laboratory training and working visits (4 ECTS)
- Mediterranean vegetation dynamics; Utrecht University (2008-2009)
- Exchange program with University of Zurich (2009-2011)

Invited review of (unpublished) journal manuscript (2 ECTS)
- Remote Sensing of Environment (RSE): comparison of trends in GIMMS and MODIS datasets (2011)
- Remote Sensing of Environment (RSE): impact of sensor degradation on trends in MODIS data (2011)
- Journal of Applied Earth Observation and Geoinformation (JAG): estimating light-use efficiency (LUE) from remote-sensing data (2011)
- International Journal of Digital Earth (IJDE): seasonal patterns in fraction of photosynthetically-active radiation (FPAR) (2011)

Competence strengthening / skills courses (4.5 ECTS)
- The art of writing; Wageningen Graduate Schools (2009)
- Entrepreneurial Bootcamp; DAFNE & Wisconsin School of Business (2009)
- Leadership & Management Summer School; University of Zurich (2010)

PE&RC Annual meetings, seminars and the PE&RC weekend (3 ECTS)
- PE&RC Weekend (2008)
- PE&RC Annual meetings: expect the unexpected (2008), intelligent nature: on the origin of communication (2009), innovation for sustainability: what are the neighbours doing? (2011)
- Other PE&RC symposia: scaling from molecules to ecosystems (2008), 3rd remote sensing symposium; organizing committee (2011)

Discussion groups / local seminars and other meetings (5.1 ECTS)
- PhD Defense mini-seminars: Raoul Zuritra-Milla, Harm Bartholomeus, Jochem Verelst (2011)
- Workshop on recent methods for monitoring of forest and land degradation; oral presentation; Wageningen (2011)
- Colloquium: is our world greening or browning; oral presentation; University of Zurich (2011)
- Spatial Methods discussion group (2008-2011)
- Remote sensing thematic group (2008-2011)

International symposia, workshops and conferences (9 ECTS)
- 7th African Association of Remote Sensing for Environment (AARSE), international conference; oral presentation; Accra, Ghana (2008)
- 33rd International Symposium on Remote Sensing of Environment (ISRSE); oral presentation; Stresa, Italy (2009)
- 2nd Dutch Remote Sensing Symposium (RSS); oral presentation; Delft, the Netherlands (2010)
- Workshop United Nations Convention to Combat Desertification (UNCCD); Bonn, Germany (2010)
- 1st Spatioal Statistics Symposium; poster; Enschede, the Netherlands (2011)
- 34rd ISRSE; oral presentation; Sydney, Australia (2011)
- 9th Swiss Geoscience Meeting (SGM); poster; Zurich, Switzerland (2011)

Lecturing / supervision of practical's / tutorials (2.4 ECTS)
- Academic Master Cluster (AMC) II; 3 days (2008)
- Remote sensing with ERDAS, introduction; 5 days (2010)

Supervision of 2 MSc students; 5 days (1.5 ECTS)
- Vegetation degradation in South Africa
- Use of degraded land for palm oil in Indonesia